

Aus dem Fachbereich Biophysik
Theoretische Medizin und Biowissenschaften
der Medizinischen Fakultät
der Universität des Saarlandes, Homburg/Saar

Impacts of bystander cells and external Ca^{2+} on NK/CTL-mediated cytotoxicity

*Dissertation zur Erlangung des Grades eines Doktors der
Naturwissenschaften*

der Medizinischen Fakultät
der UNIVERSITÄT DES SAARLANDES

2017

vorgelegt von: Xiao ZHOU

geb. am: 03.08.1986 in Hunan, China

Tag des Promotionskolloquiums:

Dekan:

Vorsitzender:

Berichterstatter:

Contents

1. Abstract	1
1. Zusammenfassung	3
2. Introduction	5
2.1. The orchestra of immune system.....	5
2.2. Immune cell education: a process about selections.....	8
2.3. Immunological synapse (IS) guarantees specificity	9
2.4. Downstream cascades of immunoreceptor activation	11
2.5. Ca ²⁺ - a key player in the immune response.....	13
2.6. Bystander cells at battlefields.....	14
2.7. Purpose and goals	16
3. Materials and methods.....	18
3.1. Reagents	18
3.2. Cells.....	18
3.2.1. Cell lines.....	18
3.2.2. Peripheral blood mononuclear cell (PBMC) preparation.....	18
3.2.3. CD8 ⁺ cell stimulation and positive isolation.....	19
3.2.4. Negative isolation of CD8 ⁺ and NK cells from PBMCs	19
3.3. Real-time killing assay	20
3.4. Electroporation	21
3.5. Protein conjugation.....	21
3.6. Fluorescence-activated flow cytometry (FACS).....	22
3.7. Degranulation assay	22
3.8. Viability assay by CellTiter Blue	23
3.9. Amplex UltraRed assay	23
3.10. Single cell Ca ²⁺ imaging.....	24
3.11. Time-lapse imaging with Cell observer.....	25

3.12.	Total internal reflection fluorescence microscope (TIRFM) imaging.....	25
3.13.	3D live cell imaging.....	27
3.13.1.	Gel preparation.....	27
3.13.2.	3D image acquisition.....	27
3.14.	Data analysis.....	28
4.	Results.....	29
4.1.	Impact of bystander cells on cytotoxicity.....	29
4.1.1.	Non-target bystander cells enhance CTL-mediated cytotoxicity.....	29
4.1.2.	Bystander cells enhance NK cell-mediated target killing.....	37
4.1.3.	Bystander cell enhanced killing is not generally caused by the conditioned medium.....	41
4.1.4.	Bystander cells do not influence NK cell degranulation.....	43
4.1.5.	Bystander cells enhance NK cell migration.....	44
4.1.6.	Increase in local motility of killer cells by bystanders decreases the search time to locate target cells.....	47
4.1.7.	Mechanisms mediating the bystander cell enhanced NK migration.....	53
4.1.8.	Impacts of Treg as bystander cell on NK-mediated killing.....	60
4.2.	$[\text{Ca}^{2+}]_{\text{ex}}$ dependence of LG release.....	62
4.2.1.	$[\text{Ca}^{2+}]_{\text{ex}}$ alters the killing efficiency of CTLs.....	62
4.2.2.	Antigen concentration-dependent Ca^{2+} influx correlates with CTL-mediated cytotoxicity.....	64
4.2.3.	A certain stimulus intensity is necessary for effective killing.....	65
4.2.4.	LG fusion is correlated with optimized $[\text{Ca}^{2+}]_{\text{ex}}$	66
5.	Discussion.....	70
5.1.	Bystander cell enhanced killer cell cytotoxicity.....	70
5.1.1.	The role of bystander cell in killer cell mediated killing.....	70
5.1.2.	The role of H_2O_2 in killer cell cytotoxicity.....	72
5.1.3.	The role of β integrin in bystander cell enhanced cytotoxicity.....	74

5.1.4. Antigen transfer between cells 75

5.2. The $[Ca^{2+}]_{ex}$ dependence of killing..... 76

5.2.1. Optimal $[Ca^{2+}]_{ex}$ dependence for killer cell function 76

5.2.2. Potential mechanism(s) mediating the $[Ca^{2+}]_{ex}$ dependence in killer cells 78

6. References 80

7. Publications 89

8. Acknowledgements 90

9. Curriculum Vitae 91

1. Abstract

Immune killer cells, mainly cytotoxic T lymphocytes (CTLs) and natural killer (NK) cells, serve a crucial role in eliminating pathogen-infected cells and cancer cells. The specificity of immune cytotoxicity relies on the formation of the immunological synapse (IS) between the killer cell and the target. While killer cells search and eliminate targets, environmental components like the non-target bystander cells and extracellular calcium ($[Ca^{2+}]_{ex}$) are important factors relevant for the killer cell' functions. To date, the impact of bystander cells and $[Ca^{2+}]_{ex}$ on killer cell cytotoxicity remains poorly understood. To address this question, I investigated the role of the bystander cells and $[Ca^{2+}]_{ex}$ for killer cell functions. In the first part of this work, I focused on bystander cells. I found that the presence of bystander cells enhanced the killing efficiency of both CTLs and NK cells without affecting the degranulation of cytotoxic lytic granules (LG). Live cell imaging showed that the killer cells migrate with a faster velocity and a higher persistence in the presence of bystander cells. The persistence, but not the velocity of killer cells was reduced by the blockade of integrin β chains 1, 2 and 7 on the killer cells with neutralizing antibodies. Furthermore, bystander cell-generated H_2O_2 elevates the killer cell migration velocity, but not the persistence and degranulation. In the second part, based on coworkers' observation, I investigated how $[Ca^{2+}]_{ex}$ affects CTL-mediated cytotoxicity. I reproduced that CTLs show the best killing when $[Ca^{2+}]_{ex}$ was reduced to 130-800 μM , higher or lower $[Ca^{2+}]_{ex}$ impaired the killing efficiency. The same tendency was confirmed for LG release in CTLs with the same $[Ca^{2+}]_{ex}$ using total internal reflection fluorescence microscopy (TIRFM). I could show that the Ca^{2+} signal at the site where vesicles fused is lower than in the LG-free cytosol and the site a vesicle stayed non-fused. In summary, this work suggests that bystander cells enhance NK/CTL-mediated cytotoxicity by promoting killer cell migration through bystander-derived H_2O_2 and by killer cell β integrins. CTLs

execute the cytotoxicity in a $[Ca^{2+}]_{ex}$ dependent manner, and the release of LG correlates with a Ca^{2+} microdomain which contains relatively low Ca^{2+} at the IS. These results suggest a positive role of the bystander cells in facilitating killer cell to pinpoint the target, and uncover the potential utility of tuning $[Ca^{2+}]_{ex}$ to modify killer cell cytotoxicity, therefore allowing new insights into the possible impact of the microenvironment on immune surveillance.

1. Zusammenfassung

Die wesentlichen Killerzellen des Immunsystems, Zytotoxische T Lymphozyten (CTL) und Natürliche Killerzellen (NK), spielen eine entscheidende Rolle bei der Eliminierung von Pathogen-infizierten Zellen und Krebszellen. Die Spezifität der Zytotoxizität des Immunsystems hängt dabei von der erfolgreichen Bildung der Immunologischen Synapse (IS) zwischen Killer- und Zielzelle ab. Die Suche nach und Abtötung von Zielzellen wird wahrscheinlich von verschiedenen Faktoren des Mikromilieus beeinflusst: U.a. könnten sogenannte Bystanderzellen, die selbst nicht von den Killerzellen erkannt werden, wie auch die extrazelluläre Calciumkonzentration ($[Ca^{2+}]_{ex}$) eine wichtige Rolle für die Funktion der Killerzellen spielen. Beide Faktoren sind allerdings bis jetzt nicht eingehend untersucht worden. Daher hat meine Arbeit zum Ziel die Rolle von Bystanderzellen und von $[Ca^{2+}]_{ex}$ auf die Funktion von Killerzellen zu analysieren. Im ersten Teil der Arbeit habe ich mich auf die Bystander-Zellen fokussiert. Ich habe herausgefunden, dass die Effizienz von CTL und NK Zellen bei der Abtötung von Zielzellen durch die Anwesenheit von Bystander-Zellen positiv beeinflusst wird, ohne dass diese dabei die Degranulation der lytischen Granula (LG) beeinflusst. Mittels bildgebender Verfahren konnte nachgewiesen werden, dass CTL und NK Zellen in der Anwesenheit von Bystander-Zellen schneller migrieren und dabei auch eine höhere Migrations-Persistenz aufweisen. Dabei wird die Persistenz nicht aber die Geschwindigkeit der Migration durch eine Blockade der Integrin β -Untereinheiten durch neutralisierende Antikörper reduziert. Im Gegensatz dazu erhöht H_2O_2 , welches von den Bystander-Zellen produziert wird, die Geschwindigkeit aber nicht die Persistenz der Migration, ohne dabei die Degranulation der LG zu beeinflussen. Im zweiten Teil der Arbeit habe ich die Abhängigkeit der CTL Zytotoxizität von $[Ca^{2+}]_{ex}$ untersucht, basierend auf vorhandenen Ergebnissen von anderen Labormitgliedern. Ich habe reproduziert, dass CTL bei einer $[Ca^{2+}]_{ex}$ von etwa 130-800 μM ein Optimum bezüglich Zytotoxizität gegenüber Zielzellen haben, höheres oder niedrigeres $[Ca^{2+}]_{ex}$ reduziert die Abtötungseffizienz. Dieselbe Abhängigkeit von $[Ca^{2+}]_{ex}$ habe ich für die Freisetzung von LG an der IS mittels Totaler-Interner-Reflektions-Mikroskopie (TIRFM) gemessen. Zusätzlich konnte ich zeigen, dass intrazelluläre Ca^{2+} Signale in Bereichen niedriger sind, in denen LG Fusion stattfindet, und höher in Bereichen, in denen keine Fusion stattfindet. Zusammenfassend zeigt die Arbeit, dass Bystander-Zellen die Zytotoxizität von CTL und NK Zellen erhöht, und zwar durch eine H_2O_2 -abhängige Erhöhung der Migrationsgeschwindigkeit und eine Integrin-

abhängige Erhöhung der Migrationspersistenz. Die zytotoxische Funktion ist Ca^{2+} -abhängig mit einem relativ niedrigen Ca^{2+} -Optimum und relativ niedrigen Ca^{2+} Konzentrationen an der IS. Diese Ergebnisse weisen auf eine positive Rolle von Bystander-Zellen bei Abtötung von Zielzellen hin, und sie zeigen eine Möglichkeit auf, $[\text{Ca}^{2+}]_{\text{ex}}$ zu nutzen, um die Zytotoxizität der Killerzellen zu modulieren. Beide Ergebnisse unterstreichen darüber hinaus die fundamentale Rolle des Mikromilieus bei der Immunabwehr.

2. Introduction

For thousands of years, human beings survived an environment filled with numerous threats, including natural disasters or wild animal attacks, but also diseases caused by pathogenic microbes or uncontrolled cell proliferation like cancer. Human beings utilize a sophisticated immune system to fight the potential pathogens and pathogenic cells. The immune system is serving crucial roles of eliminating invading microbes and abnormal cells, therefore providing the individuals with proper protection against a plethora of diseases.

2.1. The orchestra of immune system

The vertebrate immune system is an elaborate system that functions through the collaboration of a complex network of protein mediators, cells, and other factors. For human beings, it provides us with the defense lines against infectious agents and also with a surveillance system to monitor the integrity of host tissues. The immune system is composed of two parts: the innate immune system and the adaptive immune system, which complement each other to guard the individuals and protect us from illness in most cases [1].

The innate immune system serves as the first protection line to respond immediately to infectious agents. It combines two levels of protection: The physical barrier comprising the skin and the humoral innate immune components. The skin acts as a physical barrier to keep invaders outside of the body [2]. In addition, glands like sudoriferous and salivary glands, secrete various liquids to flush away or deteriorate the attached microbes from environment, thus remove the potential pathogen [3]. Mucus is another important liquid system which is a viscous product containing different kinds of enzymes, immunoglobulins, salts and proteins. Mucus exists in different organs and plays a role in protecting the lining of the tubes in the

respiratory, gastrointestinal and other systems. It provides an environment which favors beneficial microbes but prohibits harmful microbes [4], [5].

If invaders managed to bypass the physical barriers, the second line of defense, the cellular innate immune system, provides immediate protection. The cellular part of the innate immune system is pre-activated to recognize the invaders or ‘danger signals’ from the damaged tissue. The cellular innate immune system contains leukocytes including phagocytes, mast cells and natural killer (NK) cells [6]. The cellular innate immune system recognizes pathogen families that are typically associated with infectious agents. In most cases, the cellular innate immune system serves to remove the invader or pathological cells directly. Meanwhile, it recruits other immune cells and activates the complement cascade, as well as the adaptive immune system to carry out further immune activities. Usually, the innate immune functions are exerted by NK cell-mediated cytotoxicity, macrophage- and neutrophil-mediated phagocytosis, complement-mediated attacks, extracellular enzymes mediated digestion and so on. In addition, activation of naive T cells requires antigen presentation by innate immune cells, in particular, dendritic cells [7], [8].

The adaptive immune system is also known as the acquired immune system. It has (or develops) a high specificity and is tailored against specific molecules (antigens) of the infectious agents. The term ‘acquired’ means that the function of this sub-system is not present at birth but has to be adapted during the lifetime of the organism. The adaptive immune function is mainly carried out by two key players, T and B lymphocytes [9], which possess a huge receptor repertoire that can recognize an almost limitless range of structures.

Under physical conditions, DCs circulate with the blood and check the tissues. If the cell in tissue carries the right self-identity molecules called human leukocyte antigen (HLA), it will not activate the immune response [10]. When the cell is infected or transformed, most likely

foreign antigens are presented or HLA is lost, DCs will be activated and integrate the specific antigen to MHC molecules and be ready to present these antigens to naïve cells. The activated DCs subsequently migrate and accumulate in the lymph node to activate the naïve cell with the corresponding receptor. Once the naïve cell is activated by antigen presenting cells (APC), it undergoes massive expansion in response to the recognition of this antigen by the immunoreceptors. The engagement of the antigen with the receptor induces proliferation and differentiation, therefore efficiently amplify the respective lymphocyte capable of recognizing the particular antigen that triggers the response [11].

The rapid proliferation and activation of B lymphocytes will result in the abundant production of cytokines and specific antibodies which can neutralize the pathogen or mark them for further interactions with other immune components [12]. Aside from the B lymphocytes, the expanding T lymphocytes primarily serve the role of eliminating pathogen infected cells or transformed cells [13]. After the infected cells or abnormal cells have been eradicated, most of the effector cells undergo programmed death, except that a small portion of the T and B cell population survives and keeps proliferating to form the reservoir of memory cells [14]. At the second encounter with that same pathogen, the memory cells undergo polyclonal response to mount a faster and stronger response, therefore respond to the pathogen that the cells encountered before much more efficiently.

The innate and the adaptive immune system establish a comprehensive protection against pathogens by complementing each other to ensure the efficient eradication of the harmful organisms and antigens. It is important that the lymphocytes only recognize and eliminate the cells turned ‘nonself’, otherwise, autoimmune diseases occur because of the immune activation initiated by normal cells, therefore induce dysfunction of the organ locally or globally [15].

2.2. Immune cell education: a process about selections

Immune cells arise from haematopoietic stem cells in the bone marrow and generate two stem cell populations: one is the myeloid progenitor that gives rise to granulocytes, macrophages, dendritic cells and mast cells; and the other is the lymphoid progenitor that differentiate into NK cells and other lymphocytes such as T and B cells [16], [17]. Dendritic cells are the professional antigen-presenting cells, and the lymphoid progenitor-derived lymphocytes develop to execute the immune cytotoxicity.

During the immune surveillance, it is of crucial importance to target the pathogen infected cells or tumorigenic cells but in parallel tolerate self-antigens. Lymphocytes manage this specificity via education during the development and maturation procedure, which takes place in the lymphatic organs (Fig. 1). The bone marrow-derived immature T cell progenitors lack both of the immune cell marker CD4 and CD8 molecules, therefore they are defined as double negative (DN) cells. When the DN cells arrive at the thymus, they migrate through the thymic cortex towards the outer subcapsular zone. Then DN thymocytes start to express a functional β -chain of the T cell receptor (TCR) and form the pre-TCR complex containing TCR β proteins associated with the CD3 δ , ϵ , and γ chains as well as an invariant pT α chain. These cells subsequently develop to express both CD4 and CD8 molecules and become double-positive (DP) cells. Only those DP cells expressing the invariant α -chain and ultimately pair with a β -chain successfully survive and proceed to proliferate, thus the pre-TCR serves as a molecular sensor for effectively selecting the cells that have productive TCR β gene rearrangements. This process has therefore been denoted by β selection [18], [19]. Afterward, the DP cells undergo positive selection, during which they are exposed to the self-antigens presented by the cortical epithelial cells expressing major histocompatibility complex (MHC)-I or MHC-II molecules. DP cells bind with the self-antigens with a proper affinity to induce the survival signal and survive the selection, otherwise, cells undergo apoptosis [20].

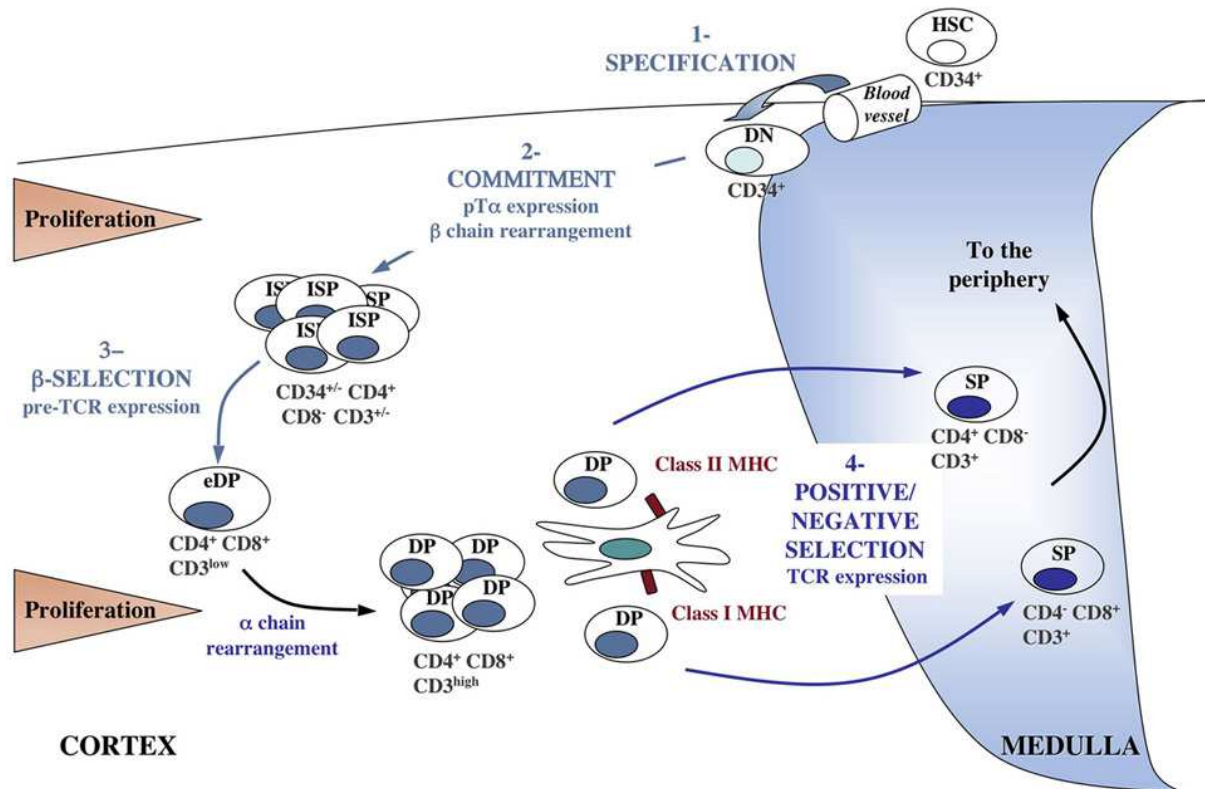


Figure 1. Sequential events during lymphocyte maturation. After entering the thymus, DN T cells rearrange the TCR complex to accomplish the commitment procedure. Then T cells undergo the β selection. The survived cells express both CD4 and CD8 molecules to become the DP cells. Subsequently, DP cells interact with the cortical epithelial cells expressing MHC molecules with a high enough affinity to survive the positive selection. Then the cells undergo the negative selection, during which the cells interact with the bone-marrow derived APC with a high enough affinity undergo apoptosis. These selections are dependent on self-peptides and MHC-self-peptides complex, which are independent on pathogen. The scheme was modified from Ref. [21].

DP cells that interact well with MHC class I molecules will eventually differentiate into CD8⁺ cells, while those interact well with MHC class II molecules mature into CD4⁺ cells. Later on, cells proceed to the negative selection, during which cells displaying TCR with high affinity to self-MHC molecules or MHC⁺ presented self-peptides undergo apoptotic death [22]. These selections ensure that the lymphocytes that exit the thymus possess the potential to carry mature TCR $\alpha\beta$ and recognize foreign antigens but do not interact with self-antigens presented by self-MHC molecules.

2.3. Immunological synapse (IS) guarantees specificity

Killer cells exert their cytotoxic function via two principal mechanisms: a non-cytolytic pathway through the death receptor and a cytolytic pathway through the fusion of lytic granules

(LG) to release lethal proteins like perforin (PFN) and granzyme B (GZB) or other granzymes [23]. The cytolytic pathway is dependent on the fusion of LG at the tight conjugation formed between the killer cell and the target upon immunoreceptor activation, termed immunological synapse (IS) [24].

The formation of the IS is a precisely controlled process: For instance in CTL (Fig. 2), in case a target cell presents the cognate antigen to the killer cell, the engagement of TCR with the corresponding antigen results in a transient IS formation between the CTL and the target. CTL subsequently polarizes towards the interface and re-orientates several intracellular components like the microtubule organizing center (MTOC) as well as the entire microtubule network and LG towards the contact area [25]. In addition, CTL undergoes a series of molecular interactions, including adhesion molecule ligation and co-receptor activation. As a result, the activation of these adhesion molecules, co-stimulatory molecules as well as the co-receptors in the complex form a bull's-eye-like structure, which is known as the supramolecular adhesion complex (SMAC).

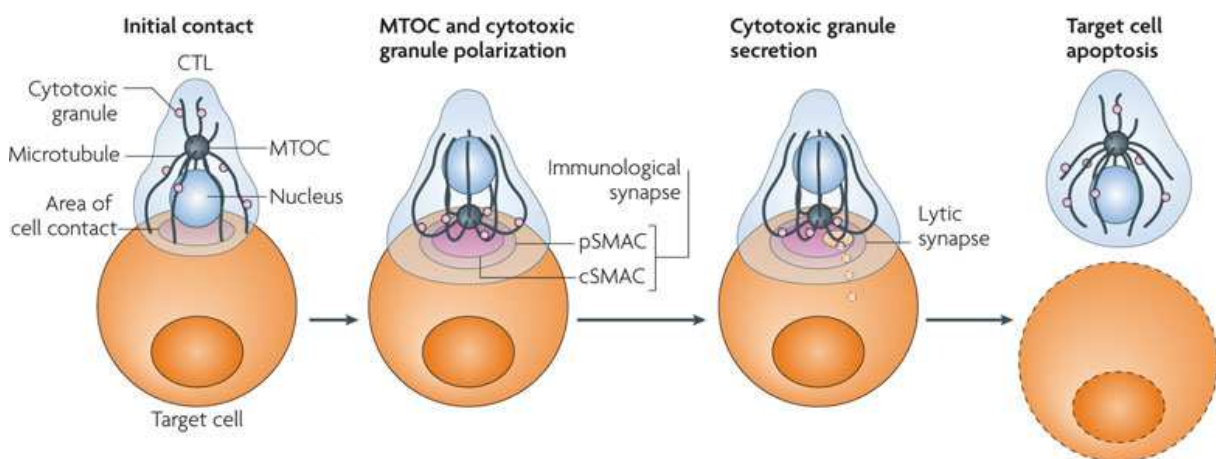


Figure 2. Sequential events during an IS formation between a CTL and a target cell. The recognition of the antigen on a target cell induces CTLs to form a tight conjugate with the target cell. The CTL rapidly polarizes MTOC and the microtubule network towards the contact site, where an immunological synapse (IS) is formed. The IS is organized into a central supramolecular activation complex (cSMAC), containing the signaling molecules and T cell receptors (TCRs). cSMAC is surrounded by the peripheral SMAC (pSMAC). Following IS formation, cytotoxic granules (also known as lytic granule, LG) are polarized along microtubules and then cluster around the MTOC. LG are fused with the cell membrane and their content is released into the secretory cleft (yellow) formed between the CTL and target cell. The release of LG content containing perforin and granzymes induce target apoptosis. The scheme was modified from Ref [27].

The IS ensures a sealed cleft between CTL and the target cell membrane with an enclosed actin ring [26]. The SMAC is composed of two different parts, which are called the central SMAC (cSMAC) and the peripheral SMAC (pSMAC). cSMAC which locates right at the center of the ring structure is enriched in TCR and the activated signaling proteins like phosphorylated LCK, PKC θ , and other proteins, therefore it is also known as the activating zone. This activating zone is surrounded by an actin ring and other cytoskeleton associated proteins, composing the pSMAC. At the pSMAC, the adhesion molecules such as lymphocyte function associated antigen-1 (LFA-1) are also enriched to stabilize the IS and induce further downstream signal activation [28]. Upon maturation of IS and fine-tune of the intracellular Ca^{2+} ($[\text{Ca}^{2+}]_{\text{in}}$), LG are fused into the secreting cleft. The exocytosis of LG results in the release of lethal proteins such as PFN and GZB. PFN binds to the target membrane and consequently form pores on it, GZB then enter the target cells in both passive and active manner through the PFN induced pores [29]. Subsequently, GZB induces the apoptosis cascade activation inside the target cell. Aside from the PFN-GZB induced cytolytic pathway, Fas ligand (FasL) interacts with the Fas receptors on the target cell and initiates the target death receptor signals to induce target cell apoptosis [30].

2.4. Downstream cascades of immunoreceptor activation

Upon the activation of the immunoreceptors, the signals are transduced into a series of intracellular reaction. The signaling cascade is initiated by the interaction of immunoreceptors with antigenic complex, such as TCR with MHC-peptide and NK Fc receptor with the IgG-antigen complex [31]. For instance (Fig. 3), TCR is responsible for recognizing antigen bound to the MHC molecules, together with the ζ -chain and CD3 molecules to constitute the TCR complex. TCR activation leads to phosphorylation of immunoreceptor tyrosine-based activation motifs (ITAMs) on the TCR complex by lymphocyte protein tyrosine kinase (Lck). The protein tyrosine phosphatase activates Lck and other Src family tyrosine kinases. The TCR

complex subsequently recruits and activates in situ the Zeta-chain-associated protein kinase (Zap-70) to promote further recruitment and phosphorylation of downstream components. Zap-70 phosphorylates different substrates like lymphocyte cytosolic protein 2 (LCP2) and promotes the recruitment of a series of proteins such as the adaptor proteins and inducible T cell kinase (Itk). Itk activates phospholipase C (PLC) and induces the generation of the second messengers diacylglycerol (DAG) and inositol trisphosphate (InsP₃). InsP₃ diffuses in the cytosol and binds to the InsP₃ receptor (InsP₃R) on the endoplasmic reticulum (ER) membrane. The ligation of InsP₃R opens the InsP₃R Ca²⁺ channels, which leads to the release of Ca²⁺ from the intracellular Ca²⁺ stores of ER. Depletion of the intracellular Ca²⁺ stores triggers the opening of Ca²⁺ release-activated channels (CRAC) [32].

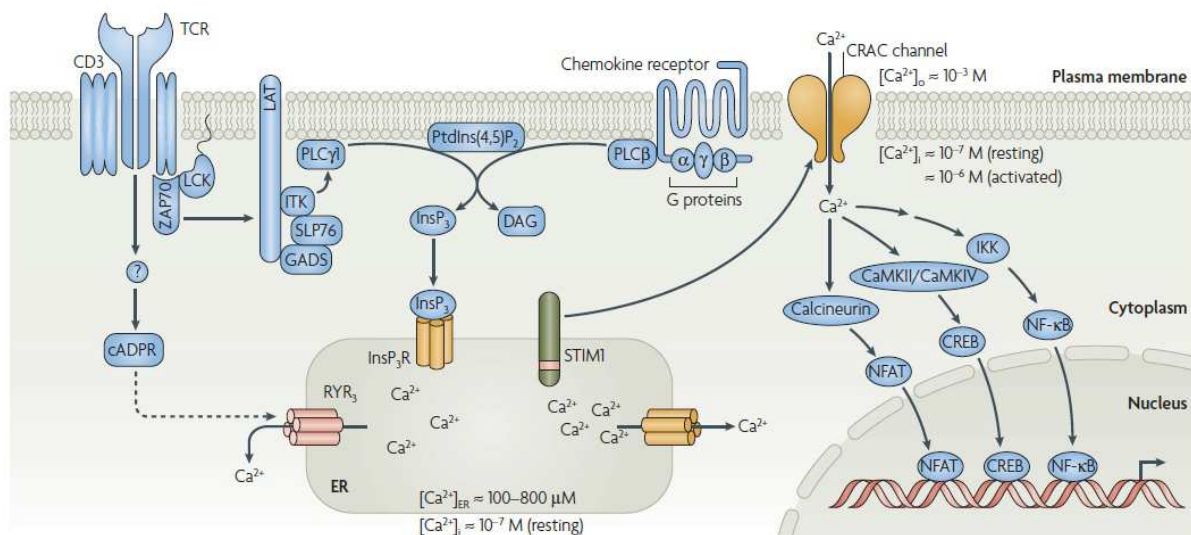


Figure 3. TCR cascade and the Ca²⁺ influx through CRAC channels upon antigen stimulation. Antigen recognition by TCR results in the tyrosine kinase like LCK and ZAP70 activation inside the T cell. Subsequently γ PLC 1 is phosphorylated and activated to produce InsP₃ and DAG. The InsP₃ receptor located in the ER is activated and allows the output of calcium from the ER lumen. STIM1 senses the reducing calcium deposits by the N-terminal region of the ER lumen. STIM1 rearrange in the ER membrane and activates the CRAC channel, Orai1. Intracellular calcium change activates the NF- κ B, NFAT, and other pathways. This scheme was adapted from Ref [34].

2.5. Ca^{2+} - a key player in the immune response

Ca^{2+} is a universal secondary messenger in many cells and tissues and it exerts important roles in mediating immune functions, ranging from cell growth, proliferation, apoptosis to other behaviors like cytokine secretion and cell migration [35]. In the human serum, the free Ca^{2+} concentration is kept at around 1.2 mM, while it is maintained at 0.1 μM in the resting cytoplasm [36]. This is achieved by Ca^{2+} -ATPases in the plasma membrane that maintain the extraordinary concentration gradient. In response to receptor stimulation, the free Ca^{2+} concentration may increase about 10 times in the cytosol. Ca^{2+} binds to proteins that contain for instance C2 Ca^{2+} binding motifs or EF-hand domains, thereby activating these proteins to mediate specific functions [37]. Ca^{2+} changes in lymphocyte can be generally subdivided into different forms: short-term, rapid changes which do not involve gene transcription and long-term responses that alter gene transcription [38]. The strength and duration (and maybe also frequency) of Ca^{2+} signals generated by this mechanism are key regulators of T-cell responses to the immunoreceptor activation [31], [39]. For instance, lymphocyte motility regulation and IS formation are dependent on short-term Ca^{2+} processes. The APC-T cell interaction is quickly followed by an elevation of intracellular Ca^{2+} mediated by Ca^{2+} release and influx. Within minutes, the transient, rapid Ca^{2+} influx regulates changes in T cell shape, interruption of migration and movement of actin network, MTOC polarization as well as the LG fusion [40], [41]. Long-lasting Ca^{2+} is required for the initiation of development and differentiation programs. Long lasting Ca^{2+} change emanating from the TCR responses and store-operated CRAC channels is usually sustained for hours to days. The long-lasting Ca^{2+} influx governs the activation pattern of nuclear factor of activated T cells (NFAT) signal. NFAT is one of the most important transcription factors in T cells. NFAT responds directly to Ca^{2+} signals, by which it can differentially regulate gene expression [42], [43]. The transcriptional responses upon sustained Ca^{2+} signals shape the outcomes of lymphocyte activation via altering the

protein expression pattern which determines the lymphocyte effector functions. These include normal responses to antigen, naive T cells differentiation, immature T cell development, but also unresponsiveness such as anergy [34].

In addition, Ca^{2+} also plays important roles in cancer development. Cancer cells often bear alterations in calcium channels, pumps, and exchangers in terms of their expression level, subcellular localization, activity, which are mostly regulated through post-translational modification or genetic mutations [44]. These changes often result in alterations in Ca^{2+} transport across the plasma membrane or the intracellular organelles. Many if not all of the Ca^{2+} channels, like voltage-gated Ca^{2+} channels, TRPV and ORAI channels as well as the plasma membrane calcium ATPases (PMCAs) are all implicated in the occurrence and development of cancer [45]–[47]. Changes in Ca^{2+} channel expression in carcinoma are correlated with the functional alternation involving cell proliferation and apoptosis. Other ion channels like K^+ and Cl^- channels are also correlated with the tumor growth via controlling the membrane potential and thereby the opening probability of the voltage-gated Ca^{2+} channels and the driving force for all Ca^{2+} channels [48]. Aside from tumorigenesis, tumor cell behavior is also highly correlated with altered Ca^{2+} signals. Higher expression of Ca^{2+} channels and consequently more Ca^{2+} influx enhance the proliferation, migration, invasion, metastasis and drug resistance [49], [50]. In summary, Ca^{2+} is tightly correlated with the immune escape and the tumor behaviors during the tumorigenesis.

2.6. Bystander cells at battlefields

IS formation is triggered in case that cells present the right antigen to the killer cells, otherwise, the cells are considered non-target cells for the specific cytotoxic response and are classified as bystander cells [51]. In both scenarios, infections and tumorigenesis, target cells are surrounded by non-target cells, either healthy or infected, in tissue, especially at early-stages of

disease development. Cancer, for instance, usually starts with the single mutated cell or a group of mutated cells, which is able to survive the immune surveillance. Subsequently, this phase proceeds into a multistep process involving further mutation and evolution of a progressively enhanced capacity of proliferation, survival and finally also invasion and metastasis [52]. In the tumor microenvironment (TME), many cells are non-target cells, in term bystander cells, including (but not limited to): infiltrated immune cells, healthy somatic cells as well as malignant cells that do not present matching antigens to initiate recognition of killer cells.

During immune surveillance, various types of immune cells infiltrate into the battlefield, a tumor or inflammation sites, to fight tumorigenic or infected cells. Among them, macrophages, differentiated from monocytes, are quickly recruited to battlefields, producing large amounts of reactive oxygen species (ROS) to kill intracellular bacteria [53]. Macrophages also act as professional antigen-presenting cells to activate T cells [54]. In addition, regulatory T lymphocytes (Treg) are also often found in tumors [55]. Primarily, Treg play an essential role in preventing autoimmune responses by suppressing the activation of conventional T cells [56]. However, tumor cells can take advantage of these Treg properties to escape immune surveillance, resulting in a negative correlation between the presence of Treg in tumor and promising prognosis [57], [58].

Apart from the recruited immune cells, there are other types of bystander cells presented at the battlefield. At early stages of disease development, tumor or inflammation, the aberrant cells are very often surrounded by healthy somatic cells. Healthy somatic cells bear self-antigens [59] and do not present tumor specific antigens, at least in most cases [60], therefore they will not be recognized as target cells by NK cells or tumor-specific CTL.

In addition to the health somatic bystander cells, malignant cells, to some extent, can also serve the role of bystander cells. For instance, malignant cells present cytomegalovirus peptide cannot

be recognized by the glioblastoma specific CTLs, and *vice versa* [61]. Meanwhile, NK cells become activated in the absence of sufficient signaling by their HLA-I specific receptors. Therefore, other malignant cells that present sufficient HLA-I receptors are not recognized and killed [62]. Thus, these malignant cells either with the unmatched antigen or sufficient HLA-I signals could act as bystander cell for CTLs and NKs, respectively.

Although bystander cells are a major component, at least in number, in tumor microenvironment or at inflammation sites, their direct impact on CTL or NK cell-mediated killing is not yet fully understood.

2.7. Purpose and goals

As described above, the immune system is always competing with the malignant cells. The immune cells are educated to recognize the infected or transformed cells in a specific manner and therefore tend to eliminate them efficiently. On the contrary, the malignant cells keep gaining different features to survive and spread, and hijack the environment to favor their growth and development. The communication of transformed cells with non-malignant cells of the environment shapes the tumor growth. As part of the TME, the non-target bystander cells have long been neglected in tumor development. What remains unclear are how and if bystander cells participate in mediating tumor progression and/or tumor immunity and if yes, what the mechanisms are. Meanwhile, immune cells function in the complex environment with distinct concentrations of soluble factors involving Ca^{2+} . Despite that the function of Ca^{2+} in both physiological and pathological conditions of T cell activation has been widely studied, it remains elusive that what the optimal extracellular concentration of Ca^{2+} is for immune killer cells to exert their cytotoxicity. Considering the points discussed about bystander cells and Ca^{2+} concentrations we set the following two goals for my thesis work:

1. Understanding the impacts of non-target bystander cells on the NK/CTL cytotoxicity and the respective mechanisms.
2. Investigating the Ca^{2+} dependence of CTL killing and the underlying mechanisms.

3. Materials and methods

3.1. Reagents

Fluorescent dye like Calcein-AM (C3100), CellTrace Calcein Red-Orange, AM (C34851), Hoechst 33342 (H1399) and LysoTracker red-AM (L7528) were purchased from ThermoFisher Scientific. Anti-integrin α -L (ITGAL) antibody (ABIN135680) was from Antibodies-online (Aachen, Germany). Human integrin β 1 antibody (MAB17781) and human integrin β 2 polyclonal antibody (AF1730) were from R&D Systems, Inc. (MN, USA). Anti-human/mouse integrin β 7 antibody (321218) was from Biolegend (CA, USA). Polybead[®] Polystyrene Microspheres (15 μ m, 18328-5) were purchased from Polyscience, Inc. (PA, USA). Type 1 Collagen (5133-A) was from Advanced BioMatrix, Inc (CA, USA). All chemicals and reagents not specifically mentioned were from Sigma.

3.2. Cells

3.2.1. Cell lines

Raji cells, P815 cells, and K562 cells were maintained in the laboratory with RPMI 1640 medium (21875, Invitrogen) supplemented with 10% FCS (10270-106, Invitrogen) and 100 U/ml P/S (15140-122, Life Technologies). All cell lines were maintained in the incubator at 37°C with 5% CO₂ and provided by Cora Hoxha, Carmen Haessig, Gertrud Schwaer and Sandra Janku.

3.2.2. Peripheral blood mononuclear cell (PBMC) preparation

Human blood was obtained by Carmen Haessig from healthy donors at the local blood bank as described before [63]. Briefly, blood cells were taken either from a Leucoreduction system chamber or the Amicus system, and they were diluted with HBSS solution and filtered with the

LSM medium at the condition of 450 g for 30min. The mononuclear cells were collected and washed with HBSS. After reducing the red blood cells with the erythrocyte-lysis-buffer, PBMCs were kept in chilled PBS containing 0.5% BSA.

3.2.3. CD8⁺ cell stimulation and positive isolation

Human CD8⁺ T cells were stimulated and purified as described before with minor modifications [63]. PBMCs were suspended at a density of 1.25×10^8 cells/ml in the complete medium (AIMV+10% FCS) and pulsed with 0.1 µg/ml SEA for 1 h at 37°C. Afterwards, the pulsed PBMCs were kept at a density of about 1.67×10^6 cells/ml in complete AIMV medium supplemented with 100U/ml interleukin-2 for 5 days in the incubator. On day 5, cells were positively isolated using a Dynabeads CD8 Positive isolation kit. Cells were diluted in PBS with 0.5% BSA at a density of 1×10^7 cells/ml, the antibody conjugated beads were added at the ratio of 0.8 bead per cell to the suspension and incubated at 4°C for 15 min with tilting. Afterward, the CD8⁺ cells were collected by magnetic accumulation on a magnet. After 3 times washing with PBS, cells were resuspended in RPMI-1640 with 1% FCS. The detaching reagent was added and the cells were incubated with tilting at RT for 45 min. After washing with RPMI medium, the beads were removed by magnetic separation and the supernatant was harvested by the centrifugation. Purified CD8⁺ T cells were resuspended in complete AIMV medium at the density of 1.5×10^6 cells/ml until being used for experiments.

3.2.4. Negative isolation of CD8⁺ and NK cells from PBMCs

For the TIRF imaging and the experiments performed with transfected cells, CD8⁺ T cells were negatively isolated by applying the Dynabeads® Untouched™ human CD8 T cell isolation kit. NK cells were also negatively isolated from PBMCs by the Dynabeads untouched human NK cell kit. Briefly, PBMCs were resuspended in PBS containing 0.5% BSA at the concentration of 1×10^8 cells/ml. The cells were incubated with the antibody cocktail against other cell types

at 4°C for 20 min. After 1 wash, cells were resuspended at the density of 1×10^8 cells/ml and mixed with the pre-washed beads. After 15 min incubation at RT, the mixture was undergoing a magnetic separation. The suspension of the magnetic procedure was collected and the cells were spun down at 300 g and 4°C for 8 min. Then NK cells were maintained at the concentration of 2×10^6 cells/ml in the complete AIMV medium and ready for use. CD8⁺ cells were stimulated by the CD3/CD28 activator beads at a cell to activator ratio of 1:0.8 at a density of 1.5×10^6 cells/ml for 3 days. On day 3, the activator beads were magnetically removed and the cells were ready for further electroporation.

3.3. Real-time killing assay

The cytotoxic capability of killer cells was detected by a real time killing assay previously introduced by Kummerow et al. [64]. Briefly, target cells were incubated with 500 nM Calcein-AM in AIMV containing 10 mM HEPES at RT for 15 min with gentle tilting. For CTLs, the target cells were pulsed with 1 µg/ml SEA in the complete AIMV medium for 30 min in the incubator before loading with Calcein-AM. Afterward, cells were washed once and resuspended at the density of 1.25×10^6 cells/ml in FCS-free AIMV medium with HEPES. The volume of 200 µl of cell suspension was added into a black clear-bottom 96 well plate (BD Falcon). Killer cells were resuspended in FCS-free AIMV according to killer:target ratio and added carefully into each well. Immediately after that step, the plate was read by a fluorescence reader (GENios Pro M200, TECAN, CA, USA). The bottom read function (Ex 488/Em 520 nm) was used to measure the fluorescence every 10 min over 4 h at 37°C.

To quantify killing with different amount of bystander cells, 2.5×10^4 target cells alone or mixed with the designed number of bystander cells were resuspended in 200 µl FCS-free AIMV and added into each well. For experiments using beads as bystanders, 2.5×10^4 Calcein-

AM loaded target cells were mixed with 7.5×10^4 polystyrene microspheres and a killing assay was performed.

To harvest the supernatant for killing assay, target K562 cells without Calcein-AM loading alone or together with the triple amount of bystander P815 cells were co-incubated with NK cells in the incubator for 4 h. After 4 h incubation, the supernatant was collected accordingly by centrifugation at 12000 g for 10 min. Afterwards, fresh K562 cells were loaded with Calcein-AM in FCS-free AIMV. The target cells were resuspended accordingly in the supernatant from different conditions to perform the real-time killing assay by adding 2.5×10^4 NK cells into each well.

3.4. Electroporation

Transfection of the CD8⁺ T cells was done as preveriously described [65]. Briefly, CD3/CD28 bead activated CD8⁺ T cells (5×10^6 cells for each transfection) were gently centrifuged at 100 g for 8 min. Cells were resuspended in 100 μ l pre-warmed transfection reagent and gently mixed with 0.75 μ g GZB-mCherry construct (or other designed constructs), the mixture was electroporated in the cuvettes by using the P3 primary cell nucleofection kit with the program Stimulated-T cell in Lonza 4D Nucleofacter™. Afterwards, cells were maintained in CO₂-pre-equilibrated complete medium (1.5 ml per one transfection). After 6 h incubation, the transfection reagent was removed by gentle centrifugation (100 \times g, 8 min) and fresh complete medium containing 10% FCS and 100 U/ml IL-2 was applied to the cells at the volume of 2 ml per transfection. After 24 to 30 hours cultivation post electroporation, cells were used for experiments.

3.5. Protein conjugation

An Atto 633 protein labeling kit (51253, Sigma) was used to label SEA with the fluorescent dye Atto 633. The conjugation was done by following the manual step by step. Briefly, the

protein was dissolved at a concentration of 2 mg/ml with PBS. The Atto-633 dye dissolved in 20 μ l DMSO was added quickly into the protein solution and incubated at 4°C for 2-4 hours with gently stirring in dark to complete the reaction. A PD-10 column with an exclusion size limit of 5 kDa was equilibrated with water and subsequently PBS. The labeling mixture was added to the column and 5 ml PBS was added to start the elution. The separated bands of the dye-labeled protein and non-conjugated dye became visible and the first band of the dye-conjugated protein was collected. The loading efficiency was detected following the instruction by using the fluorescence reader. Also, the conjugation efficiency was tested by loading the Raji cells with this dye-conjugated protein and checked under a fluorescent microscope.

3.6. Fluorescence-activated flow cytometry (FACS)

For detecting the transportation of antigens, Raji cells were pulsed with Atto-633 conjugated SEA or the normal SEA for 30min, another batch of Raji cells were incubated CD19-Alexa 488 for 30 min. After 2 washes the SEA pulsed Raji cells were mixed with the CD19 labeled Raji at the ratio of 1:1. The mixture was incubated in AIMV with 10% FCS for different time points. Afterward, the mixture was washed twice and fixed with 4% PFA on the ice. The fluorescence was detected by FACSVerse™ flow cytometer (BD Biosciences) equipped with 488 nm and 640 nm lasers. Cells which were not labeled or labeled with the vehicle were FACSeD using the same settings for gating. Each detection was based on 10,000 sorted events. Data were analyzed with FlowJo_V10 (FLOWJO, ICC).

3.7. Degranulation assay

To detect the degranulation level of the killer cells, FACS was employed to quantify the amount of exocytosed CD 107a, which is a degranulation indicator on the cell surface. Killer cells were cultivated in complete medium for certain days. For each detection, 1.0×10^5 target cells with or without 3×10^5 bystander cells were seeded onto the 96-well plate in 200 μ l

complete medium containing 10% FCS. After the cells were settled, 1×10^5 NK cells in 50 μ l medium were added into the well containing the pre-seeded cells. Alexa Fluor 488 conjugated anti-human CD107a antibody (Biolegend, 1:40) and Golgi stop Protein Transport Inhibitor (BD biosciences, 1:200) were added to the mixture. Cells were incubated at 37°C with 5% CO₂ for 4 h. Afterward, the mixture was resuspended gently and the cells were spun down at 200 g for 5 min. Cells were then resuspended in 100 μ l PBS containing 5% FCS and 0.5% BSA. APC/Cy5.5 anti-human NKG2D antibody or anti-CD16 antibody (Biolegend, 1:100) for NK cell or Alexa-647 anti-human CD3 antibody (Biolegend, 1:50) was added to the suspension and stained for 30 min on ice, meanwhile, killer cells incubated with just PBS were used as controls for gating. The fluorescence was detected by FACSVerse™ flow cytometer (BD Biosciences) equipped with 405nm, 488nm and 640nm lasers and the BD FACSuite™ software. Data were analyzed with FlowJo_V10 (FLOWJO, ICC).

3.8. Viability assay by CellTiter Blue

To detect the cell viability, the CellTiter-Blue assay (G8081, Promega) was used to check the capability of the cells to convert a redox dye (resazurin) into a fluorescent end product (resorufin). Briefly, the cells were resuspended at a density of 1.25×10^5 cells/ml, and 200 μ l of the cell suspension was added to the 96 well plate; to make the results more precise, triplicates were set. H₂O₂ at different concentrations or the vehicle (H₂O) was added to the cells and the cells were incubated at 37°C for 4 h. Afterwards, each well was supplemented with 20 μ l CellTiter-Blue reagents. After 2 h incubation, the plate was measured with the GENios Pro plate reader (TECAN) with the Ex/Em at 535 nm/590 nm.

3.9. Amplex UltraRed assay

To detect the concentration of extracellular H₂O₂, a direct peroxidase assay was employed by using Amplex UltraRed (A36006, Invitrogen). Briefly, 2.5×10^4 target cells alone or together

with 7.5×10^4 bystander cells in 100 μ l phenol red free DME-F12 supplemented with 10mM HEPES were seeded in the 96 well plate. Twenty minutes after the cells were seeded, NK cells, in 10 μ l DMEM-F12 medium, were added carefully onto the top of the pre-seeded cells. As a background control, DMEM F12 without adding any cells was added. The freshly mixed 50 μ M Amplex ultra-red reagent together with 10 U/ml SOD and 0.1 U/ml HRP in the phenol red free DMEM F12 were added into wells immediately after the NK cell addition. The plate was immediately measured on a GENios Pro microwell plate reader (TECAN) at excitation/emission of 535 nm/590 nm with controlling the temperature at 37°C. The plate was measured every 4 min using the bottom read mode for 60 cycles. The concentration of H₂O₂ was calculated based on a standard calibration curve obtained by serial dilution of H₂O₂. To check if chelating of the [Ca²⁺]_{in} of bystander cells affects the H₂O₂ generation, the bystander cells were pre-incubated with 100 mM EGTA-AM at 37°C for 30 min, and subsequently, the cells were mixed with the target cells. For catalase function detection, 10 U/ml catalase was added to the well bottom, and afterwards, the designed concentrations of H₂O₂ in FCS-free DMEM-F12 were applied to the catalase-containing wells, followed by fluorescence detection with the GENios pro reader.

3.10. Single cell Ca²⁺ imaging

For detecting antigen-induced Ca²⁺ influx, 2×10^5 CTLs were incubated with 2 μ M Fura-2 AM in FCS-free AIMV medium at 37°C for 30 min, meanwhile 1×10^6 Raji cells were pulsed with SEA as described before. The washed CTLs were attached to a Φ 25 mm poly-ornithine coated cover glass and assembled in the chamber to fit the stage of the Olympus IX71 microscope equipped with an Olympus UPLSAPO 20 \times (NA 0.75) lens. Cells were excited at 340 and 380 nm with a polychrome V monochromator (TILL Photonics) using an ET Fura2 filter set (Chroma Technology Corp). The emitted light at wavelength > 400 nm (T400 lp dichroic beamsplitter, ET510/80 nm emission filter) was acquired by the CCD camera (SensiCam,

TILL Imago). The ratiometric images were recorded every 5 s for 300 frames. At 100 seconds, Raji cells were applied in AIMV to the attached CTLs by suction. The images were analyzed by TILL Vision software.

3.11. Time-lapse imaging with Cell observer

To monitor NK migration with or without bystander, calcein-labeled 2.5×10^4 target cells were seeded per well with or without beads or P815 bystander cells (incubated with either CellTrace Calcein Red-Orange-AM labeled or with EGTA-AM or other dyes). The mixture of target and bystander cells in FCS-free AIMV supplemented with 10 mM HEPES was added together and settled onto the black clear-bottom 96 well plate. NK cells without any treatment or incubated with neutralizing antibodies or vehicle at 37°C for 60 min were added into the designed wells at 1×10^5 cell/well. The cells were monitored on a Zeiss cell observer microscope equipped with a 10× (Plan/Apo, N.A. 1.0) objective. Green channel (Ex 488/ Em 525 nm) and deep red channel (Ex 561/ Em 600 nm), as well as the wide field, were recorded at the intervals of 20-40 seconds over 4 hours at 37°C. ImageJ with the speckle trackerJ plugin was applied to track movements of killer cells manually. For each experiment, only migrating cells were tracked. Velocity and trajectories were calculated by Igor Pro program with home-made macros programmed by Carssten Kummerow.

3.12. Total internal reflection fluorescence microscope (TIRFM) imaging

A LEICA TIRF microscope setup configured with the following components was used: a solid-state laser 85 YCA that emits at 561 nm (Melles Griot), a dual-view camera splitter (Visitron) to separate the red and green excitation waves, a Visichrome Monochromator (Visitron) to acquire epifluorescence images. For vesicle fusion recording, the GZB-mCherry or PFN-mCherry overexpressing human CTLs were settled for 5 min on anti-CD3/anti-CD28/anti-LFA

Materials and Methods

antibody-coated coverslips in 0 mM $[Ca^{2+}]_{ex}$. Cells forming IS with the cover glass were imaged every 40 ms for around 15 min at the excitation wavelength of 561 nm with the laser power of 15%. After 5 s acquisition, a solution with 4, 132 or 798 mM external Ca^{2+} was applied to the cells by perfusion. For the global and local Ca^{2+} influx experiments, human CTLs were loaded with 2 μ M Fura-red AM for 30 min at 37 C. After one wash the cells were allowed to settle onto the anti-CD3/anti-CD28/anti-LFA antibody-coated coverslips in 0 mM $[Ca^{2+}]_{ex}$. Afterward, cells were imaged with the excitation of 405 nm and 488 nm and excitation of 525 nm in both TIRF mode and the EPI mode for 100 cycles. To record the Ca^{2+} signals locally at the IS and globally, cells were recorded at 110 nm penetration depth above the cover glass, the focus panel of EPI mode was adjusted to around 0.5 μ m higher above the TIRF panel. Cells were firstly recorded in the TIRF mode, then the focus automatically was moved to 0.5 μ m above TIRF mode and the cells were recorded. These two procedures were looped and repeated for 40 cycles. At cycle 10 the external Ca^{2+} was applied carefully to the cells without disturbing the sample position.

The lytic granule release was analyzed by ImageJ configured with the time series analyzer 2.0 plugin. Vesicles were marked in the region of interest (ROIs) and the average fluorescence intensity was monitored over time. For global and local Ca^{2+} analysis, a customized macro was used to create ratiometric images. The image stacks excited at both 405 and 488 nm were subtracted by the corresponding background. Afterwards, the ratiometric stack was made by dividing the image excited at 488 nm into that at 405 nm frame by frame. ROIs on cells in the ratiometric stack were monitored for average fluorescence intensity over time.

3.13. 3D live cell imaging

3.13.1. Gel preparation

Type I collagen (5.9 $\mu\text{g/ml}$) was used as 3D matrix. To make the working solution of collagen, one part of pre-chilled 10 \times PBS and 8 parts of the chilled collagen solution were mixed and the pH was carefully adjusted by adding sterile 0.1 M NaOH to 7.2-7.4.

NK cells were pre-loaded with 10 $\mu\text{g/ml}$ Hoechst 33342 in complete AIMV medium for 30 min and then recovered for at least 2 h in the incubator. Afterwards, the cells were incubated with 10 $\mu\text{g}/\mu\text{l}$ anti-integrin $\beta 1$, $\beta 2$, and $\beta 3$ antibodies or 10 $\mu\text{g}/\mu\text{l}$ LFA-1 antibody in the complete medium for 1 h. Target cells were labeled with 500 nM calcein-AM and bystander cells were stained with 500 nM CellTrace Calcein Red-Orange-AM as described before in the killing assay. 1×10^6 NK cells together with 1×10^6 targets were re-suspended in 20 μl AIMV+10% FCS medium, and afterwards mixed well with 3×10^6 (or other amounts as experimental design) bystander cells. Immediately 120 μl chilled collagen were added to the cell suspension and mixed very gently to avoid air bubbles. The capillary with filled the mixture and the capillary was kept vertically in a falcon tube to incubate at 37°C with 5% CO₂ for 1 h, during which the gelation took place. After 1 h polymerization, 1 ml complete medium was added into the falcon to let the nutrients dialyse into the polymerized gel for another hour.

3.13.2. 3D image acquisition

For 3D recordings, a Zeiss Z.1 Lightsheet setup configured with 20 \times objective (N.A. 1.0) was used with the following components: LBF 405/488/561 with no emission filter for Hoechst channel, LBF 488/561 with SBS LP 635 filter kit for the green and red channels. Images were taken at a Z step size of 1 μm and the Z volume of 60-80 μm . The cells were imaged with alternating the 405 nm, 488 nm, and 561 nm light source every 30 s over 3 h to create a time-lapse video. During the measurement, the atmosphere was set to 5% CO₂ and 37°C. The laser

power was set at 0.5% to reduce photobleaching and phototoxicity, and the exposure time was around 30 ms.

The Imaris 8.0.0 software from Bitplane was applied to analyze 3D migration of cells. Files were imported and converted into the proper format by using the Imaris format converter. The migrating NK cells were followed tracked by the software, minor corrections were applied manually afterwards.

3.14. Data analysis

Data were analyzed using Fiji (ImageJ) newest version, AxioVision (Zeiss), ZEN (Zeiss), Igor Pro (Wavemetrics), FlowJo V10 (FlowJo), GraphPad Prism 6 (GraphPad Software) and Microsoft Excel (Microsoft). All values are given as mean \pm SEM if not mentioned specifically. In case, data points were normally distributed, an unpaired two-tailed student t-test was used, and Wilcoxon signed-rank test is used for distribution-free comparison. Values are stated in the figure legends and a p-value less than 0.05 is considered significant. * P<0.05, ** P<0.01, *** P<0.001.

4. Results

To analyze the impact of environmental bystander cells and extracellular Ca^{2+} ($[\text{Ca}^{2+}]_{\text{ex}}$) on killer cell cytotoxicity, this study was carried out in two parts: 1) in 4.1, I studied the impact of bystander cells on NK/CTL-mediated cytotoxicity and analyzed molecular mechanism(s); 2) in 4.2, I examined the correlation of $[\text{Ca}^{2+}]_{\text{ex}}$ and killing efficiency of killer cells, in particular for CTL, to identify the optimal $[\text{Ca}^{2+}]_{\text{ex}}$ for CTL cytotoxicity, and I investigated the potential mechanism of the $[\text{Ca}^{2+}]_{\text{ex}}$ dependence.

4.1. Impact of bystander cells on cytotoxicity

In this part, I focus on studying whether the cytotoxicity of killer cells is influenced by the non-target bystander cells, and, if so, what is the mechanism behind the bystander-induced killing regulation. The immune cells are circulating in the circulatory system and migrating through tissues, which are packed with healthy cells. During immune surveillance, the lymphatic killer cells have to examine each object they encounter. It is reasonable to assume that with bystander cells around, the killer cell would need more time to check each cell to pinpoint the right target cells, therefore the killing efficiency would be reduced by the presence of bystander cells. Given the potential that cancer therapy would target the environment to remove the cancerous cells, it would also be beneficial to understand what role(s) bystander cells play while killer cells approaching and eliminating their target cells.

4.1.1. Non-target bystander cells enhance CTL-mediated cytotoxicity

To test killer cell mediated cytotoxicity, a fluorescence-based real-time killing assay was employed to detect the kinetics of target cell lysis [66].

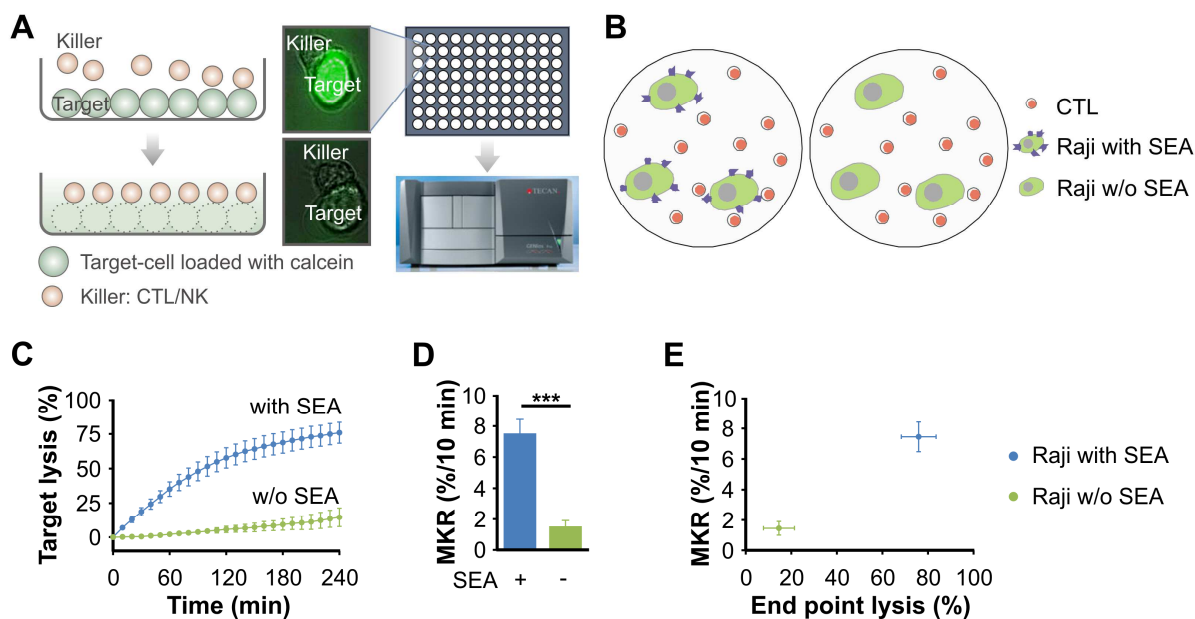


Figure 4. Kinetics of CTL-mediated cytotoxicity against SEA bearing Raji cells. (A) Sketch of the real-time killing assay. Target cells are loaded with fluorescent calcein. Due to the lysis of target cell, membrane damage results in the intracellular fluorescence decrease, which is detected at 488/525 nm by the plate reader. The sketch is modified from Kummerow *et al.* 2014 [66]. (B) Schematic cartoon of the experimental design. Raji cells pulsed with SEA (purple) were the correct target for SEA-stimulated CTLs, and Raji cells unpulsed with SEA were a negative control. (C) Killing efficiency of CTLs at the E:T ratio of 20:1. The SEA pulsed or unpulsed Raji cells were labeled with 500 nM calcein-AM, 2.5×10^4 cells/well is settled, 5×10^5 cells/well CTL were applied to the cells, the plate was recorded by the plate reader for 4 h (D) The maximal killing rate (MKR) analyzed from C, ***, $P < 0.001$. (E) Maximal killing rate as a function of the end point lysis form C, data is shown as mean \pm SEM from 4 experiments.

As is shown in Fig. 4A, target cells were loaded with calcein-AM, therefore, these cells were green by using 488 nm excitation and 525 nm emission detection. The recognition of target cells by a killer cell results in the damage of membrane integrity due to the target cell death, which was shown in Fig. 2. The loss of fluorescence in the target cells was monitored every 10 min to assess the percentage of killed target cells. Fig. 4B shows the principle of how the experiment was done. Here CTLs served the role as killer cells (effector) to eliminate the target cells, which were staphylococcus enterotoxin antigen (SEA)-pulsed Raji cells. 2.5×10^4 target cells were loaded with calcein-AM and settled onto the bottom of the plate. SEA-stimulated CTLs were afterward added on top of the target cells at an effector to target (E:T) ratio of 20:1. After 4 h, 80% of SEA-pulsed target cells were killed. In case the Raji cells were not pulsed with SEA, there no killing was observed (Fig. 4C). Thus, they can be considered non-target cells. We also analyzed the maximal killing rate (MKR) that is defined as the highest killing

rate calculated from the killing kinetics determined by the plate-reader. We found that CTLs show an MKR at around 8% per 10 min against the SEA pulsed Raji cells, and this decreases to less than 2% per 10 min while Raji cells were not SEA pulsed (Fig. 4D). To quantify the killing, the final killing efficiency was plotted against the maximal killing rate (Fig. 4E). The high maximal killing rate correlated with a high final killing efficiency, whereas the Raji cells, not pulsed with SEA, showed a low maximal killing rate as well as the final killing.

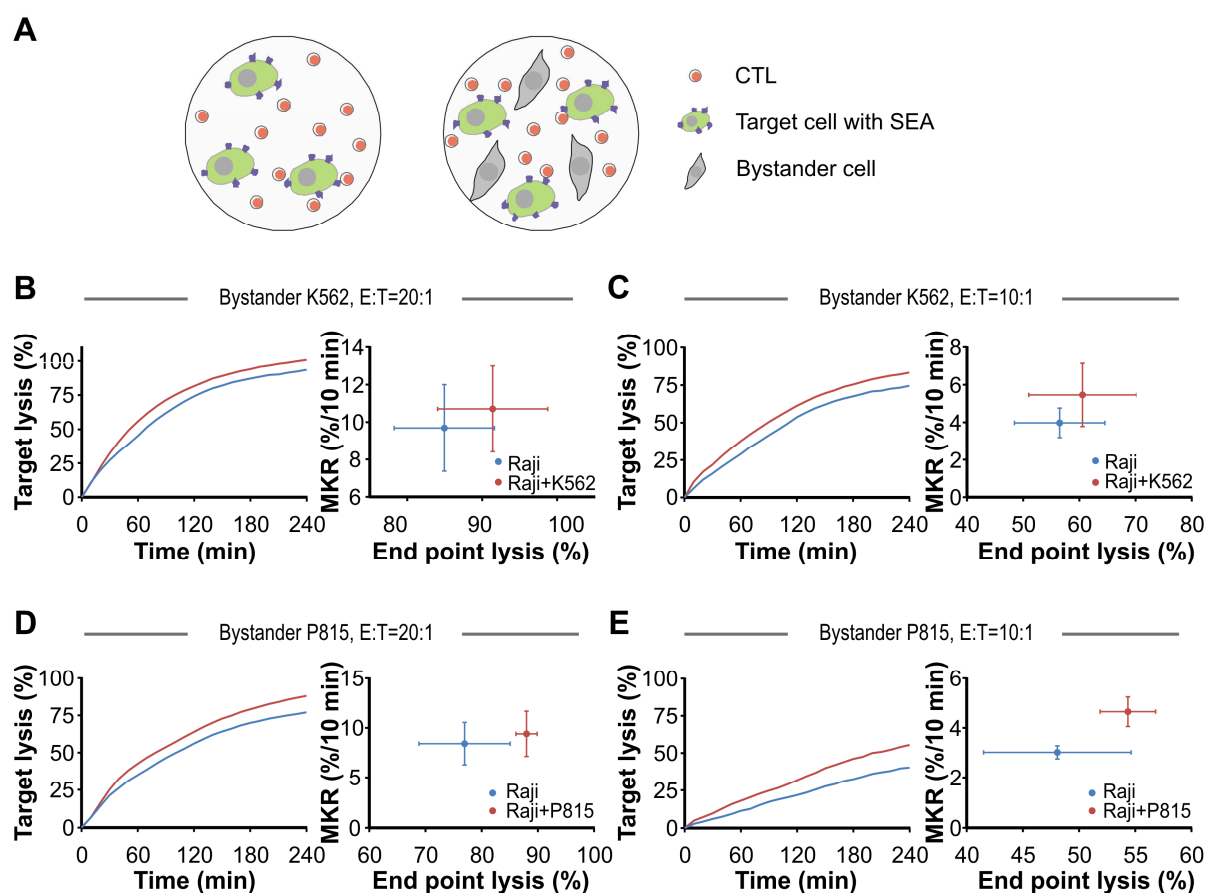


Figure 5. Bystander cells enhance CTL-mediated cytotoxicity. (A) Sketch of the experimental design. Target cells (purple) were SEA pulsed and calcein-AM loaded, non-target bystander cells were not treated and mixed with the target cells at the ratio of 1:1. (B) Characterization of the killing kinetics of human CTLs against target cells with or without bystander K562 cells from one experiment. The maximal killing rate against the end point lysis shows the mean \pm SEM of 4 independent experiments. (C) Characterization of the killing kinetics of human CTLs against target cells with or without bystander K562 cells from one experiment at the E:T ratio of 10:1. The maximal killing rate against the end point lysis shows the mean \pm SEM of 4 independent experiments. (D) Characterization of the killing kinetics of human CTLs against target cells with or without bystander P815 cells from one experiment. The maximal killing rate against the end point lysis shows the mean \pm SEM of 4 independent experiments. (E) Characterization of the killing kinetics of human CTLs against target cells with or without bystander P815 cells from one experiment at the E:T ratio of 10:1. The maximal killing rate against the end point lysis shows mean \pm SEM of 4 independent experiments.

Using this real-time killing assay I checked the initial hypothesis that the presence of non-target bystander cells would impair the killing efficiency. K562 cells, a human myelogenous leukemia line, do not express the proper MHC complex and cannot be killed by CTLs and are therefore non-target cells for the SEA-stimulated CTLs. Fig. 5A shows the experimental design. Target cells alone or together with the same amount of the non-target cells (=bystander cells) were settled on the bottom of the plate. Subsequently killer cells were applied to each well and target cell lysis was measured with the real-time killing assay. 2.5×10^4 SEA pulsed Raji cells were loaded with calcein-AM, alone or together with 2.5×10^4 K562 cells with no fluorescence labeling, and were settled onto the plate. SEA-pulsed Raji cells were successfully killed by CTLs up to 90% at the E:T ratio of 20:1 (Fig. 5B). Surprisingly, when the target cells were mixed with the same amount of bystander K562 cells, instead of impaired, the killing efficiency was increased by the presence of bystander cells. The plot of the maximal killing rate against the end point lysis showed that CTLs had a higher maximal killing rate as well as higher total target killing in the presence of bystander K562 cells. When the E:T ratio went down to 10:1, the killing efficiency of CTLs against the SEA-pulsed Raji cells was still elevated by the bystander K562 cells (Fig. 5C). To exclude that this effect is caused by K562 cells specifically, I switched the bystander K562 cells to a murine mastocytoma cell line, P815 cells. Consistent with the former observation, bystander P815 elevated the CTL killing efficiency at the E:T ratio of 20:1 (Fig. 5D) and 10:1 (Fig. 5E). This suggests that the enhancement of killing efficiency is independent of the bystander cell type.

In vivo target cells are often outnumbered by bystander cells. To mimic the *in vivo* situation, I increased the amount of bystander cells to check how the killing efficiency of CTLs was influenced (Fig. 6).

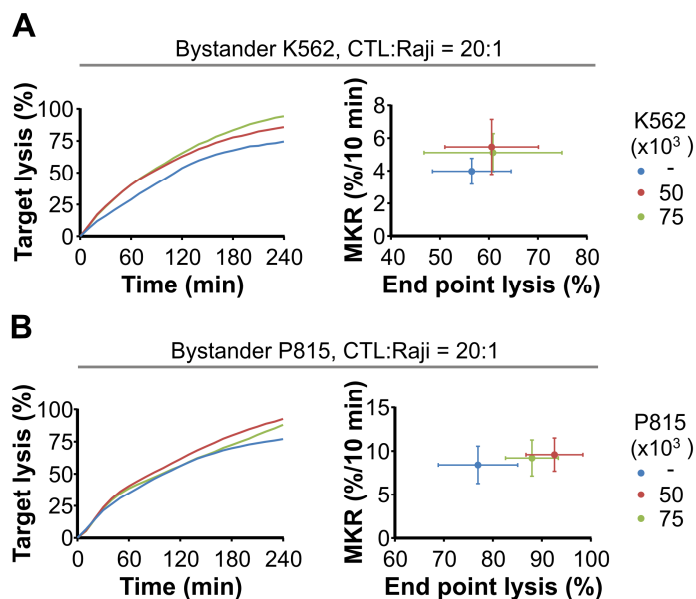


Figure 6. High numbers of bystander cells also enhance CTL-mediated killing. (A) Characterization of the killing kinetics of primary CTLs against the target cell. 2.5×10^4 cells/well Raji cells with or without 5.0×10^4 or 7.5×10^4 bystander K562 cells were settled, 5.0×10^5 CTLs were applied to the target for the 4 h killing assay. One representative killing is shown, and the maximal killing rate (MKR) against end point lysis were the mean \pm SEM of 4 independent experiments. (B) Characterization of the killing kinetics of primary CTLs against target Raji cells with or without 5.0×10^4 or 7.5×10^4 bystander P815 cells. One representative killing is shown, and the maximal killing rate against end point lysis was the mean \pm SEM of 4 independent experiments.

The killing of target cells together with a massive number of bystander cells was also significantly elevated. CTLs killed the target cells with faster kinetics and higher final killing efficiency. Both bystander K562 (Fig. 6A) or P815 (Fig. 6B) enhanced the CTL-mediated target killing by around 20%.

One question is that whether the bystander cells could be accidentally killed by CTLs and the lysis could harm the target cells. To check this, I performed the real-time killing assay with bystander cells loaded with calcein with no target cells present (Fig. 7A). As is shown in Fig. 7, the bystander K562 (Fig. 7B and D) or P815 cells (Fig. 7C and E) were not killed by CTLs, whereas the killing function of CTLs against target cells was normal either at the E:T ratio of 20:1 or 10:1.

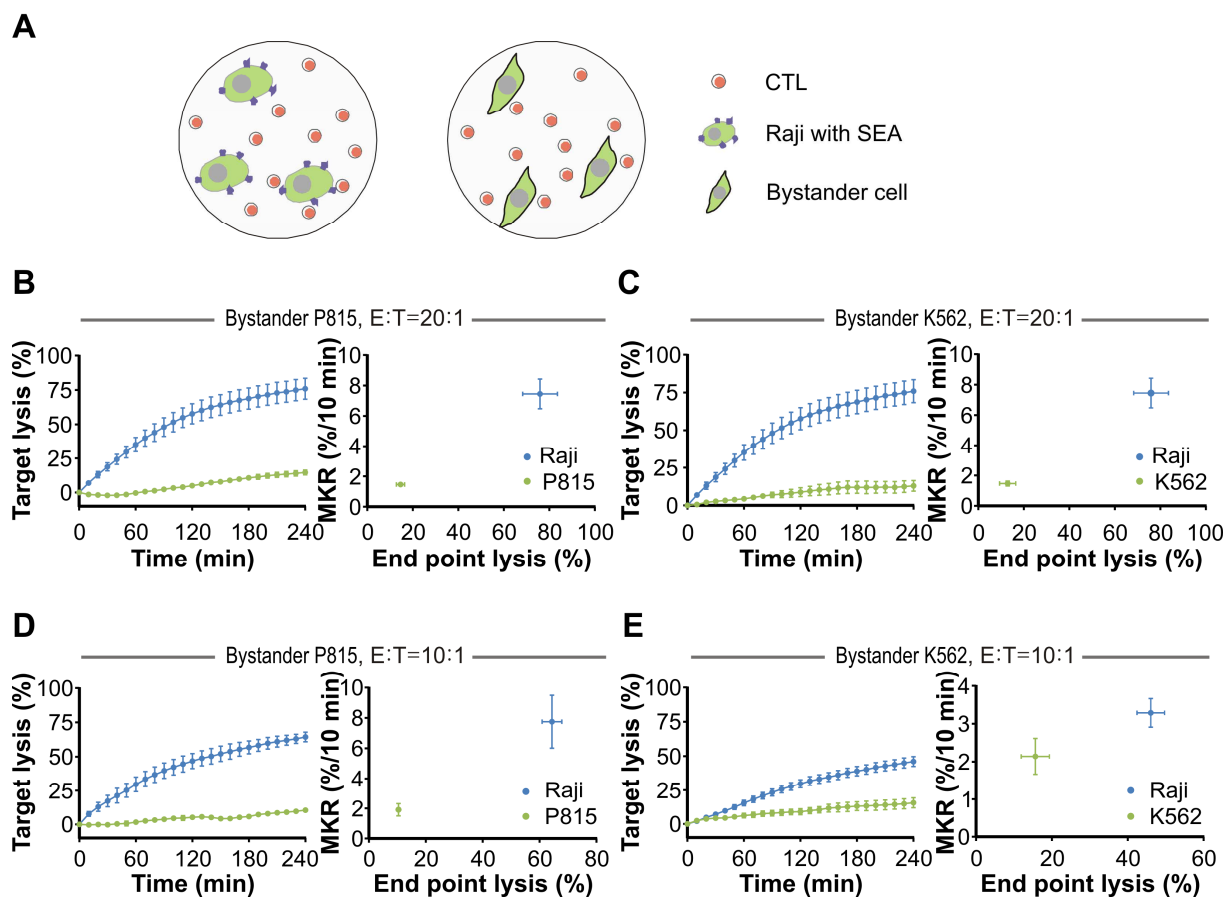


Figure 7. Bystander cells are not killed by CTLs. (A) Scheme of the experimental design. Calcein-AM loaded Raji cells alone, pulsed with SEA, or P815 or K562 cells alone were exposed to CTL. **(B)** Quantification of the killing kinetics of human CTLs against target Raji cells or bystander P815 cells. 2.5×10^4 cells/well Raji or P815 were calcein loaded, 5×10^5 cells/well CTLs were applied for a 4 h assay. **(C)** Quantification of the killing kinetics of human CTLs against target Raji cells or the bystander K562 cells following the protocol of A. **(D)** Same as B, but with E:T ratio of 10:1 **(E)** Same as C, but with E:T ratio of 10:1

Furthermore, I tested if the bystander cells are also killed by CTL when CTLs killing their target cells (Fig. 8A). The cytotoxicity of bystander cells (underlined) which is together with calcein-free Raji cells were tested by the killing assay. At an E:T ratio of 20:1, CTLs killed almost all the Raji cells (80% total lysis at 240 min), the bystander P815 cells (Fig. 8B) or the K562 cells (Fig. 8C) were not killed when they were together with the target Raji cells.

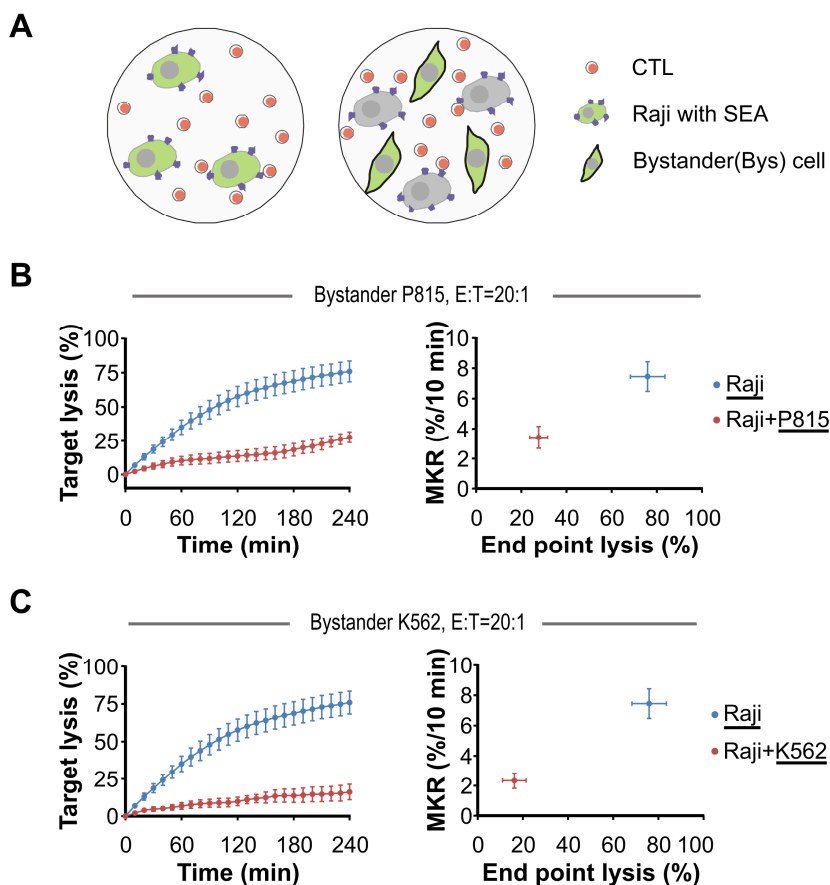


Figure 8. Bystander cell is not affected when CTLs kill their targets. (A) Scheme of the experimental design. Raji cells pulsed with SEA (purple) but not loaded with calcein were used as targets of CTLs, and the calcein loaded Raji bystander cells (without SEA) were mixed with the same amount of target cells. **(B)** Characterization of bystander P815 cell killing in the presence of the target. 2.5×10^4 cells/well SEA-Raji loaded with calcein alone or unloaded Raji together with 2.5×10^4 cells/well calcein loaded P815 cell were settled, 5×10^5 cells/well CTL were applied for the killing assay. **(C)** Characterization of bystander K562 cell killing in the presence of the target. Same as **B** but the bystander cell is K562. Cells loaded with calcein were underlined in the notation. Results are shown as mean \pm SEM of 4 independent experiments.

Raji cells that do not carry SEA molecules are not recognizable to CTLs, therefore unpulsed Raji cells should behave like other bystander cells. To test this point, I performed the real-time killing assay as shown in Fig. 9A. Calcein-AM loaded Raji cells not pulsed with SEA were mixed with the SEA pulsed Raji cells (but not loaded with SEA). I found that around 70% of the unpulsed Raji cells were killed when they were surrounded by the SEA-pulsed Raji cells (Fig. 9B). This could be explained by the possibility that the untreated Raji cells capture SEA molecules from the pulsed Raji cells. Since SEA molecules can induce CTL-mediated Raji killing at an extremely low concentration, I tested the binding efficiency of SEA on Raji cells. For this purpose, SEA conjugated with the fluorescent dye Atto-633 was used, which can be detected via FACS.

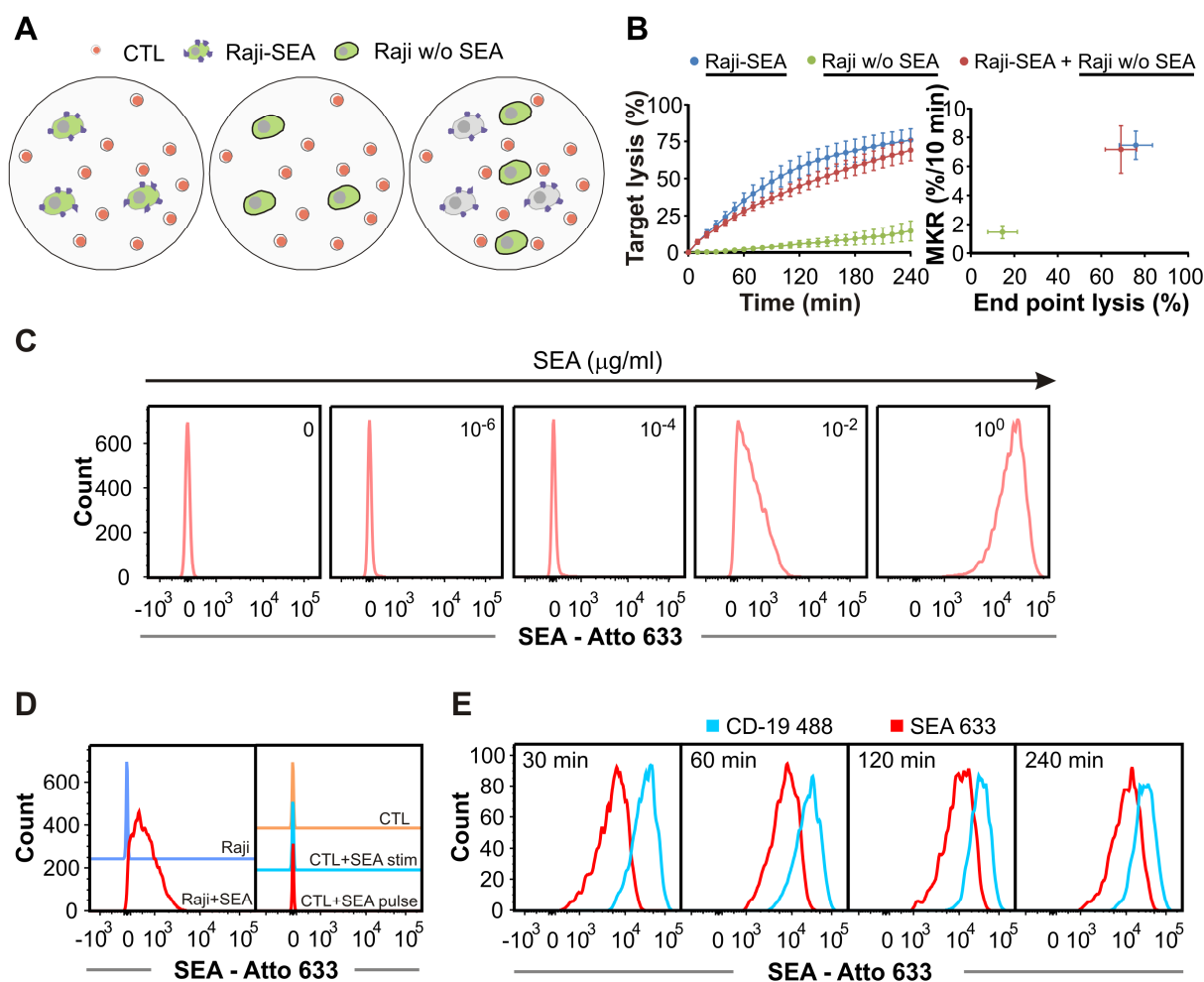


Figure 9. SEA transportation induces killing to bystander Raji cells. (A) Scheme of the experimental design. Raji cells are either pulsed with SEA (left panel) or unpulsed (middle panel). Unpulsed Raji cells were used as bystander cells mixed with SEA-pulsed target Raji cells (right panel). Green cells indicate the cells loaded with calcein. (B) Killing kinetics of SEA-loaded Raji cells and unpulsed bystander Raji cells. Raji cells were treated and plated as shown in A. Cells loaded with calcein are underlined. Results are shown as mean \pm SEM of 4 independent experiments. (C) The binding efficiency of SEA with Raji. Raji cells were pulsed with indicated concentrations of SEA-Atto-633 for 30 min. The signal of SEA was detected by FACS without cell fixation. One representative measurement out of 2 independent experiments is shown. (D) Remaining SEA on CTLs. Raji cells were pulsed with 1 μ g/ml of conjugated SEA or vehicle for 30 min (left panel). Or CTLs were either expanded from SEA stimulation (CTL+SEA stim) or incubated with 1 μ g/ml of conjugated SEA for 30 min (CTL+SEA pulse). After one wash with PBS, cells were FACSed without fixation (right panel). (E) Transport of SEA from the pulsed Raji cells to the untreated Raji cells. SEA pulsed Raji cell are mixed with Alexa488 CD19 labeled, SEA unpulsed Raji for the desired time. The signal from SEA on unpulsed Raji was detected by FACS. Results are shown as one representative measurement out of 2 independent experiments.

Raji cells did not show much SEA binding when pulsed with concentrations lower than 1×10^{-4} μ g/ml SEA. SEA binding was detected when the pulsing concentration was raised to 1×10^{-2} μ g/ml or 1 μ g/ml (Fig. 9C). Since the CTLs were SEA-stimulated, I checked if there is any SEA molecules remaining on CTLs to induce the unpulsed Raji cell death. In Fig. 9D, Raji cells efficiently bound with SEA after 30 min pulse, while CTLs do not show SEA signal. This

is irrelevant with whether CTLs are pulsed transiently or incubated with SEA for 5 days. However, when the unpulsed portion of Raji (CD19-488labeled, blue) was co-incubated with SEA pulsed Raji cell portion (Atto 633 positive), the unpulsed portion gain SEA molecules from the pulsed Raji cells with time going on (Fig. 9E). These results confirm that SEA can be transferred from SEA-pulsed Raji cells to unpulsed Raji cells and induce killing of the originally unpulsed Raji cells.

4.1.2. Bystander cells enhance NK cell-mediated target killing

Apart from CTLs, NK cells are the most relevant cytotoxic cells involved in the elimination of infected cells and carcinoma. To access if bystander cells have the same impact on NK cell-mediated cytotoxicity, I performed real-time killing assays to test if NK cell killing against one of their commonly used targets, K562 cell [67], is influenced by the presence of bystander cells.

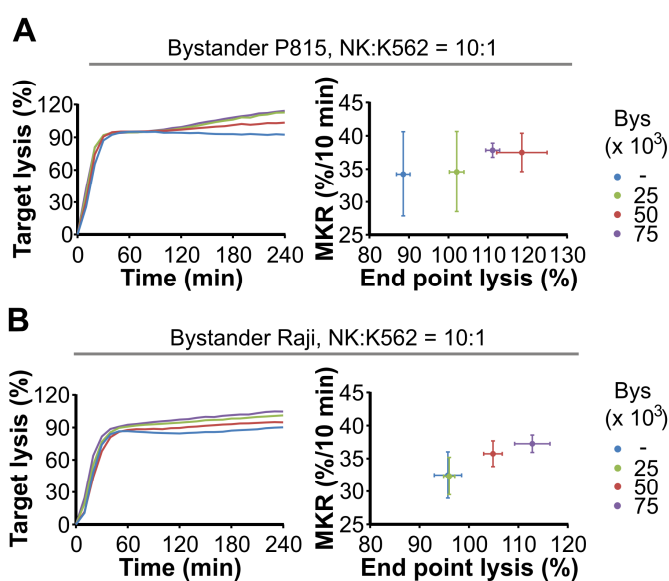


Figure 10. Bystander cells slightly enhance NK cell-mediated cytotoxicity. (A) Quantification of killing kinetics of primary NK cells against K562 cells with or without bystander P815 cells. One representative killing is shown, and the maximal killing rate was plotted against end point lysis. Results are shown as mean \pm SEM from 4 independent experiments. (B) Quantification of the killing kinetics of primary NK cells against target cells with or without bystander Raji cells. One representative killing is shown, and the maximal killing rate was plotted against end point lysis. Results are shown as mean \pm SEM from 4 independent experiments.

At an E:T ratio of 10:1, NK cells killed their target with a high efficiency (Fig. 10A, B, blue curve and dots). The presence of bystander P815 cells (Fig. 10A) or Raji cells (Fig. 10B) slightly enhanced the NK killing efficiency.

The very high efficiency of target cell killing by NK cells at a E:T ratio of 10:1 might mask bystander effects. Therefore I reduced the E:T ratio in Fig. 11 to values between 5:1 and 1:1. I observed that bystander P815 cells enhanced NK cell-mediated K562 killing even further at low ratios, especially at 1:1, compared to 5:1 (Fig. 11A, B and C).

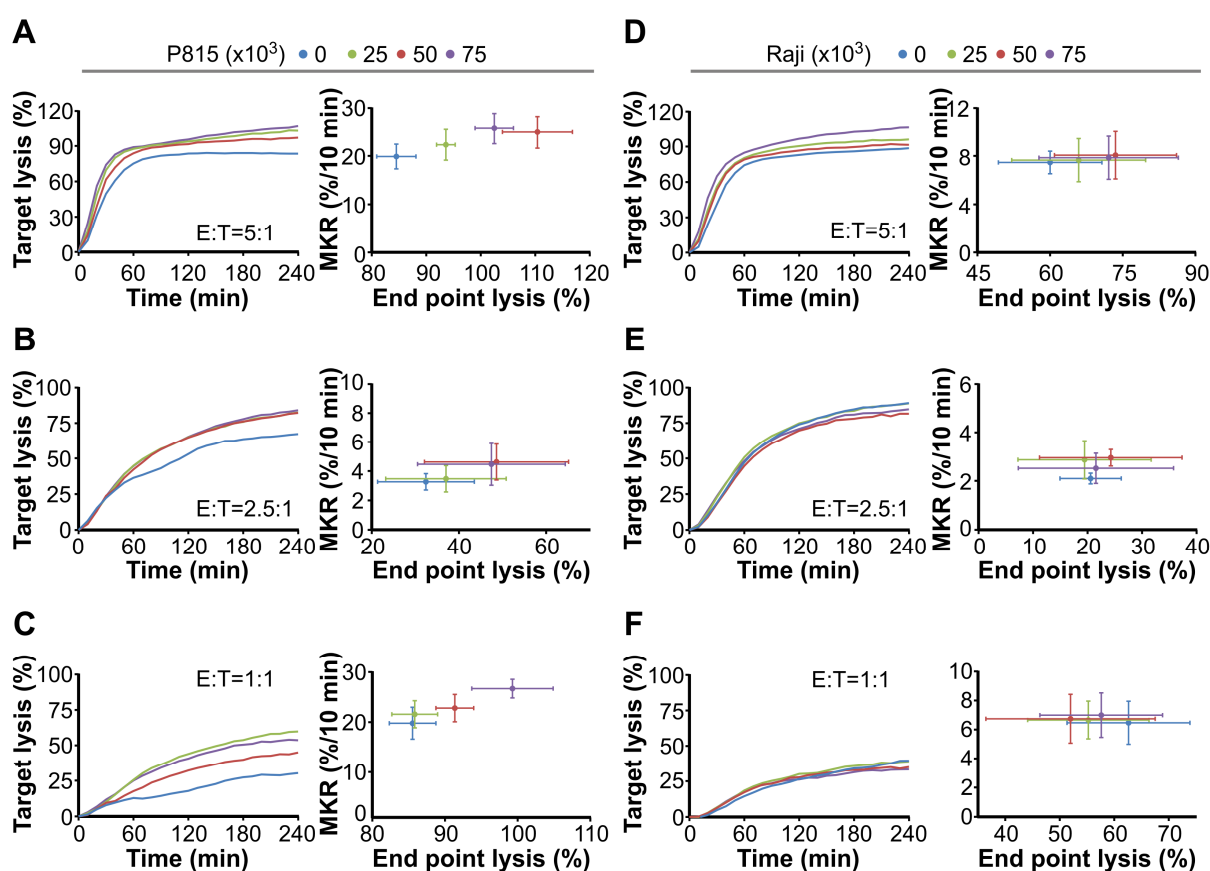


Figure 11. Bystander cells enhance NK-mediated cytotoxicity at lower E:T ratios. Quantification of the killing kinetics of NK cell against K562 cells with or without bystander P815 cells at the E:T ratio of 5:1 (A), 2.5:1 (B), and 1:1 (C). 2.5×10^4 cells/well K562 alone (blue) or together with 2.5×10^4 cells/well P815 (green), 5×10^4 cells/well P815 (red), 7.5×10^4 cells/well P815 (purple) were used and the desired amount of NK was added for each killing assay. The killing efficiency is shown as one representative experiment and the maximal killing rate as a function of the end point-lysis plotting is shown as mean \pm SEM of 4 independent experiments. NK cells kill the target cells in the presence of bystander Raji cells at the E:T ratio of 5:1 (D), 2.5:1 (E), and 1:1 (F). 2.5×10^4 cells/well K562 alone (blue) or together with 2.5×10^4 cells/well Raji (green), 5×10^4 cells/well Raji (red), 7.5×10^4 cells/well Raji (purple) were used and the desired amount of NK was added for killing assay. Killing curves are from one representative experiment and the maximal killing rate against the end point-lysis plotting is shown as mean \pm SEM of 4 independent experiments.

Differently, the bystander Raji cells (Fig. 11D) did not increase NK cell-mediated K562 killing at low ratios (2.5:1 and 1:1) (Fig. 11E and F), although bystander Raji cells could enhance NK cell-mediated K562 killing to a similar level as P815 cells at the E:T ratio of 5:1 (Fig. 11D).

Given that the SEA-stimulated CD8⁺ cells contain several subpopulations and not all of the subpopulations are capable of killing (*e.g.* naïve cells not), killing at lower E:T ratio was tested only on NKs, although CTLs show the same phenomenon at the E:T ratio of 10:1.

Similarly as for CTL, I also tested if NK cells can kill the bystander cells. As shown in Fig. 12, bystander P815 cells and Raji cells were not killed by NK cells, neither alone (Fig. 12A and C, green, Fig. 12B and D, green) nor with target cells (Fig. 12, red curve and dot).

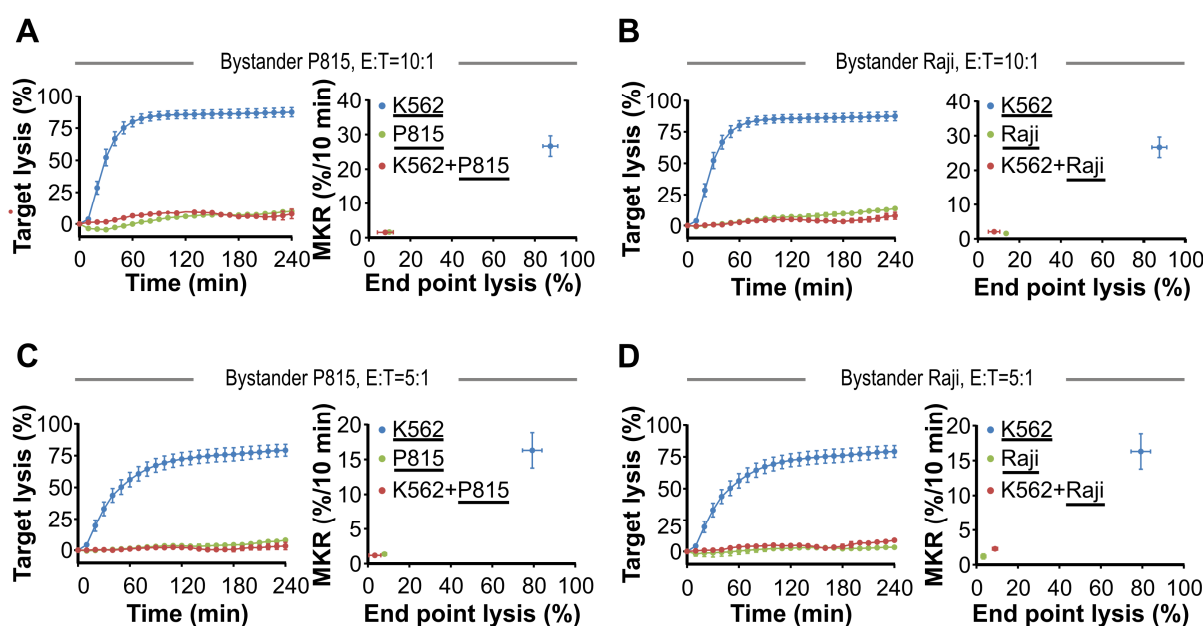


Figure 12. Bystander cells are not affected when NK cells kill the target. (A, B) Killing kinetics of NK cells at the E:T ratio of 10:1. Underlined cells were loaded with calcein and were monitored for cell lysis. (C, D) Killing kinetics of NK cells at the E:T ratio of 5:1. Underlined cells were loaded with calcein and were monitored for cell lysis. Results are always shown as mean \pm SEM of 4 independent experiments.

Up to this point, bystander cells used to analyze effects on the killing of target cell by CTL and NK cells were all neoplastic cells, which does not reflect the reality *in vivo*. To test if the non-neoplastic bystander cells have the same effect on killing, freshly isolated primary human cells were applied as bystander cells. Primary human monocytes and PBMCs without NK cells (=LO) were tested as bystander cells. As a control we monitored again P815 cells as bystanders which enhanced the NK cell-mediated killing as usual (Fig. 13A). The addition of bystander monocytes had qualitatively and quantitatively the same effect to enhance NK killing as P815. Although it was a bit weaker, NK cell depleted PBMCs (=LO) showed the same tendency to enhance the killing efficiency. Furthermore, I also tested the bystander effect with the adherent, non-neoplastic HUVEC cells as the bystander cells which showed the same effect (Fig. 13B).

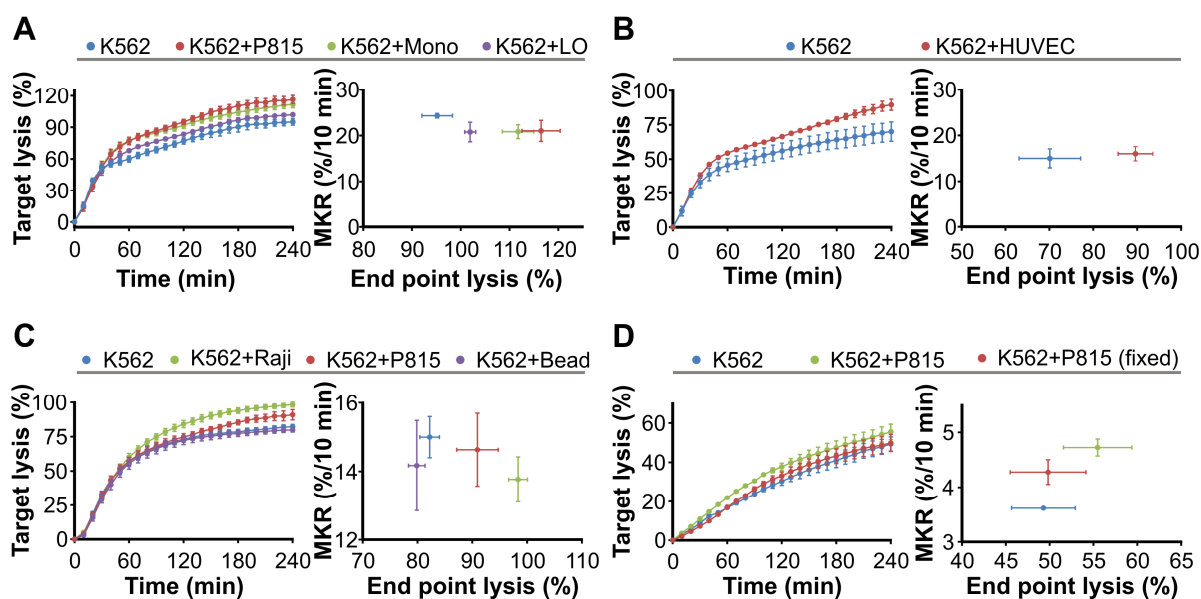


Figure 13. Non-neoplastic primary human bystander cells enhance NK killing while beads or fixed cells do not. (A) Quantification of the killing kinetics of NK cells against K562 cells with or without bystander monocytes or PBMCs without NK cells (LO). 2.5×10^4 cells/well K562 alone (blue) or together with 7.5×10^4 cells/well P815 (red), 7.5×10^4 cells/well monocytes (green) or 7.5×10^4 cells/well PBMCs (purple) were settled in the wells; 2.5×10^5 cells/well NK cells were applied for killing (B) Quantification of the killing kinetics of NK cells with or without bystander adherent HUVEC cells. 2.5×10^4 cells/well K562 alone (blue) or together with 7.5×10^4 cells/well HUVEC (red) were used for the killing assay (C) Characterization of the killing kinetics of NK cell with or without beads. 2.5×10^4 cells/well K562 alone (blue) or together with 7.5×10^4 cells/well beads (purple) or the control bystander Raji (green) and P815 (red) were applied for killing assay. (D) Characterization of the killing kinetics of NK cell with or without fixed bystander cells. 2.5×10^4 cells/well K562 alone (blue) or together with 7.5×10^4 cells/well fixed P815 (red) or the control bystander P815 (green) were applied for killing assay. Results are shown as mean \pm SEM from 4 independent experiments.

Large numbers of bystander cells of course occupy a lot of otherwise open space between targets. To exclude the possibility that the enhancement of killing by bystander cells resulted from the reduction of space to be searched, cell-sized polystyrene beads with similar size than bystander cells were used to mimic the bystander cells. As shown in Fig. 13C, beads failed to elevate the killing efficiency and the kinetics also showed that bystander beads had no effect on NK killing. Since beads are rigid spheres, I also tested if with fixed bystander cells, which have denatured surface proteins, could mimic the bystander effect. As shown in Fig. 13D, the fixed bystander cells did not elevate the killing efficiency of the NK cells, while the normal bystander cells enhanced the killing efficiency by around 20% as usually.

In summary, primary human bystander cells and neoplastic cell lines enhance CTL and NK cell-mediated cytotoxicity against target cells. This effect is only caused by living cells and cannot be mimicked by cell-sized beads or dead cells proving that the bystander effect is not mediated by a mere space occupancy of the bystander cells.

4.1.3. Bystander cell enhanced killing is not generally caused by the conditioned medium

An obviously important question is how the bystander effect is mediated. I thus designed experiments to test the underlying mechanisms how bystander cells enhance killer cell-mediated cytotoxicity. Since activated killer cells secrete numerous soluble factors into the environment and potentially enhance the immune activity, I checked if the enhancement of killing efficiency was introduced by the soluble factors in the conditioned medium. Target cells were respectively co-incubated with killer cell either with or without bystander cells and the supernatant was harvested afterwards to be used in the real-time killing assay (=conditioned medium). As shown in Fig. 14, NK cells killed the target with lower efficiency and slower kinetics in conditioned medium, when compared to the killing in fresh medium.

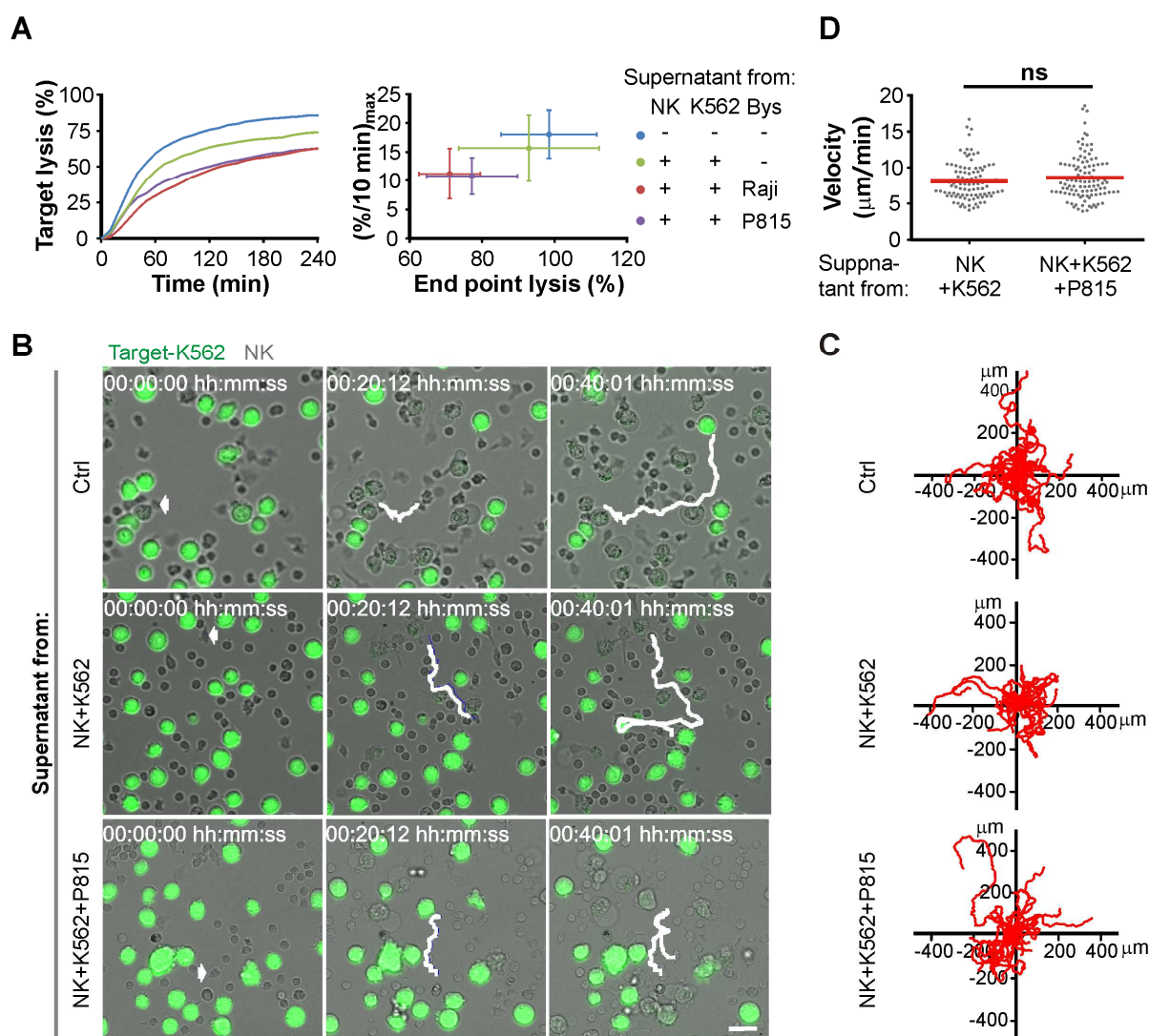


Figure 14 Supernatant of the killing with bystander cells does not enhance the NK cell killing and migration velocity. (A) Characterization of NK killing in the supernatant from the mixture of killing. Target cells alone or together with bystander cells as usual killing assay were incubated with NK cells for 4 h. The supernatant afterward was harvested and applied to the freshly settled target and NK cell. One representative killing curve is shown and the quantitative data of 4 independent experiments is shown as mean \pm SEM. (B) Representative figures of a migrating NK cell at different time points within the supernatant as in A. The supernatant was harvested from the killing system as in A, NK cells were monitored with target cell alone or together with P815 cell every 20 s for 2 h at 37°C. Green labels the target cells and the unlabeled are NK cells. White arrows indicate the starting point of the NK cell and the solid white line covers the footprint of the migrated NK cell. Scale bar=20 μm . (C) Trajectories of the NK cells migrating in the fresh medium or supernatant harvested from NK with target or NK with target and bystander cells. (D) Migration velocity of NK cells in the supernatant.

It was reduced by around 20% in the conditioned medium from the killer-target-bystander mixture compared to the conditioned medium from only killer and target cells, the latter of which was not changed significantly compared to fresh medium (around 5% lower) medium (Fig. 14A). Since killer cell migration is an important parameter influencing serial killing of target cells, I designed experiments to test if the conditioned medium influences this parameter.

Time-lapse imaging was applied to visualize NK cell migration. Target cells were labeled with calcein and settled on the well bottom and non-labeled NK cells were added into the well. NK cell migration was recorded every 20 s for 1 h. The representative pictures also show that NK cells migrated similarly in the different media. In the fresh medium or in killer-target-bystander or killer-target conditioned medium, NK cells migration persistence was also similar (Fig. 14B, C). In addition, similar patterns of the trajectories were observed (Fig. 14C). The velocity of NK cells showed no significant differences between in the killer-target-bystander conditioned medium or in the killer and target conditioned medium: it was always around 8 $\mu\text{m}/\text{min}$ (Fig. 14D). These results suggest that the bystander cell enhanced killer cell mediated cytotoxicity is not caused by a global change of soluble factors, for instances cytokines, released into the supernatant.

4.1.4. Bystander cells do not influence NK cell degranulation

Exocytosis of LG towards the target cell is of central importance for NK/CTL cell-mediated killing. To test if the degranulation was affected by bystander cells, a degranulation assay was employed to detect the exocytosis of LG by killer cells in the presence or absence of bystander cell (Fig. 15). CD107a is a marker on the cell membrane to indicate LG fusion. When LGs fuse, CD107a is exposed to the fluorescence-conjugated antibody, therefore, the LG fusion level could be detected by flow cytometer (FACS). NK cells showed no degranulation without target cell stimulation as expected. In addition, bystander cells alone did not induce NK degranulation, which is consistent with the real-time killing measurement. In the presence of target cells, CD107a fluorescence and thus NK degranulation was significantly increased to around 28% which was however not change by the addition of bystander cells (Fig. 15A). The corresponding quantification and statistic confirm that bystander cells do not influence NK cell degranulation (Fig. 15B).

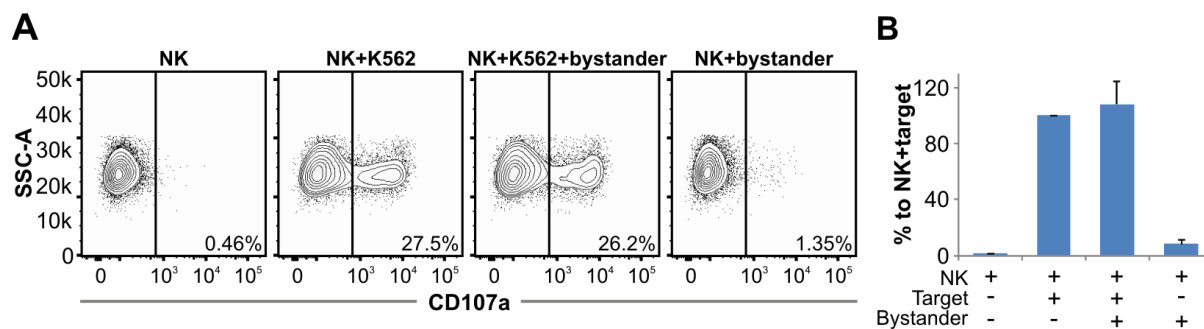


Figure 15. Bystander cells do not influence NK cell degranulation. (A) Degranulation assay of NK cells with or without target and bystander cells present. Results are shown as one representative experiment out of five. 2.5×10^4 target cells were used to stimulate 2.5×10^5 killer cells, bystander P815 cells were added at the amount of 7.5×10^4 for each condition. (B) Quantitative analysis of degranulation assay, each column was normalized to the value of killer cells with target cells present. Data are shown as mean \pm SEM from five independent experiments. Figure is provided by Renping Zhao and adapted from Zhou *et al.* 2017 [68].

4.1.5. Bystander cells enhance NK cell migration

As already mentioned above, migration of killer cells is a critical aspect that affects the cytotoxicity [69], [70]. While the media (fresh or conditioned) had no influence on overall migration (see 4.1.3), bystander cells themselves could of course influence killer cell migration independent of global concentration changes of any released substance. To check if bystander cells had any impact on killer cell migration, I used the time-lapse imaging to track the NK cell migration with or without the bystander cells present. As shown in Fig. 16A, NK cells migrated at a velocity of around $6 \mu\text{m}/\text{min}$ with only target cells but no bystander cells present. Intriguingly, the migration velocity of the NK cells was raised by around 50% to around $9 \mu\text{m}/\text{min}$ by the bystander cells. Migration persistence, defined as the displacement between the start and end point divided by the total length of the trajectory, was also changed in case bystander cells were presented. Without bystander cells, the persistence of the NK cell migration was around 0.4, and it was significantly elevated to around 0.5 by the addition of bystander P815 cells (Fig. 16B). Furthermore, I analyzed the distribution of the migration step size, which is the distance moved between two sequential frames. With only target cells present, around 50% of the NK cells moved with a step size of 0-2 μm , 30% of the cells moved 2-4 μm per step and around 18% percent of the cells migrated with a step size of 4-6 μm .

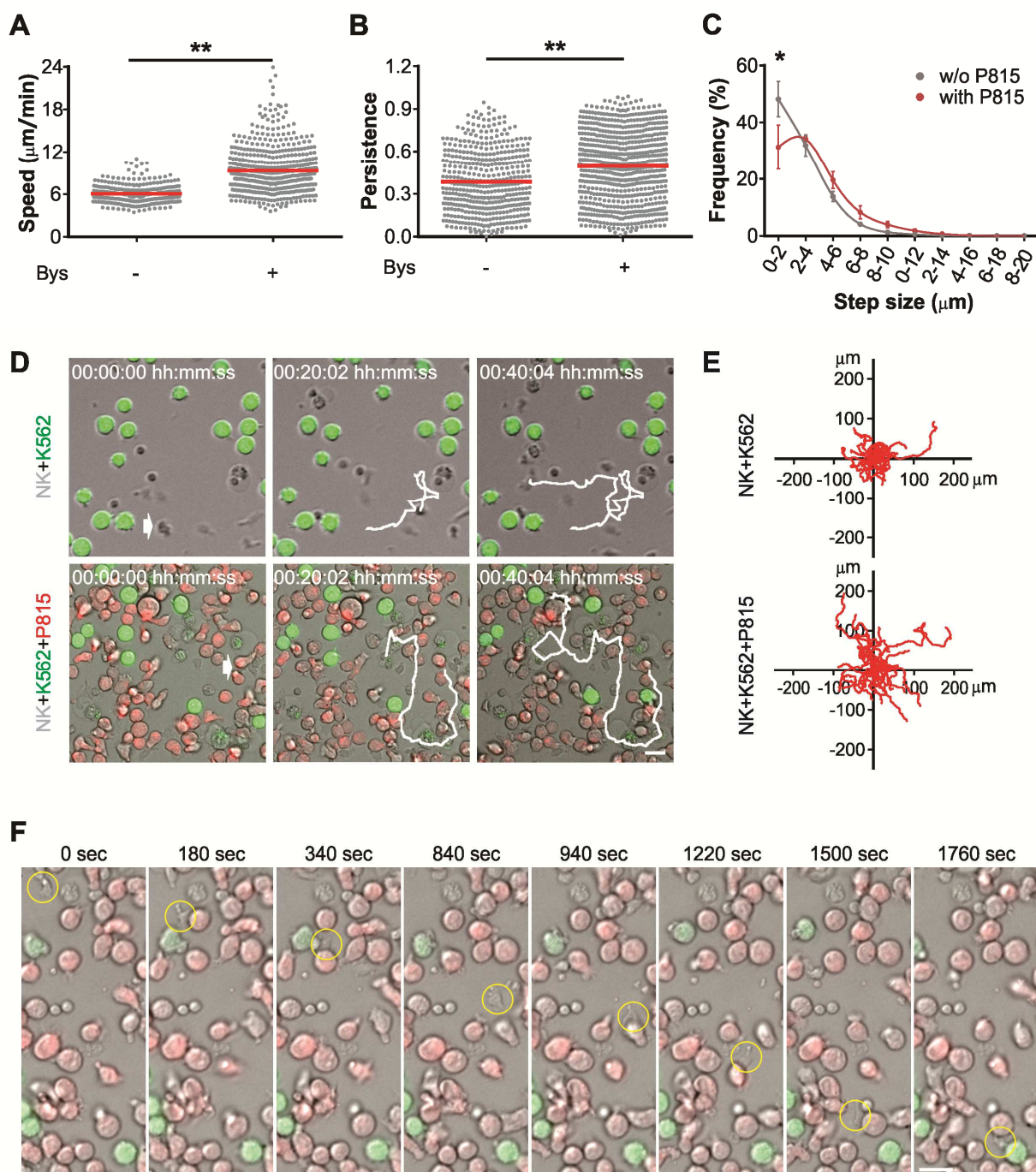


Figure 16. Bystander cells enhance NK cell migration. (A) Quantitative analysis of the migration velocity of the NK cells with 2.5×10^4 target cells in the presence or absence of 7.5×10^4 bystander cells. (B) Persistence analysis of the NK cells calculated from A. (C) Distribution of the migration step size of the NK cells analyzed from A. (D) Representative images of the cells from A. White arrows show the starting point of the cells and the white lines show the footprint of the migration trajectory. (E) Trajectories of the NK cells in the absence and presence of bystander cells. (F) Representative images of one migrating NK cell directed by bystander cells, the yellow circle indicates the position of the NK at each time point, scale bar is 20 μm . *, $p < 0.05$, **, $p < 0.01$. Part A, B, C, E and F are from Zhou *et al.* 2017 [68].

However, the step size distribution was changed dramatically by the addition of bystander cells.

Only around 30% of the NK cells migrated with a 0-2 μm step size, and the percentage of cells

migrating with larger step sizes were increased (Fig. 16C). NK cells migrate in a random fashion without ‘knowing’ the destination in the open space. In the presence of bystander cells NK cell displacement was larger than in the absence of bystanders (Fig. 16D). With bystander cells present, NK cells migrated in a more directed fashion, and a longer path (Fig. 16D, E). Looking at many individual cells, there is a tendency that NK cell migration tends to be directed by several individual bystander P815 cells from one to the other until it finally reaches a target (compare example in Fig. 16F). Together, these data suggest that bystander cells accelerate NK cells locally in their vicinity, thereby allowing a faster and potentially more persistent migration. This hypothesis is tested further by a mathematical model and additional experiments in 4.1.6.

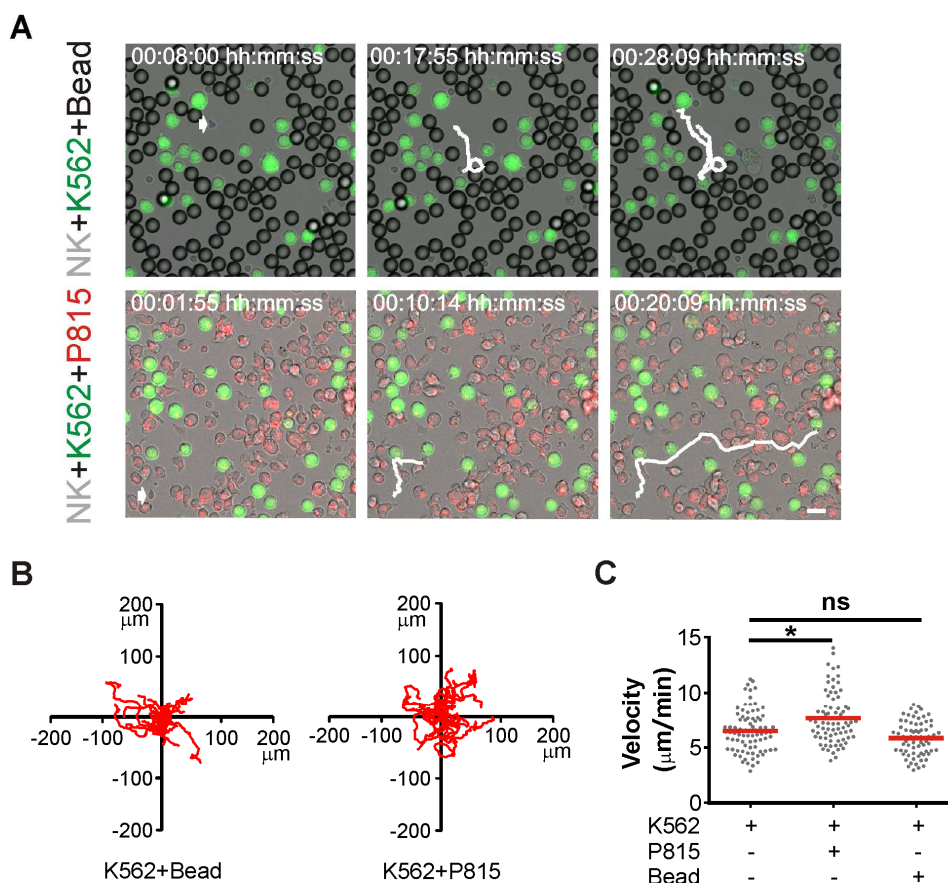


Figure 17. Nonfunctional bystander spheres do not enhance the NK cell migration. (A) Representative figures of a migrating NK cell at different time points with the presence of bystander beads or bystander cells. White line indicates the footprint of an NK cell. **(B)** Trajectories of the NK cells migrating with the cell-sized spheres or the bystander cells. **(C)** The velocity of the NK cell migration either with the spheres or the same amount of bystander cells. *, $P < 0.05$; Scale bars are 20 μm .

To confirm that this acceleration is caused by the living bystander cells and not by any space-occupying obstacle, I also analyzed NK migration with the addition of cell-sized polystyrene beads, which physically mimicked the space occupancy by bystander cells. As shown in Fig. 17A and B, NK cell displacement is reduced in the presence of the beads compared to bystander cells during the same time. The trajectories show that the presence of non-functional beads did not mimic the effect of bystander cells on NK cell migration. Furthermore, NK cells migrated with a higher velocity with bystander cells present compared to NK cell migration in the presence of beads or target cells alone (Fig. 17C). Taken together, I conclude that bystander cells, but not the beads, significantly facilitate the migration velocity, displacement and the persistence of NK cells.

4.1.6. Increase in local motility of killer cells by bystanders decreases the search time to locate target cells.

While bystander cells significantly facilitate the migration of killer cells, it is not clear that the enhanced migration velocity and persistence should necessarily lead to a better killing efficiency. This hypothesis can be tested with a mathematical model. By collaborating with physicists, we developed a random search model in a two-dimensional environment to simulate this scenario (Data of this session 4.1.6 is provided by Karsten Schwarz, Matthieu Mangeat, Mohamed Hamed, Volkhard Helms, and Heiko Rieger, and the text is adapted from Zhou *et al.* 2017[68]).

Mathematical model simulation: At first, the question whether a behavior like it is shown in Fig. 11 could be the result of a simple volume exclusion effect by passive obstacles was studied. For doing so, the event-driven kinetic Monte-Carlo Algorithms [71], [72] called GFRD or FPKMC (continuous in space and time) for the simulation of diffusive search processes in the presence of circular obstacles were performed. Fig. 18A sketches the

simulation setup in a unit square for the case of immobile circular obstacles of radius r_{obs} and mobile killers and targets of radii r_{killer} and r_{target} . Furthermore, the case of mobile obstacles was also studied.

In all cases, two competing effects which occur in the presence of obstacles were observed. On one hand, there is a reduced volume to be searched in and once a searcher is close to a target, the obstacles behave like traps, which decrease the likelihood of separating again without having found before. On the other hand, on larger time- and length-scales, the diffusion of the searchers is slowed down to a smaller effective diffusion constant. For a higher target density, as it is in the experiments and simulations, the first effect wins this competition. Hence it is possible to reduce $t_{1/2}$ in our simulations by adding a small number of obstacles. But as soon as the target density becomes smaller, the second effects dominates and no parameter sets were found to create curves like Fig. 11, where a high density of bystanders is favorable for all times. Exemplarily, Fig. 18B showed the ratio of $N_t(t)/N_t(0)$ for the scenario of immobile obstacles. Especially for larger time (*i.e.* lower densities of targets), the presence of obstacles is inefficient. Fig. 18C shows $t_{1/2}$ as a function of the obstacle number N_b for different radii r_{obs} .

The model data indicate: Bystanders do not behave like passive obstacles. In consequence, bystanders were added to the model. For numerical reasons, now two lattices based reaction-diffusion models with discrete time steps Δt in two dimensions, including four different types of particles- N_k killers, N_t targets, N_o obstacles and N_b bystanders were considered. The simulations take place on a 60×60 square lattice (and its dual lattice, see discrete Model 2) with periodic boundary conditions and simple exclusion (no/one particle per lattice side). The lattice size was checked to be large enough to avoid finite-size effects at particle densities $(N_k+N_t+N_o+N_b)/(60 \times 60)$.

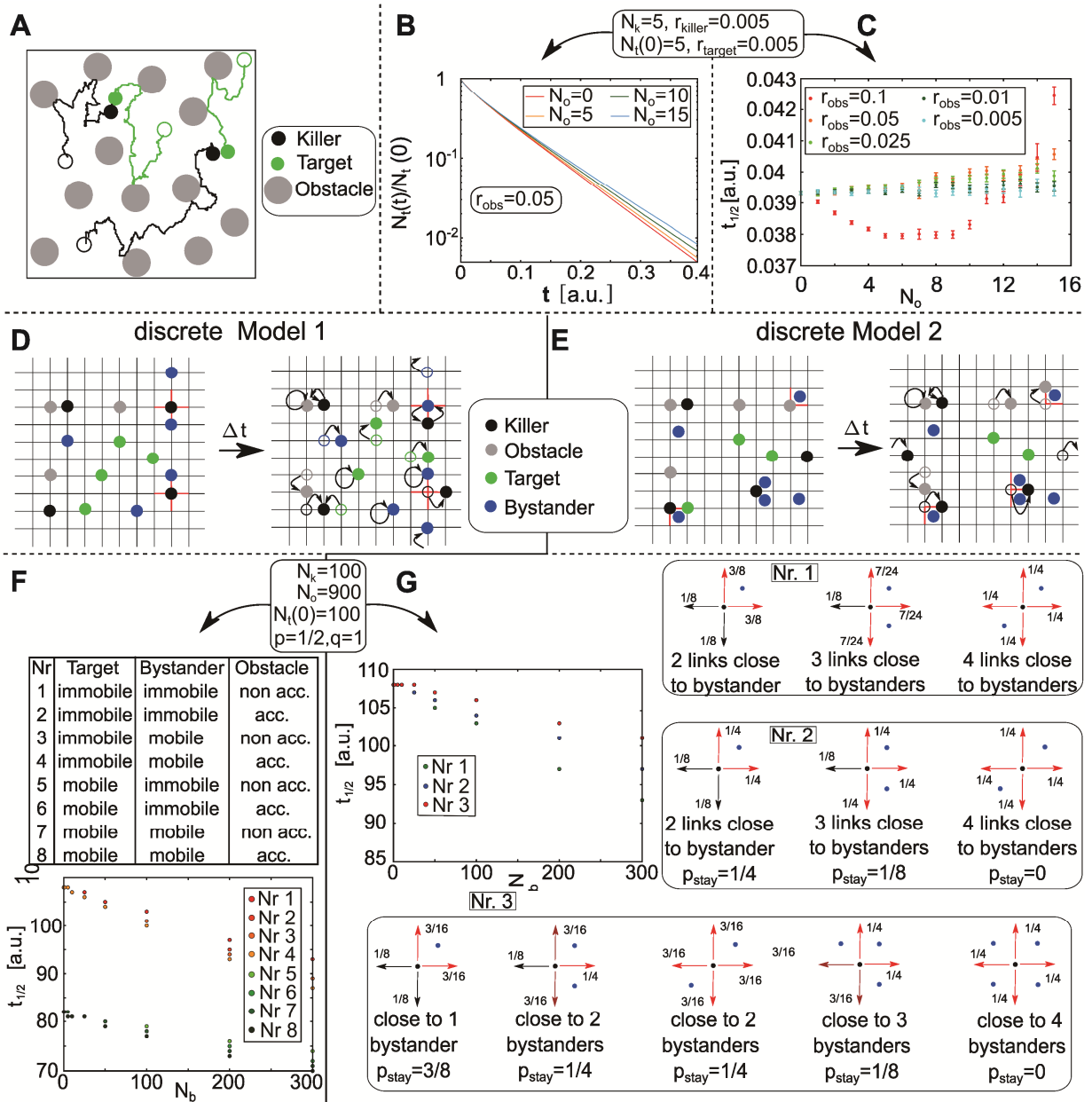


Figure 18. Mathematical model simulation. (A) Sketch of the simulation setup without bystanders in continuous space and time: circular killers (black) and targets (green) of radii r_{killer} and r_{target} diffuse in the presence of immobile obstacles (gray) of radius r_o . A target is eliminated at the time it touches a killer for the first time. (B) Log-Plot of the ratio of survived targets as a function of time for $N_k=5$ killers, $N_t(0)=5$ targets and different numbers of obstacles. (C) The half time $t_{1/2}$ as a function of N_o for different values of r_o for the same number of killers and targets. (D) Sketch of the stochastic process for the discrete Model 1: Killers, targets, obstacles and bystander are placed on the same periodic lattice. With probability $p/4$ a particle will hop to its neighbor spot. In the neighborhood of obstacles the hopping probability is increased to $q/4$ (indicated in red). (E) Sketch of the stochastic process for the discrete Model 2: Killers, targets, and obstacles are placed on the same periodic lattice, immobile bystanders on the corresponding dual lattice. With probability $p/4$ a particle will hop to its neighbor spot if there is no other particle. In the neighborhood of obstacles the hopping probability is increased (indicated in red). (F) Half time $t_{1/2}$ as a function of the number of bystanders for different update scenarios in Model 1. (G) Half time $t_{1/2}$ as a function of the number of bystanders for different update scenarios in Model 2 (provided by Karsten Schwarz and Heiko Rieger, adapted from Zhou *et al.* 2017 [68]).

In both investigated models, the searchers, targets, and obstacles (representing inactive killers) share the same lattice. In the first model (discrete Model 1) the bystanders were also placed on

this lattice. In the second model (discrete Model 2), the bystanders are always immobile and placed on the dual lattice. A sketch of the setup for both models is shown in Fig. 18D and E. In both models a target is found by a killer when they are located at the same lattice side at the same time. The killer goes on with its movement, the target disappears. The normal hopping probability of a mobile particle is given by $p/4$ (usually $p=1/2$) in each of the four directions. A special role is always given to the bystanders, as they increase the hopping probability in their nearest neighborhood. Several different scenarios have been investigated for the increased hopping rates of the stochastic processes in both models.

Model 1: Particles (killer and obstacles, the latter representing inactive killers) which are accelerated by bystanders increase their hopping rate to an allowed direction to $q/4$ (with $q>p$).

Fig. 18F shows the half time $t_{1/2}$ for different setups as a function of the number of bystanders.

Model 2: Targets and bystanders are immobile in this model. Killers and obstacles (*i.e.* inactive killers) are accelerated by bystanders. Several different scenarios for the acceleration have been investigated. Fig. 18G explains them and shows the half time $t_{1/2}$ for these scenarios as a function of the number of bystanders. In both models, three update schedules for the particles have been applied: a sequentially ordered update, a sequential update with stochastic order and a totally randomized choice of particles, they all deliver the same results. The model was set up to mimic the experimental conditions as best as possible: as in the experiment, the cells move randomly in a confined two-dimensional area. For the densities realized in the experimental setups described in this method, the obstacles form an “archipelago” [73] that leads to an effective, distance dependent diffusion constant that is much smaller than the one of the freely diffusing particle. Since a decreasing diffusion constant implies an increasing search time for mobile or immobile targets, the bystanders cannot merely be obstacles for the killer cells but must have an efficiency-enhancing effect. Therefore these conditions were modeled.

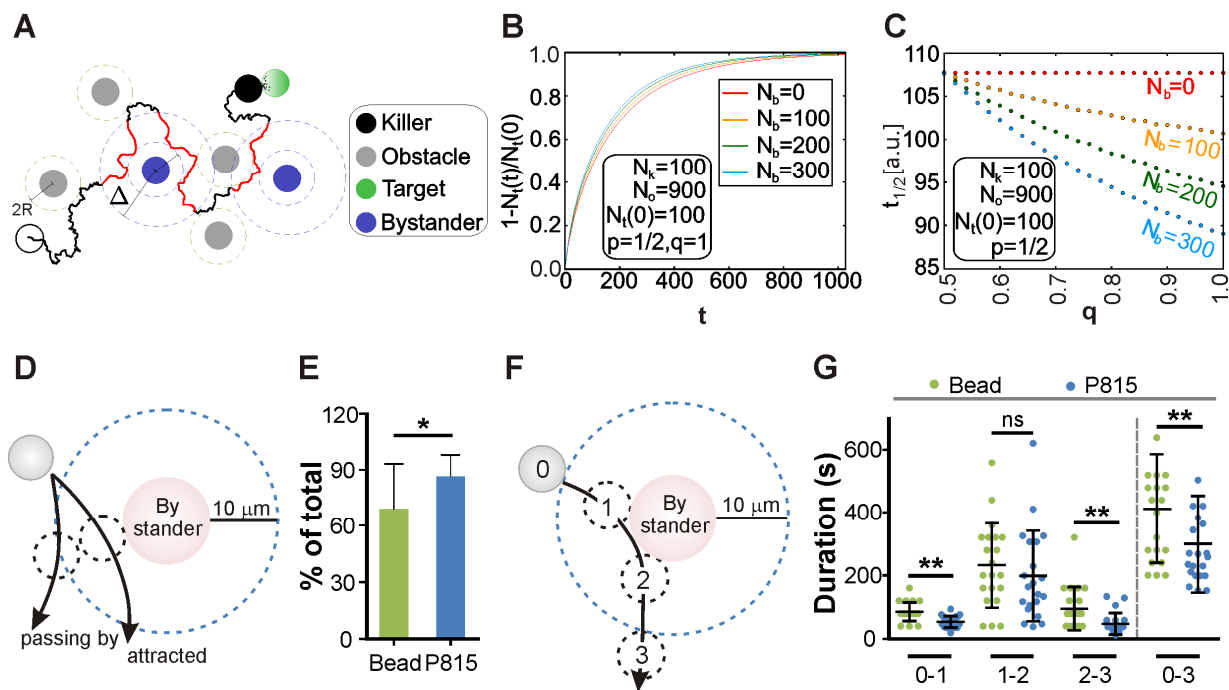


Figure 19. Mathematical prediction and experimental evidence that bystander cells enhance killer cell migration. (A) Sketch of the theoretical model: Killers (black), obstacles (gray), targets (green) and bystander (blue) are represented by circles of radius R . The search trajectory of a killer is indicated in black when its distance to the nearest bystander is larger than $2R$ and its diffusion constant is D_{normal} , and it is indicated in red when its distance to the nearest bystander is smaller than Δ and its diffusion constant is $D_{\text{fast}} > D_{\text{normal}}$ implying a faster movement along the red parts. When a target is reached by a killer, the target is eliminated. (B) Percentage of found targets as a function of time for $N_k=100$ killers, $N_o=900$ obstacles, $N_t(0)=900$ targets at time $t=0$ and different numbers of bystanders N_b , on a 60×60 square lattice (corresponding to a maximum occupancy of 3600 cells). (C) The half time $t_{1/2}$ as a function of the acceleration probability $q > p=1/2$ for the same particle numbers as in B (provided by Karsten Schwarz and Heiko Rieger). (D) Scheme of the attraction of a migrating NK by the bystander objects. Trace a was defined as passing by and b was attracted. (E) Quantitative analysis of NK cell attracted by the bystander cell or beads. (F) Scheme of the 3 different time frames during the attraction of a migrating NK cell in the vicinity of the bystander objects. Numbers are indicating the different phases during the attraction. (G) Quantitative analysis of NK cell attracted by the bystander cell or beads. 0-1 shows the time between entering the territory and contacting bystander, 1-2 shows the time of NK cell contacting bystander and 2-3 shows the time between detaching the bystander and leaving the territory, 0-3 is the total duration of NK cell in the territory of a bystander cell or bead. *, $p < 0.05$, **, $p < 0.01$. (A, B, and C are from Karsten Schwarz and Heiko Rieger and adapted from Zhou *et al.* 2017 [68]).

Assumption: The random motion was modeled as free diffusion with a characteristic diffusion constant D_{normal} and with appropriate boundary conditions and the cells are modeled as hard, impenetrable disks of radius R . Four different cell types were considered: killers, targets, bystanders and obstacles (*e.g.* inactive killers), each having a pre-defined number at time $t=0$. When a killer touches a target cell (*i.e.* the distance between centers of two cells becomes equal to $2R$) the target is removed from the system. When the killer approaches a bystander it will increase its motility and diffuse faster with a diffusion constant $D_{\text{fast}} > D_{\text{normal}}$ as long as its

distance from the bystander is smaller than Δ , which should be larger than $2R$, since this is the minimum distance between two hard disks of radius R , but smaller or equal to the range of the microenvironment of an individual bystander cell. Fig. 19A shows the sketch of this model. It should be noted that the local acceleration modeled in this way does not provide any guiding clue towards nearby targets, nevertheless, it decreases the searching time and hence the killing efficiency of the killer cells as demonstrated now. For computational reasons a lattice version of the model described was used above, its mathematical details were delegated before (see also Fig. 18). In Fig. 19B, targets, bystanders, and obstacles are all mobile for a model version. For a varying number of bystanders (N_b), the percentage of found targets, $100\Delta(1-N_b(t)/N_b(0))$, increases monotonically with time and, in particular, increases faster with increasing N_b . The same behavior, with slightly different numbers, was observed in all other model variants considered (mobile/immobile targets, mobile/immobile bystanders, mobile/immobile obstacles). Fig. 19C shows the half time $t_{1/2}$, defined as the time after which 50% of the targets were found: $t_{1/2}$ increased monotonically with more numbers of bystander cells.

In the following the predictions of the mathematical model are tested. Fig. 19D shows the experimental approach to quantify attraction of NK cells by bystanders. When close to a bystander (in a distance of $10\ \mu\text{m}$), NK cells tend to be attracted by the bystander cells with a much higher probability compare to bystander beads (Fig. 19E). For those NK cells moving towards either the bystander cell or bead, the time of approaching, touching and leaving was analyzed. Quantification shows that NK cells needed less time to approach and leave the bystander cells compared to the beads, while the time that NK cells spent to examine bystander cells or beads was similar (Fig. 19F). As a whole, the total time that NK cell spent in the vicinity of bystander cells, including approaching, touching and leaving, was significantly shorter relative to bystander beads control (Fig. 19G), which is expected considering the shorter approaching and leaving time. This result strongly supports the prediction of the model

that the presence of bystander cell enhances the killer cell migration through local migration velocity increases.

In conclusion, the mathematical model strongly and the experimental evidence suggest that locally increased migration velocity by bystander cells decreases the target searching time and thus increase target elimination efficiency.

4.1.7. Mechanisms mediating the bystander cell enhanced NK migration

The next question is how bystander cells facilitated killer cell migration by local migration velocity enhancement in the vicinity of bystanders. Considering the literature and the tumor microenvironment, I focused on two factors which could potentially increase migration: 1) Adhesion molecules which may facilitate the NK cell migration via physical cell-cell interaction [74], [75]; and 2) Soluble pro-migration factors [76], [77].

4.1.7.1. β -integrins facilitate NK persistence but not velocity, while LFA-1 is not involved in the migration enhancement.

Considering that NK cell migration velocity is significantly elevated by bystander cells and NK cells often make contact with bystander cells, I hypothesized that surface molecules on NK cells, especially integrins, could play a crucial role in this regard. Integrins, which consist of α and β chains, are one of the most important receptors responsible for cell-cell contact [78]. Since it has been proved that α -like chain (LFA-1) as well as integrin β -chain 1, 2 and 7 are the predominant integrins on NK cells (by Eva Schwarz, [68]), the function of these surface molecules was tested. The neutralizing antibodies were used to block the integrin function on the NK cell surface. Since integrins are the major receptors to mediate the interaction with ECM, including collagen, I examined the functionality of those neutralizing antibodies in a 3D collagen matrix. Time-lapse imaging of NK cell migration shows that adding the antibody cocktail against integrin β 1, β 2 and β 7 could reduce NK velocity in collagen (Fig. 20A),

indicating that this antibody cocktail can inhibit the function of integrin $\beta 1$, $\beta 2$ and $\beta 7$. Afterwards, I tested the role of β integrin in bystander-enhanced NK migration. NK cell migration was tested in an environment which was consistent with the killing assay conditions. Representative migration of NK cells with or without β integrin blockade is shown in Fig. 20D. The trajectories showed that the migration of NK cells with β -integrin blockade was slightly restrained, and the cells migrated in a less directed way than those without the β -integrin blockade (Fig. 20E).

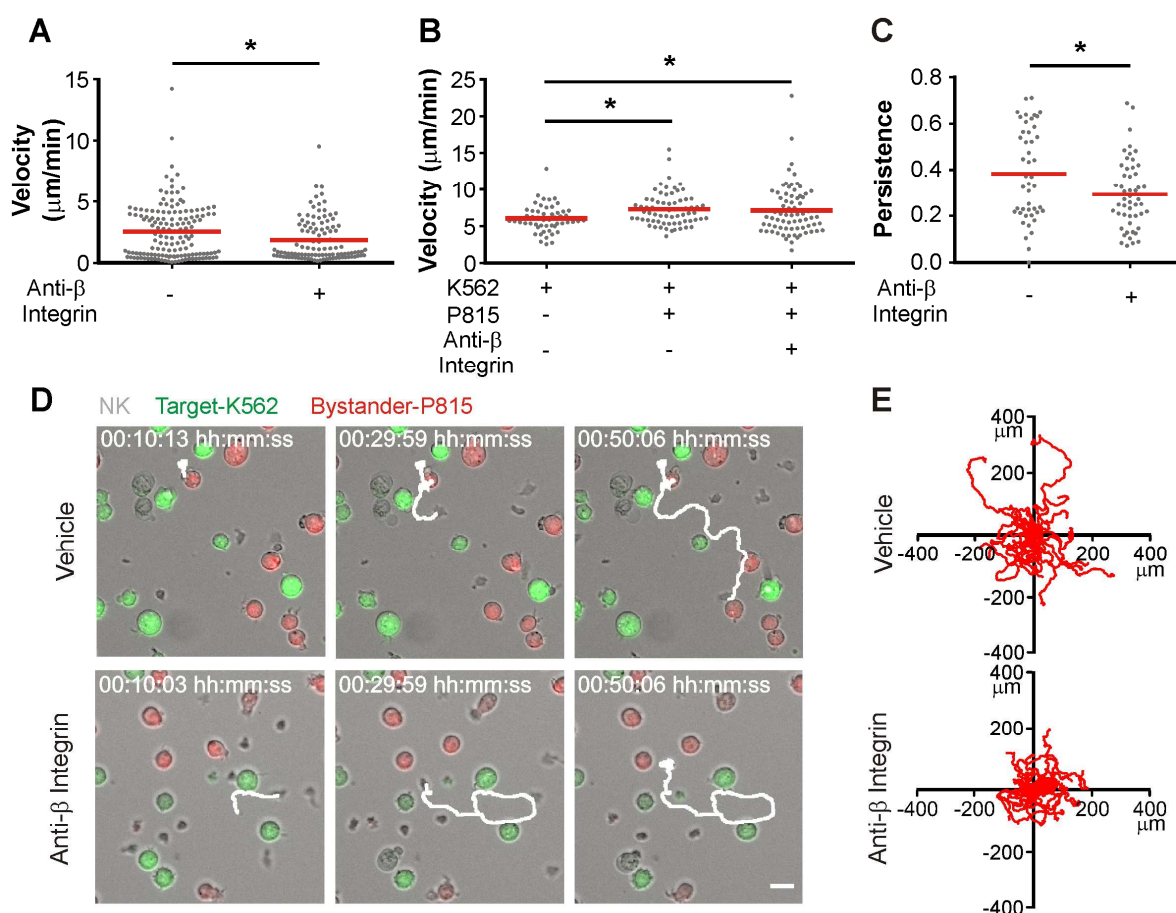


Figure 20. Integrin blockade does not abolish the bystander cell induced enhancement of NK cell migration. (A) Migration velocity of the NK cells with or without the integrin $\beta 1$, $\beta 2$ and $\beta 7$ cocktail treatment. NK cells were treated with vehicle or the cocktail for 30 min and then migration was monitored in a 3D collagen environment. (B) Migration velocity of the NK cells with the incubation of the combined anti-integrin $\beta 1$, $\beta 2$ and $\beta 7$ antibodies in a 2D environment in the presence or absence of bystander cells. (C) Persistence of the NK cell migration with or without the anti-integrin treatment. (D) Representative images of the NK cells migrating without integrin blockade or with integrin blockade. Target cells are green and bystander cells red (labelled with calcein green or red respectively). NK cells were not labeled by fluorescence. White arrows indicate the starting point of the NK cell and the solid white line covers migration over time. (E) Trajectories of the NK cell migration with or without integrin blockade during 50 min in a 2D environment. *, $P < 0.05$; **, $P < 0.01$. Part A, B, C and E are from Zhou *et al.* 2017 [68].

Further quantification shows that compared to the NK cells without β integrins blockade, the velocity of NK cells with β integrin blockade was not affected (Fig. 20B). Further analysis showed that NK cells migrated with a significantly reduced persistence when integrin β 1, 2, 7 were blocked on the NK cells. The migratory behavior of NK cells was similar when NK cells were β -integrin antibody treated or not. However, the migration persistence of NK cells with β integrin blockade was significantly impaired (Fig. 20C).

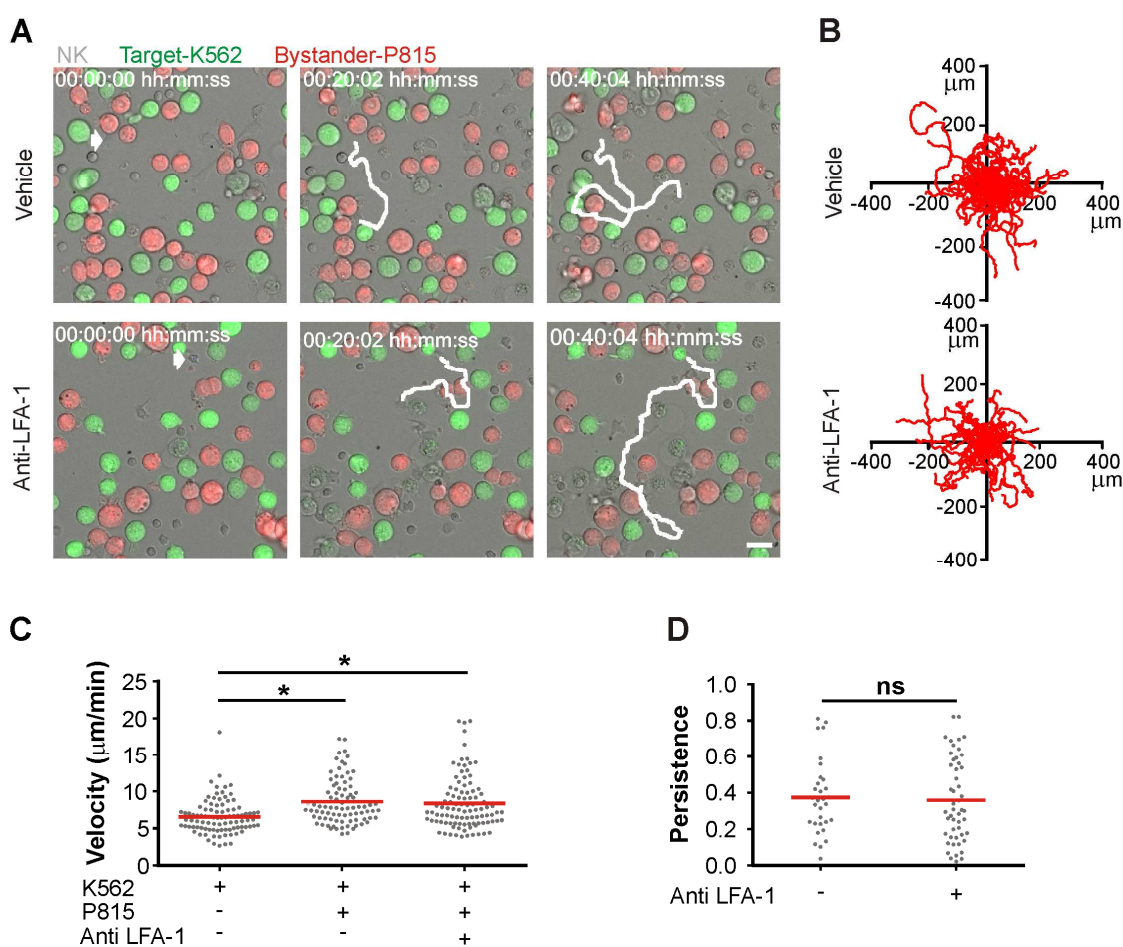


Figure 21. LFA-1 blockade does not abolish the bystander cell induced enhancement of NK cell migration. (A) Representative images of the NK cells migrating without LFA-1 blockade or with LFA-1 blockade. Target cells are green and bystander cells red (labelled with calcein green or red respectively). NK cells are not labeled. White arrows indicate the starting point of the NK cell and the solid white line follows the migrating NK cell. (B) Trajectories of the NK cell migration with or without LFA-1 blockade during 50 min in a 2D environment, $n=20$. (C) Migration velocity of the NK cells with the incubation of vehicle or the anti LFA-1 antibody in a 2D environment. (D) The persistence of NK cell migration with or without anti-LFA-1 treatment*, $P < 0.05$, scale bar is 20 μ m. Part B, C and D are from Zhou *et al.* 2017 [68].

Aside from the β chains, I also tested the function of the predominantly expressed α -like chain, LFA-1. In Fig. 21A, representative pictures of one cell in certain time shows that NK migrated in a similar fashion in the presence of bystander cells, regardless of the LFA-1 blockade on the NK cells. Time lapse imaging shows that LFA-1 antibody treated NK cells migrated almost the same as control cells (Fig. 21A). The trajectories of NK cells with or without anti LFA-1 treatment also exhibit similar length and curvature (Fig. 21B). Further quantification shows that the administration of the neutralizing LFA-1 antibody did not impair the bystander-enhanced NK migration velocity (Fig. 21C). The persistence was also not affected by LFA-1 blocking (Fig. 21D). Taken together, the results suggest that bystander cells enhance NK cell migration persistence via the activation of the integrin β chains but not LFA-1 on NK cells.

4.1.7.2. Bystander cell derived H_2O_2 promoted NK migration velocity

Considering that the enhancement of killer cell velocity was not caused by the activation of integrins on killer cells, the role of soluble pro-migratory factor was examined. Although the conditioned medium overall was not the reason to enhance the killing of NK cells, the role of the microenvironment surrounding bystander cells remains to be clarified. Considering that the bystander cells often outnumber target cells by orders of magnitude, they could be the significant sources to release factors like ATP and reactive oxygen species (ROS) into their vicinity to modulate killer cell function in the microenvironment generated by them. ROS like superoxide anion or its dismutated product H_2O_2 are particularly interesting because they are short-lived and may act locally. Given that H_2O_2 are known to facilitate cell migration [79]–[81], they are reasonable targets to be involved in the bystander-mediated NK migration acceleration.

H_2O_2 is the most popular and well-studied ROS known to play important roles in mediating cell functions, such as guiding cell migration towards higher H_2O_2 concentrations [82]. To test if bystander cell-derived H_2O_2 was involved in the bystander enhanced killing, I analyzed H_2O_2

production with or without the presence of the bystander cells using an Amplex reagent, which reacts with H_2O_2 with a 1:1 stoichiometry to generate a highly fluorescent product. Target cells produced a very low level of H_2O_2 over 4 h incubation. Bystander P815 cells alone or together with target cells significantly elevated the H_2O_2 generation (Fig. 22A). Thus it is reasonable to assume that H_2O_2 is the mediator of the bystander effect on migration velocity.

This hypothesis can easily be tested by adding similar amounts of H_2O_2 to NK cells and analyze their migration. At 2 μM H_2O_2 , which is comparable to the amount produced by bystanders, NK cell migration velocity was significantly increased when compared to vehicle (Fig. 22B). However, the persistence of NK cells was not changed by H_2O_2 (Fig. 22C). The trajectories show that the displacement of NK cells was increased in the presence of H_2O_2 (Fig. 22D). Viability of NK cells and CTLs was not affected by H_2O_2 concentrations between 10 nM and 10 μM whereas there was a slight effect on K562, P815 and Raji cells at higher H_2O_2 (Fig. 22E).

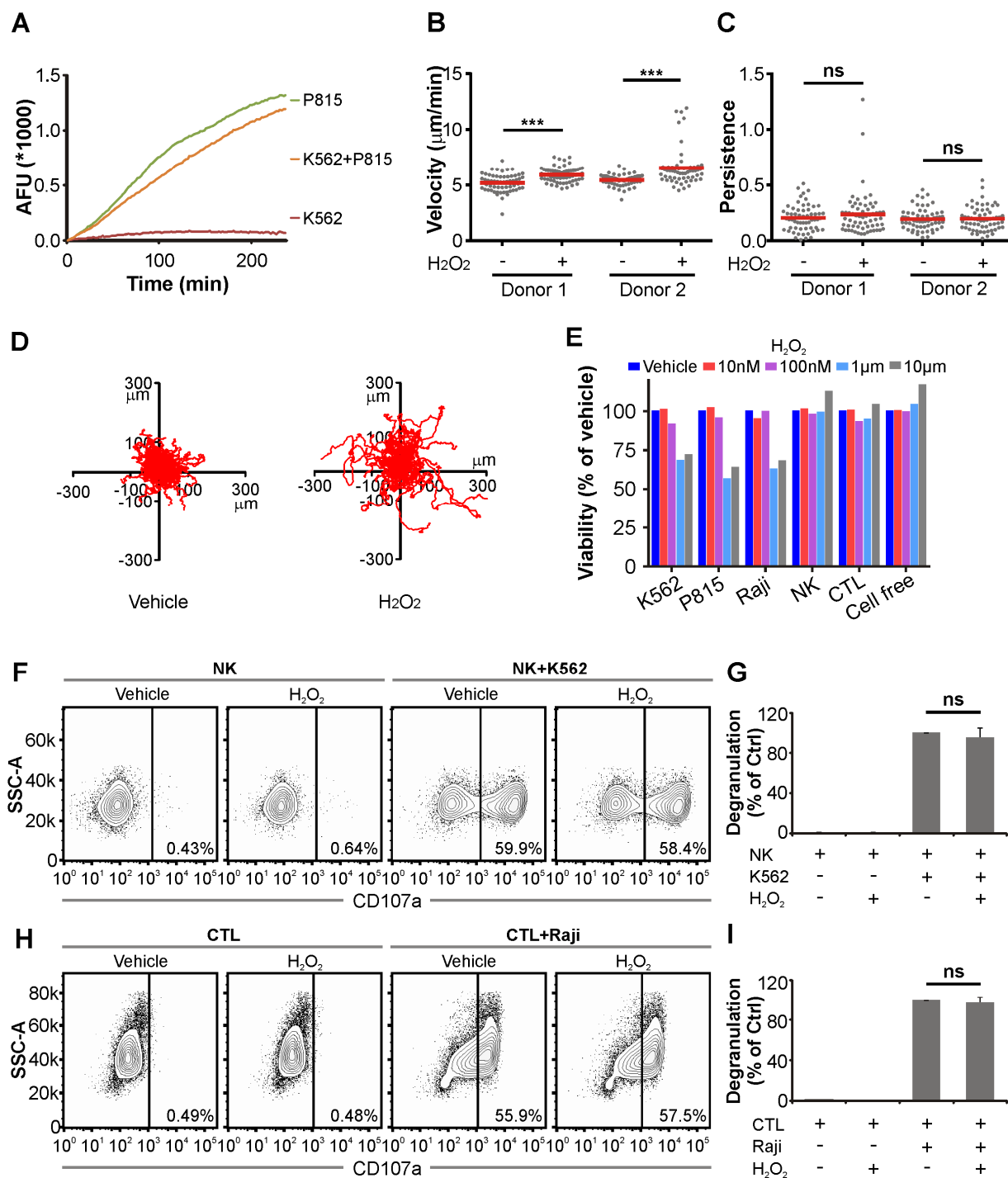


Figure 22. Bystander cell-derived H₂O₂ increases migration velocity but not persistence. (A) H₂O₂ generation of target cells and the bystander cell lines. 2.5×10^4 K562 cells, 7.5×10^4 P815 cells respectively, or mixed as indicated in DMEM-F12 medium, and measured with the Amplex assay for 4 h. (B) Quantitative analysis of the NK cell migration velocity with or without 2 μM H₂O₂ treatment. (C) Migration persistence of NK cells with or without H₂O₂ treatment from B. (D) Trajectories of the migrating NK cells with or without H₂O₂ treatment. (E) Effects of different concentrations of external H₂O₂ on the cell viability. (F) The degranulation level of the NK cells without or with 2 μM H₂O₂. (G) Quantification of F including two more experiments. (H, I) The degranulation of CTLs is not affected by H₂O₂. In the degranulation assay, CTLs, or CTLs + Raji cells were incubated with 2 μM H₂O₂ or vehicle for 4 h at 37°C. One representative experiment is shown in H. Quantification of experiments from three independent experiments is shown in I. Part B, C, D, E, F, G, H are from Zhou *et al.* 2017 [68].

To complete control experiments, it was also tested whether external H_2O_2 influenced killer cell degranulation. $2 \mu M H_2O_2$ had no significant effect on NK cell (Figs. 22F, G) or CTL (Figs. 22H, I) degranulation, indicating that cytotoxicity of both was not impaired.

To further test the function of H_2O_2 on NK cell behavior, catalase, a natural scavenger of H_2O_2 , was applied to check if the bystander enhanced NK killing and migration was reversed by depleting H_2O_2 . The efficiency of catalase was analyzed first. Fig. 23A showed that 10 U/ml Catalase successfully reduced H_2O_2 to a very low level which is around $0 \mu M$, showing a high avidity of degrading H_2O_2 . Subsequently, catalase abolished the bystander cell induced killing enhancement, in other words, the bystander cells together with the H_2O_2 scavenger failed to enhance the killing capability (Fig. 23B).

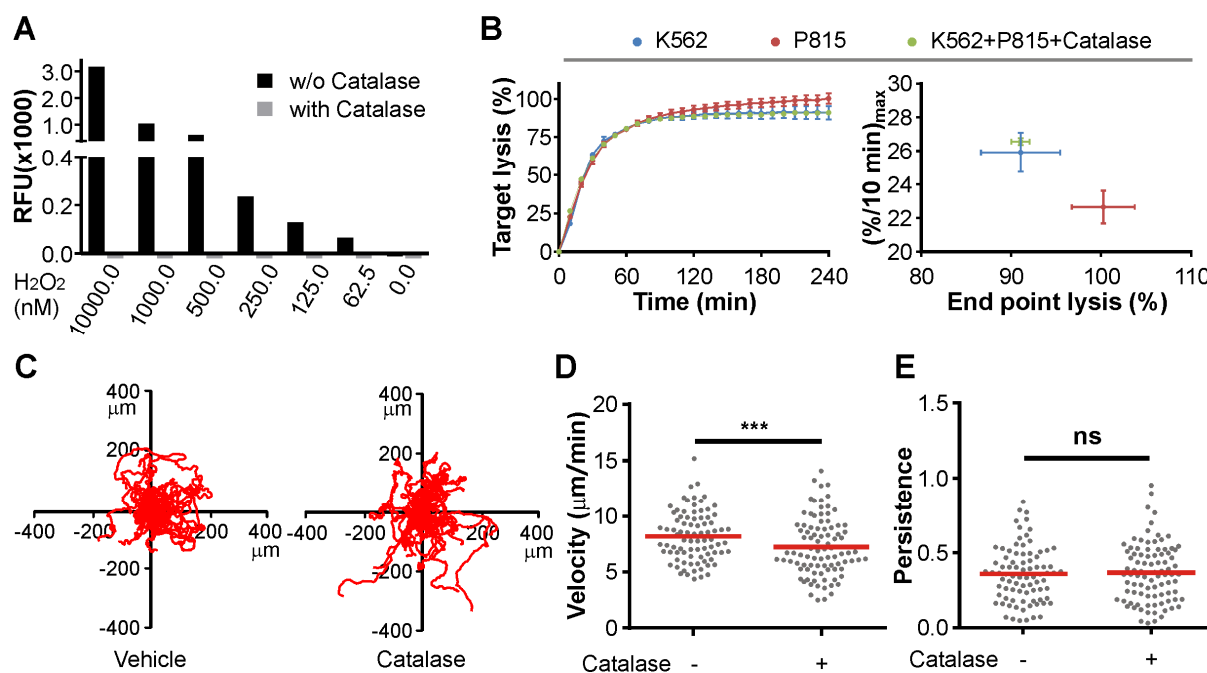


Figure 23. Catalase abolishes bystander cell enhanced target cell killing by NK cells and reduces NK cell migration velocity but not persistence. (A) Environmental H_2O_2 is depleted by 10 U/ml catalase. Various concentrations of H_2O_2 as indicated were plated, then Amplex reagent was added and measured at 535/590 nm. (B) Killing efficiency of NK cells in the presence of vehicle or catalase. 2.5×10^4 K562 cells alone or together with 7.5×10^4 P815 cells were settled in the wells. Then 10 U/ml Catalase was applied before adding 5×10^5 NK cells for killing assay. (C) Trajectories of NK migration together with target and bystander following vehicle or catalase addition. (D) Migration velocity of NK cells together with target and bystander cells in the absence of catalase. (E) Migration persistence of NK cells with or without catalase treatment in the presence of bystander cells. Part C, D and E are from Zhou *et al.* 2017 [68].

A potential effect of catalase on NK cell migration was checked by time lapse imaging. Trajectories of NK migration are shown in Fig. 23C. Further quantification shows that application of catalase significantly reduced bystander-enhanced NK migration velocity (Fig. 23D) but not bystander-enhanced NK persistence (Fig. 23E).

In summary, the bystander cell enhancement of killing efficiency was caused by the bystander cell-dependent enhancement of killer cell migration. The combination of the mathematical modeling with the experimental approaches complementary showed that the locally increased velocity was sufficient to enhance the killing efficiency. Mechanistically, integrin $\beta 1, 2, 7$ on NK cells govern the NK migration persistence, while bystander derived H_2O_2 increases NK cell migration velocity.

4.1.8. Impacts of Treg as bystander cell on NK-mediated killing

During the initial tumor development and growth, the microenvironment consists not only of non-carcinoma cells but also of other immune cells like regulatory T cells (Treg). Considering the bystander effects described so far, it is an interesting question if Treg cells can act as bystanders. Tregs express the transcription factor Foxp3 function as a critical suppressor of the T and B lymphocyte' responses and function [83], [84], but they could interact with killer cells as other bystander cells do. To test if the Treg cells have any similar effects as other bystander cells on killer cell function, I performed the killing assay in presence of Tregs to check how if they influence the killing efficiency. After 24 h co-incubation with the homologous Treg cells, the killer cells killed their target in an impaired fashion with the reduction of around 30% in total killing compared with control, while the bystander cells enhanced the killing as usual (Fig. 24A). When the Treg cells were freshly mixed with the killer cells, the killing efficiency was slightly enhanced, similarly to other bystander cells did (Fig. 24B).

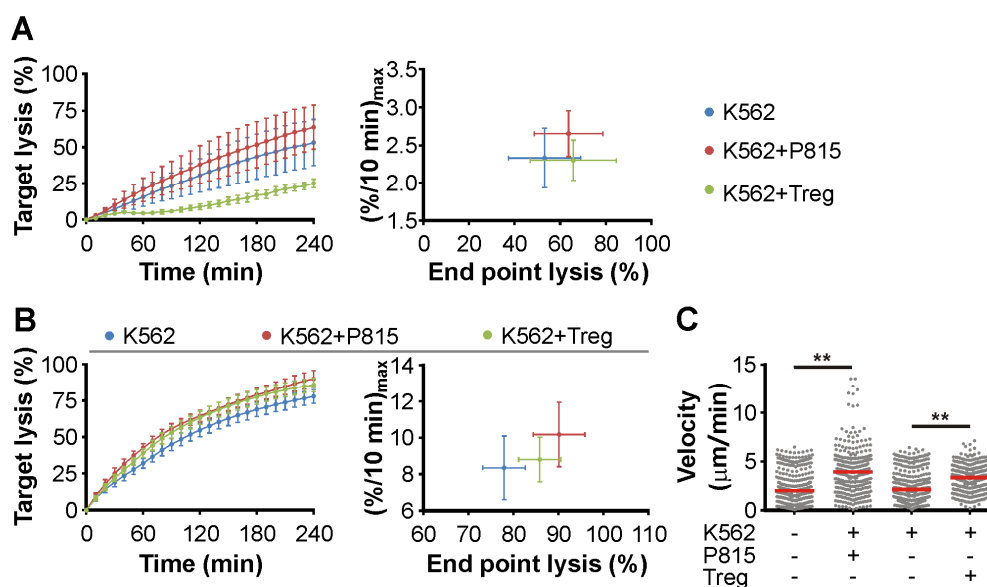


Figure 24. Impact of bystander Treg cells on NK cell's cytotoxicity and migration. (A) Characterization of the killing of NK cells with co-incubated bystander Treg. 5×10^5 cells/well of CTL alone or together with 7.5×10^4 cells/well of Treg were co-incubated for 24 h. Next day 2.5×10^4 Raji cells/well were settled. CTL or CTL-Treg mixture was applied for the killing assay. (B) Characterization of the killing of NK cells with freshly added bystander Treg. 2.5×10^4 Raji cells/well alone or together with 7.5×10^4 Tregs/well of were settled. 5×10^5 CTL/well were applied for the killing assay. Data were shown as mean \pm SEM from 3 independent experiments. (C) Migration velocity of the NK cells together with the normal bystander cells or the freshly mixed Tregs, $n=2$. **, $p < 0.01$.

I also examined the migration velocity of NK cells with freshly added Treg. The velocity of the killer cells was around 2 $\mu\text{m}/\text{min}$ with target cells, which was similar to that of NK cells themselves without any other cell type present. When the NK cells were mixed with bystander P815 cells, the migration velocity was elevated to around 4 $\mu\text{m}/\text{min}$. The freshly added Treg cells also elevated the velocity of the NK cells to 4 $\mu\text{m}/\text{min}$ (Fig. 24C). These results revealed that on the hand Treg cells could suppress killer cell function as was expected when present over extended times (24 h). However, on the other hand freshly added Tregs functioned as normal bystander cells to enhance killing capability through increased velocity. The bystander effect of Tregs may even be larger than observed considering that at the same time they start to inhibit CTL function as obvious from the incubation experiment.

4.2. $[Ca^{2+}]_{ex}$ dependence of LG release

In killer cells, Ca^{2+} serves as a key regulator to control IS formation, cytokine expression and a series of events during LG exocytoses, such as docking, priming, and fusion [85]. The Ca^{2+} dependence of target cell lysis by CTL is not well explored. Based on findings by Kim Friedmann, Cora Hoxha, Arne Knörck and Eva Schwarz, I thus focused on the impact of different concentrations of external Ca^{2+} on CTL cytotoxicity, with a focus on LG fusion and the correlation between the Ca^{2+} microdomain and LG release.

4.2.1. $[Ca^{2+}]_{ex}$ alters the killing efficiency of CTLs

The Ca^{2+} concentration is tightly regulated but it can vary dramatically from tissue to tissue, for instance, the free external Ca^{2+} in blood is around 1.2 mM and it decreases to 1.05 mM in brain [86]–[88]. It can even change in certain organs under certain conditions, for example, the Ca^{2+} concentration increases after the myocardial ischemic injury [89], [90]. In particular, when tumor occurs, the microenvironment surrounding the tumor is changing, as a major messenger, Ca^{2+} concentration also plays crucial role in cancer development [91]–[93]. Therefore, it is of great importance to elucidate whether immune functions can be regulated by extracellular Ca^{2+} .

To address this point, different concentrations of free extracellular Ca^{2+} were achieved by adding EGTA or $CaCl_2$ into the AIMV medium following the work by Friedmann, Knörck and Schwarz in our laboratory. The analysis of the Ca^{2+} concentrations in the AIMV medium shows that the free Ca^{2+} in the medium was around 800 μ M. The concentration of free Ca^{2+} in AIMV supplemented with different amounts of EGTA or Ca^{2+} was also analyzed with different methods by Kim Friedmann, Arne Knörck and Eva Schwarz (unpublished). In addition, recent work in our lab shows that increasing or decreasing Ca^{2+} in the medium can significantly tune the killing efficiency (Friedmann, Hoxha and Schwarz *et al.*, unpublished).

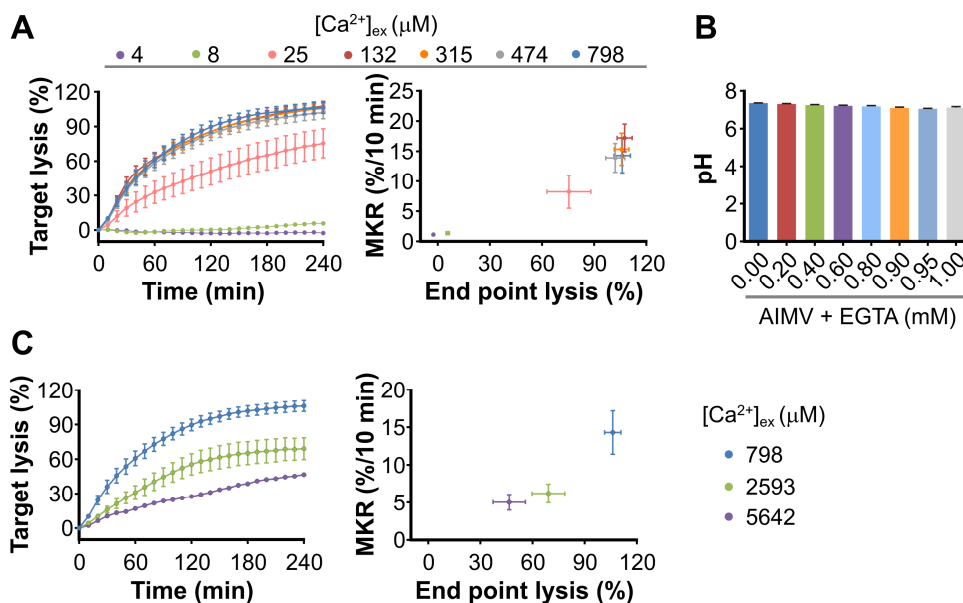


Figure 25. Manipulating $[Ca^{2+}]_{ex}$ alters the CTL killing efficiency (reproduced from the findings by Friedmann, Hoxha, Schwarz *et al.*). (A) Characterization of the killing efficiency of CTL at different Ca^{2+} concentrations (in AIMV medium). 2.5×10^4 SEA-pulsed Rajis/well were settled in the desired medium with Ca^{2+} concentrations, achieved by adding different amounts of EGTA. Free external Ca^{2+} concentration in the medium were measured by Eva Schwarz *et al.* (unpublished). 5×10^5 CTLs/well were applied for killing assays. Data is shown as mean \pm SEM from 4 independent experiments. (B) pH determination in the media after the addition of EGTA, $n=3$. (C) Killing efficiency of CTLs at high Ca^{2+} concentrations. Free external Ca^{2+} concentration in the medium were measured by Eva Schwarz *et al.* (unpublished). Data is shown as mean \pm SEM from 4 independent experiments.

Along the same line, I reproduced that CTLs have the best killing in the normal medium AIMV and the EGTA adapted AIMV, which contains 130-800 μM Ca^{2+} (Fig. 25A). While further increasing EGTA from 0.9 to 1.0 mM in AIMV, corresponding to $[Ca^{2+}]_{ex}$ of 25 to 4 μM , the killing was almost abolished (Fig. 25A). This is not due to a pH change caused by proton release from EGTA into the medium (Fig. 25B). When I further increased the free $[Ca^{2+}]_{ex}$ as Friedmann, Hoxha and Schwarz did by adding 2 mM or 5 mM $CaCl_2$, corresponding to $[Ca^{2+}]_{ex}$ of 2593 to 5642 μM , the killing efficiency was diminished rather than enhanced. The maximal killing rate as a function of final killing efficiency shows that excessive $[Ca^{2+}]_{ex}$ suppressed the CTL cytotoxicity (Fig. 25C). These results suggest that CTLs function best within the optimized Ca^{2+} range of 130-800 μM $[Ca^{2+}]_{ex}$.

4.2.2. Antigen concentration-dependent Ca^{2+} influx correlates with CTL-mediated cytotoxicity

Considering the importance of external Ca^{2+} for killing efficiency, it makes sense to analyze if the stimulus strength modifies Ca^{2+} and killing efficiency in a similar way. Different concentrations of SEA (10^{-6} , 10^{-4} , 10^{-2} and $1 \mu\text{g/ml}$) were used to pulse Raji cells. The killing kinetics of CTLs show that as expected the efficiency of target elimination is dependent on the concentration of the antigen (Fig. 26A). The killing kinetics showed that there is a clear drop in killing efficiency between 10^{-2} to $10^{-4} \mu\text{g/ml}$ SEA (Fig. 26B), suggesting that there might be a threshold of antigens to initiate the elimination of target cells.

As Ca^{2+} influx is a downstream consequence of the stimulation [94], I checked if the SEA dose-dependent killing was correlated with Ca^{2+} influx in CTLs upon target recognition. CTLs were loaded with a Ca^{2+} sensor Fura-2, and then they were incubated with the Raji cells pulsed with different concentrations of SEA. Fura-2 is a ratiometric Ca^{2+} sensor which binds to free Ca^{2+} . When excited at 340 nm and 380 nm, the ratio of the emissions at those wavelengths of Fura-2 is directly proportional to the concentration of Ca^{2+} . Using single cell Ca^{2+} imaging, I found that CTLs show the highest Ca^{2+} influx when contact with the Raji cells pulsed by $1 \mu\text{g/ml}$ and $1 \times 10^{-2} \mu\text{g/ml}$ SEA. In comparison, with the concentration of SEA down to 10^{-4} and $10^{-6} \mu\text{g/ml}$, the Ca^{2+} influx was almost in the same range as that induced by the cells treated with vehicle (Fig. 26C). It shows that the increase of intracellular Ca^{2+} reflects the intensity of stimulation and there is a threshold of stimulus (between 10^{-2} and $10^{-4} \mu\text{g/ml}$) for a full Ca^{2+} activation in CTL. Although, it should not be forgotten that antigen stimulation probably effects killing efficiency not only by Ca^{2+} but also by synaptic strength, the dose dependent killing efficiency of different antigen concentrations correlates with different Ca^{2+} signals.

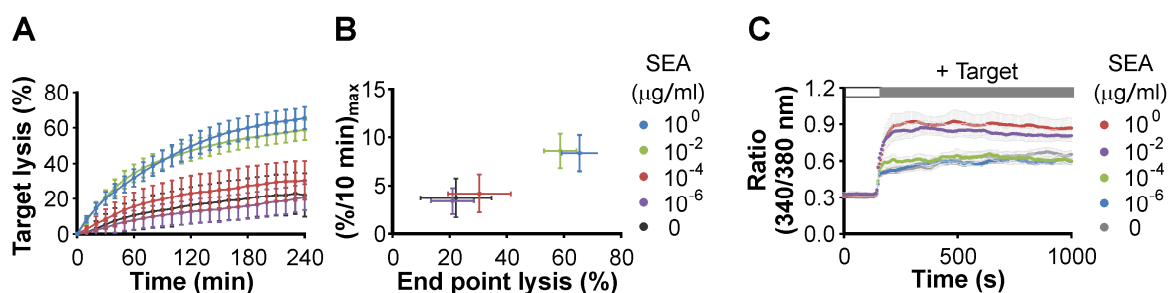


Figure 26. CTL killing efficiency is SEA dose dependent and correlates with Ca^{2+} influx. (A) Characterization of CTL killing Raji cells pulsed with different SEA concentrations. Raji cells were pulsed with the indicated concentration of SEA for 30 min at 37°C with 5% CO_2 . 2.5×10^4 Raji cells/well were settled into each well. 5×10^5 CTLs/well were applied for the killing assay. (B) The maximal killing rates are plotted against the end point-lysis from A. (C) Ca^{2+} influx of CTLs upon target recognition. CTLs were loaded with 2 μM Fura2-AM, 2×10^5 cells were settled on the cover glass. Raji cells pulsed with indicated concentrations of SEA were applied to the CTLs and Fura-2 signals were analyzed.

4.2.3. A certain stimulus intensity is necessary for effective killing

The threshold of SEA to induce sufficient target cell killing and Ca^{2+} influx suggests that the stimulus intensity is crucial for the proper target killing. Considering the dependence of killing on external Ca^{2+} concentrations and Ca^{2+} entry, the question arises, if Ca^{2+} can modulate the killing efficiency at different stimulation intensities generated by loading Raji cells with different antigen concentrations.

To address this question, I examined whether low killing efficiency induced by a low stimulus intensity could be rescued by modulating $[\text{Ca}^{2+}]_{\text{ex}}$. In Fig. 26A, I showed that 1 $\mu\text{g/ml}$ and 10^{-2} $\mu\text{g/ml}$ SEA pulsed Raji cells induce the full CTL activation, 1×10^{-4} $\mu\text{g/ml}$ and 1×10^{-6} $\mu\text{g/ml}$ SEA pulsed Raji induced lower but similar killing and Ca^{2+} influx. Therefore, I chose 1 $\mu\text{g/ml}$ and 10^{-4} $\mu\text{g/ml}$ SEA to pulse Raji cells and performed the killing assay in different $[\text{Ca}^{2+}]_{\text{ex}}$ to compare the killing efficiency. CTLs efficiently killed the 1 $\mu\text{g/ml}$ SEA pulsed target cells in 798 μM $[\text{Ca}^{2+}]_{\text{ex}}$. When SEA was reduced to the insufficient level (1×10^{-4} $\mu\text{g/ml}$), Raji cells were killed in a much less efficiently. Even when the extracellular Ca^{2+} concentration was tuned to the optimal concentration (132 μM $[\text{Ca}^{2+}]_{\text{ex}}$) for CTL cytotoxicity, the killing efficiency could not be rescued by the optimized $[\text{Ca}^{2+}]_{\text{ex}}$. The killing kinetics also clearly show that the lack of antigen is not compensated by the optimized $[\text{Ca}^{2+}]_{\text{ex}}$ (Fig. 27A).

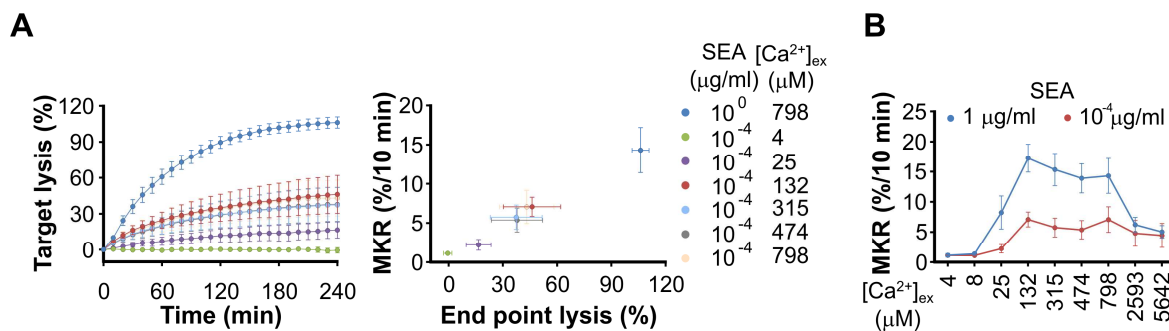


Figure 27. Modulation of Ca^{2+} concentration does not compensate the low stimulus intensity to improve killing. (A) Characterization of CTL killing with the desired amount of SEA pulsed Raji cell in different $[\text{Ca}^{2+}]_{\text{ex}}$. Raji cells were pulsed with the indicated concentration of SEA for 30 min at 37°C with 5% CO_2 . 2.5×10^4 cells/well of Raji were settled in the indicated Ca^{2+} solutions. 5×10^5 cells/well of CTL were applied for the killing assay. (B) Plotting of the maximal killing rate of the killing with target cells with sufficient or insufficient antigen pulsing. Data is shown as mean \pm SEM of 4 independent experiments.

With 1 $\mu\text{g/ml}$ of SEA pulsed target cells, CTLs showed the same Ca^{2+} dependence of target cell killing as before with the Ca^{2+} optimum at 132 μM $[\text{Ca}^{2+}]_{\text{ex}}$. Further increase or decrease of $[\text{Ca}^{2+}]_{\text{ex}}$ reduced the killing efficiency. The $[\text{Ca}^{2+}]_{\text{ex}}$ dependence of killing at low SEA concentrations (1×10^{-4} $\mu\text{g/ml}$) was similar to the one at high (1 $\mu\text{g/ml}$) stimulus intensity. In 4 to 25 μM $[\text{Ca}^{2+}]_{\text{ex}}$ or 2593 to 5642 μM $[\text{Ca}^{2+}]_{\text{ex}}$, the maximal killing rate was suppressed to a lower level. However, while the Ca^{2+} dependence is qualitatively similar between both antigen concentration, modulation of $[\text{Ca}^{2+}]_{\text{ex}}$ cannot compensate for the lack of sufficient antigen stimulation (Fig. 27B).

4.2.4. LG fusion is correlated with optimized $[\text{Ca}^{2+}]_{\text{ex}}$

One of the predominant mechanisms of the killing machinery is releasing LG containing GZB and PFN to the target cell upon the IS formation [95]. The Ca^{2+} dependence of this process is not well characterized. I applied total internal reflection fluorescence (TIRF) microscopy to visualize events that take place at the plasma membrane at the IS. CTL overexpressing mCherry-tagged GZB or PFN were settled onto the anti-CD3/CD28/LFA-1 antibody-coated coverslip in 0 mM $[\text{Ca}^{2+}]_{\text{ex}}$, and then the desired concentrations of Ca^{2+} were applied to the cells. The fastest possible acquisition time is 42 ms, which is sufficient to catch the fusion events. Fig. 28A shows a typical release event of LG at the IS.

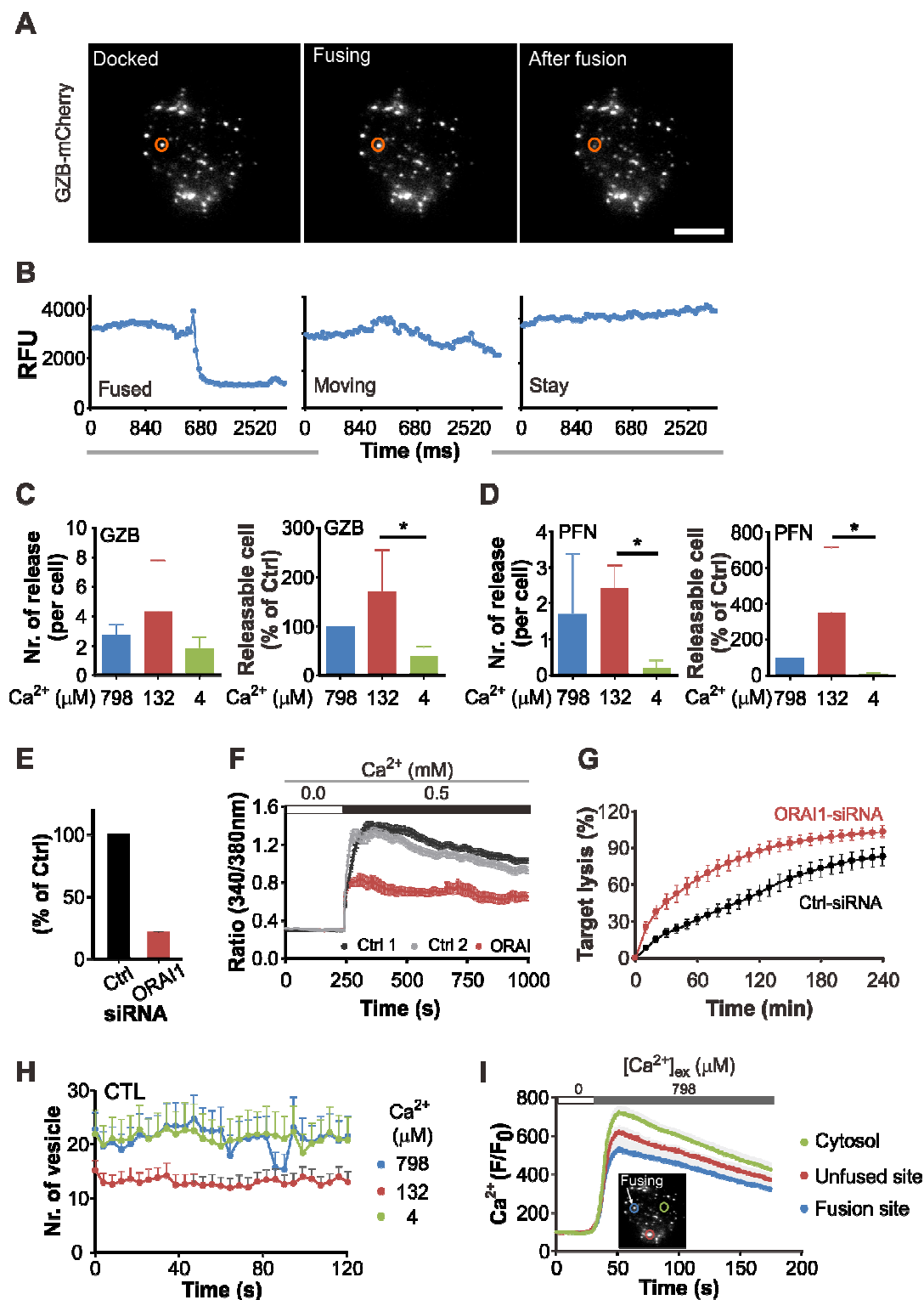


Figure 28. LG fusion at the IS in CTL is optimized at intermediate $[Ca^{2+}]_{ex}$ around 132 μM (A) Sequential images of a fusing LG at IS. CD3/CD28 stimulated CD8⁺ T cells were transfected with GZB-mCherry and settled onto the CD3/CD28 antibody coated coverslip in AIMV supplemented with 1mM EGTA, and subsequently cells were perfused with AIMV. The orange cycle indicates the fusing LG. The scale bar is 5 μm . (B) Defining LG release by analyzing the fluorescence intensity. The region of interest (ROI) covers the individual LG and the fluorescence intensity of the ROI is depicted over time. (C) Quantitative analysis of GZB or PFN positive LG fusion at different $[Ca^{2+}]_{ex}$. CD8⁺ T cells were transfected with GZB-mCherry or PFN-mCherry, respectively. The number of release events of GZB or PFN positive LG following the change to the respective Ca²⁺ concentration. (D) Quantification of the relative frequency of cell with LG release (=at least one fused LG) taken from C. n=3. *, p<0.05; **, p<0.01. (E) Quantification of ORAI1 expression in CTL. CTLs were transfected with

non-silencing siRNA (Ctrl) or ORAI1 siRNA for 3 days and the cell extract was applied for qPCR. **(F)** Intracellular Ca^{2+} signal of CTL upon target encounter. CTLs transfected with the control or ORAI1-siRNA for 3 days, 2×10^5 cells were loaded with $2 \mu\text{M}$ Fura-2 AM and seeded on the cover glass and assembled onto the chamber. 1×10^6 SEA-pulsed Raji cells were applied to CTLs. **(G)** Quantification of the killing efficiency of CTLs with control siRNA or ORAI1 siRNA. **(H)** Quantification of the accumulated GZB positive LG at IS. **(I)** Quantitative analysis of Ca^{2+} influx at different spots from IS. CD8^+ T cells were transfected with GZB-mCherry, one day after cells were loaded with $2 \mu\text{M}$ Fluo-5F at 37°C for 30 min. The cells were excited at both 488 and 561 nm by TIRF. ROIs were made at the spot in the cytosol without LG (green circle), on vesicles, which were released (blue circle) and vesicles did not release (red circle), respectively. The emission of 561 nm was monitoring the vesicle fusion and the emission of 488 nm was for Ca^{2+} signal. CD8^+ T cells were settled in 0 mM Ca^{2+} and perfused with 1 mM Ca^{2+} . Data is shown as mean \pm SEM from 3 independent measurements. Part E and G are kindly provided by Kim Friedmann, Gertrud Schwär and Eva Schwarz.

After approaching the IS LG dwell at a fixed position, indicating that it has been docked. Then the fluorescence suddenly increases during fusion because the vesicle is opening and the tagged fluorescent protein is exposed to a higher pH resulting in increased fluorescence. Afterwards, the fluorescence disappears due to the diffusion of the soluble protein into the environment. The short increase of fluorescence with the subsequent fast decline is a clear indication that the LG has been released and not been transported deeper into the cytosol away from the IS [96]. Fig. 28B shows an LG can also leave the IS, which is clearly distinguished from a released LG by the slow slope of the decreasing fluorescence. As described before, extracellular Ca^{2+} was chelated by EGTA to achieve different $[\text{Ca}^{2+}]_{\text{ex}}$ (0 mM, 0.8 mM and 1 mM EGTA, corresponding to $798 \mu\text{M}$, $132 \mu\text{M}$ and $4 \mu\text{M}$ $[\text{Ca}^{2+}]_{\text{ex}}$, respectively). After depletion of the Ca^{2+} store in Ca^{2+} -free AIMV medium and re-addition of AIMV with different concentrations of extracellular Ca^{2+} , LG accumulation and subsequent release at the IS plane was accessed. On average around one LG was released with $798 \mu\text{M}$ and $4 \mu\text{M}$ $[\text{Ca}^{2+}]_{\text{ex}}$ present, and the number of released LG was increased to around two with $132 \mu\text{M}$ $[\text{Ca}^{2+}]_{\text{ex}}$ present (Fig. 28C). Not only the number of fused LG was increased in $132 \mu\text{M}$ $[\text{Ca}^{2+}]_{\text{ex}}$, but also the percentage of CTLs which were able to release LG was also increased in $132 \mu\text{M}$ $[\text{Ca}^{2+}]_{\text{ex}}$ (Fig. 28D). Since ORAI1 is the major Ca^{2+} channel subunit, Eva Schwarz and Kim Friedmann downregulated ORAI1 expression in CTLs. After ORAI1 is partially depleted (Fig. 28E), there are less Ca^{2+} influxed into CTL upon target conjugation compared to the non-silenced CTLs (Fig. 28F). Interestingly, CTLs kill their target cells with a higher

killing efficiency when the ORAI1 channels are partially depleted (Fig. 28G). As Ca^{2+} may also be important for LG transport towards IS upon antigen recognition, the accumulation of LG at IS in different $[\text{Ca}^{2+}]_{\text{ex}}$ was also analyzed. Fig. 28H shows that around 20 GZB positive vesicles accumulated at the IS in both 798 μM and 4 μM Ca^{2+} , while in 132 μM $[\text{Ca}^{2+}]_{\text{ex}}$, the number of vesicles decreased to around 14. With these experiment, it can be ruled out that the reduced LG release at 798 μM and 4 μM compared to 132 μM is a result of reduced transport of LG to the IS. Since $[\text{Ca}^{2+}]_{\text{ex}}$ does not directly reflect the Ca^{2+} concentration at the IS, the $[\text{Ca}^{2+}]_{\text{in}}$ at IS was monitored at the IS plane by TIRF. The concentration of intracellular Ca^{2+} ($[\text{Ca}^{2+}]_{\text{in}}$) was quantified at three regions in the vicinity to the IS: the locations with no vesicles (cytosol, green circle), the locations where releasable LG were primed (fusion site, blue circle) and the locations with LG not released during the acquisition (unfused site, red circle). Analyses show that Ca^{2+} signal was the highest at the spots of cytosol (Fig. 28I, green circle). Unexpectedly, Ca^{2+} signal was lowest at fusion sites (Fig. 28I, blue circle). In comparison, the Ca^{2+} signal at unfused sites was inbetween (Fig. 28I, red circle).

In summary, both of the proteins required for cytotoxicity mediated by LG, PFN and GZB, were released in a $[\text{Ca}^{2+}]_{\text{ex}}$ dependent manner, which was in good agreement with $[\text{Ca}^{2+}]_{\text{ex}}$ dependence of the killing being optimal at intermediate $[\text{Ca}^{2+}]_{\text{ex}}$. The analysis of intracellular Ca^{2+} signals at different sites of the IS also supports the Ca^{2+} dependence of killing. Therefore, these results suggest that the $[\text{Ca}^{2+}]_{\text{ex}}$ dependent killing might be regulated by the molecules mediating LG fusion which may be Ca^{2+} sensitive to.

5. Discussion

5.1. Bystander cell enhanced killer cell cytotoxicity

In tumor or at inflammation sites, many cells are not recognized by killer cells as their targets, referred to as non-target bystander cells in this work. The impact of bystander cells on target elimination efficiency by CTL or NK cells is not yet fully understood. In this work (4.1), I show that various type of bystander cells enhance both CTL- and NK-mediated cytotoxicity via accelerating NK cell approaching and leaving the bystander cells. The acceleration is mediated by bystander-derived H_2O_2 . Combining a mathematical diffusion model, we confirmed that the migration of NK cells in the vicinity of bystander cells is locally accelerated, thereby reducing the search time to reach target cells. In addition, I found that the predominantly expressed integrins $\beta 1$, $\beta 2$, and $\beta 7$ on NK cells are involved in the bystander-enhanced NK persistence.

5.1.1. The role of bystander cell in killer cell mediated killing

Bystander cells often represent the majority of cells at tumor or infected sites, especially at early times. Thus, the role of bystander cells for the immune response is of special importance. A very likely prediction (or hypothesis) is that bystander cells physically block the path between the killer cell and the target and therefore prolong the searching time and reduce the killing efficiency. Interestingly, I found the opposite, namely that bystander cells, specifically, P815, Raji, primary human monocytes and HUVEC, enhance CTL- and NK cell-mediated cytotoxicity.

From my data, it is clear that bystander cells enhance the cytotoxicity of killer cells *in vitro*, however, physiological conditions *in vivo* are much more complex than *in vitro* conditions. There is good evidence that *in vivo*, bystander cells in zebrafish can also promote microglia cell migrate towards the injury site to clear the dead neuron by secreting glutamate [82]. It is also

possible to mimic the *in vivo* conditions better by using three-dimensional (3D) matrices *in vitro*. In our lab, the preliminary results from 3D collagen matrices show that the killer cell cytotoxicity, as well as the migration velocity, is also enhanced by the bystander monocytes (by Renping Zhao, Zhou et al. 2017 [68]). This is in line with a previous study that bystander cells promote microglia migration *in vivo* [82]. Furthermore, *in vivo* studies show that non-target CD4⁺ T cell facilitate CD8⁺ T lymphocyte mobilization towards the virus-infected tissue in mouse [97] and that bystander monocytes facilitate infiltration through the glia limitans in the mouse brain [98].

Since conditions *in vivo* can obviously not fully be reproduced *in vitro*, we applied also computer simulation to test which parameters influence the “bystander effect”. The actual work was done in Heiko Rieger’s group (Theoretical Physics) after we worked out the conditions together with them. The model shows that bystander cells reduce the search time of killer cell to find and reach target cells, without providing extra directional cues. A simple local acceleration close to the bystander cells is sufficient to produce the “bystander effect” and enhance the killing efficiency. This suggests that in tissues, the presence of bystander cells could provide the killer cells with an optimal microenvironment to direct the killer cells faster to their target cells.

An important question is which cell types can induce the “bystander effect”. In principle, all H₂O₂-producing non-target cells should act as bystanders to accelerate killer cell migration and therefore enhance killing efficiency. We found that living cells like Raji, P815 and HUVEC but not beads or the fixed cells produced the bystander effect. However, particular cell types should not be considered as bystander cells, although they are clearly non-target cells for killer cells. These include cells that support the tissue structure or cells that form the physical barrier to hinder immune cell infiltration [99]. Interestingly, as suppressor T cell, although a long co-incubation of Treg and CTL reduces the cytotoxicity of CTL, Treg cells also enhance killing

efficiency of CTL when they are acutely added into the microenvironment containing CTLs cells and target cells (Fig. 24), indicating that bystander cells naturally have the potential to enhance the killing efficiency.

In this study, bystander cells enhance the cytotoxicity mainly depends on accelerating killer cell migration. In addition to this, there are other means of enhancement on cytotoxicity by bystander cells. For example, T cells cooperate with CD4⁺ T cells to induce killing of cancer cells or directly enhance the killing capability of CD8⁺ cells by secreting IFN- γ and IL-1 β [100] [101], [102]. In principle, H₂O₂ could also contribute to the T helper cell-enhanced killer cell cytotoxicity.

5.1.2. The role of H₂O₂ in killer cell cytotoxicity

Bystander-derived H₂O₂ was found to accelerate killer cells, thereby increasing cytotoxicity. The concentration of bystander cell-generated H₂O₂ was determined to be between 1-3 μ M (data not shown). We also found that H₂O₂ 2 μ M of extracellularly H₂O₂ enhanced migration whereas catalase could inhibit it. Together with the results from the modelling and since H₂O₂ does not affect the viability of target and killer cells (Fig. 22E), our data clearly indicate that the enhanced killing efficiency is caused by H₂O₂ produced by bystander cells. These results are in a good agreement with other studies. It is reported that H₂O₂ accelerates the microglia migration *in vitro* [103]. Niethammer *et al.* show that H₂O₂ gradients serve as directional cues for leukocytes to migrate towards the wound sites [104]. Thus we hypothesize that low concentrations of H₂O₂ in the range of 1 μ M accelerate cell migration which in case of CTL and NK cells leads to enhanced cytotoxicity. Through their local killer cell acceleration by H₂O₂ production, bystander cells can thus be considered cytotoxicity enhancers.

H₂O₂ accelerates killer cell migration via velocity enhancement (Fig. 22B), leaving persistence not affected (Fig. 22C). Since I have reported integrin β 1, 2 and 7 are involved in the bystander

cell enhanced persistence but not velocity, it is unlikely these integrins are effector molecules of external H_2O_2 on these killer cells. To differentially enhance the migration velocity from the persistence, H_2O_2 must activate some distinct signaling pathways to determine the migration velocity. Previous studies show that the migration velocity is regulated by the motility-driving forces which are aerated by actin, microtubules and intermediate filaments networks, while the persistence is highly correlated with the velocity of protrusions and the ruffle frequency at the leading edge [105]–[107]. Numerous signals are involved in the actin networks to facilitate the migration of the cells. For instance, receptor tyrosine kinases (RTKs) and G protein-coupled receptors (GPCRs) control the cytoskeleton reorganization, and trimeric G proteins, small G proteins, lipid kinases, Ca^{2+} -dependent protein kinases, ROCK, and MAPKs influence the migration motility [108]. Further studies focusing on the mechanism of H_2O_2 -mediated acceleration are needed to gain a better understanding of the differential regulation of the cytoskeleton dynamics and the protrusion stability at the leading edge.

In addition, the spatial-temporal relationship of the H_2O_2 generation during the killer-target-bystander cell interaction remains unclear. The overall H_2O_2 in the killing environment was measured; however, the Amplex assay only determines the H_2O_2 concentration at a population level. It is reasonable to assume that H_2O_2 peaks at the time that killer cells encounter the bystander cells. To investigate the spatial-temporal relationship between H_2O_2 generation and killer cell behavior, the approaches with a single cell resolution are required. Combining microscopy and direct H_2O_2 detection approaches offers a possibility to measure the H_2O_2 in real time and indicate the spatiotemporal relationship of H_2O_2 generation and cell behaviors [109]. Besides, the H_2O_2 sensor proteins provide another valid tool to monitor H_2O_2 at a single cell level, as well to determine H_2O_2 concentration in different organelles at a subcellular level [110], [111].

The next question is whether all cells produce identical amount H_2O_2 in different tissues. In this study, the major resources producing environmental H_2O_2 are bystander cells. In comparison, killer cells and target cells generate little H_2O_2 , much lower than bystander cells (data not shown). H_2O_2 is mainly generated from the most prominent ROS member-superoxide anion (O_2^-), which is produced by either the mitochondrial electron transport chain [112], [113], or by NAD(P)H oxidases (NOXs) [114]. The O_2^- is rapidly converted to H_2O_2 by distinct superoxide dismutases (SODs). It is reported that ROS production is increased in various tissues, such as lung tissues [115], liver [116] and kidney [117]. At inflammation sites, a big amount of H_2O_2 is produced by immune cells, such as monocytes [118]. In some organs, for example in kidney, H_2O_2 -producing enzymes NADPH oxidases are expressed in a regional and cell-specific manner [117]. Therefore, it is to be expected that the bystander effect may be different and depend on the organ/tissue. Various cell types could function differently as bystanders in different tissues/microenvironments of tumor or inflammation sites.

5.1.3. The role of β integrin in bystander cell enhanced cytotoxicity

As the adhesion molecules, integrins have numerous biological functions via interacting with the ECM, which is important for cell adhesion, migration and immune function of NK and T cells [119]–[121]. The findings from our lab show that the three predominantly expressed integrin β -chains in killer cells are $\beta 1$, $\beta 2$, and $\beta 7$ (by Eva Schwarz, unpublished). The blockade of integrin $\beta 1$, $\beta 2$, and $\beta 7$ on killer cell surface diminishes only the bystander-enhanced NK persistence, but not NK velocity (Fig. 20). It is reported in human breast carcinoma cells that integrins are involved in regulating protrusion formation, which influences directional cells migration [122], [123]. For example, $\beta 1$ integrin functions in the persistent migration of cells in the developing posterior gonad arm of *C. Elegans* [124]. Dysfunction of $\alpha v \beta 3$ suppresses only the persistence but not the velocity of the migrational fibroblasts [125].

The soluble ECM competitor reduces the persistence of long-term cell migration and the stability of transient membrane protrusions [126].

Noticeably, how migration velocity and persistence is differentially regulated remains unclear. There are numerous mechanisms regulating directional migration without influencing velocities, such as PCP/non-canonical Wnt signaling pathway, small GTPases, and focal adhesion molecules [127]–[129]. Integrins can interact with small GTPase, lipids or protein kinases C [130] to steer the cell migration and adhesion. Therefore, in NK cells, one of these mentioned pathways or a hub of these signals could be a promising candidate to mediate integrin-regulated NK persistence.

5.1.4. Antigen transfer between cells

Above the discussed bystander cells and target cells are from different origins. In this regard, bystander cells enhance CTL- and NK-mediated cytotoxicity. When I test if unpulsed Raji cells as bystander can promote CTL-mediated cytotoxicity, I observed that the superantigens can be transferred from pulsed Raji cells to unpulsed Raji cells, leading to killing of the bystander unpulsed Raji cells (Fig. 9) therefore reducing target specific killing. Remaining SEA in the supernatant cannot explain this observation, since low antigen concentration (10 ng/ml) exhibited very limited killing (Fig. 26). This result is in line with other studies that tumor antigens are able to be transported from cancer cells to the antigen presenting cells [131], and certain cancer cells can transfer their antigens to the neighboring stromal cells, thus result in the bystander cell elimination [100]. This finding suggests that under certain circumstances, target cells could transfer their antigen to bystander cells. By this means, target cells could decrease the possibility to be killed by CTL in two ways: 1. Target cells reduce their own antigen concentration, which might lead to reduced killing. 2. By transferring antigens to innocent bystanders, killer cells will spend time to kill the bystanders thereby losing time to attack the real target cells.

The question arises, what the mechanism involved in the antigen transfer is. A likely possibility involve microvesicle pathways which are involved in mediating intracellular antigen transportation including trans-endocytosis, trogocytosis, exosomal transport, shuttle through nanotubes, and cell-contact-dependent intercellular transfer [132], [133]. For instance, dendritic cells release exosomes containing certain antigens to transfer the antigens to the tumor cells, thus trigger a strong CD8⁺ T-cell-dependent immune response against this tumor [134]. Tumor cells or pathogen-infected cells may use similar mechanism to transfer their antigen to innocent bystander cells, especially from the same origin, to partially escape immune surveillance.

5.2. The $[Ca^{2+}]_{ex}$ dependence of killing

As one of the most important second messenger in cells, Ca^{2+} plays a central role in the regulation of CTL functions. However, how environmental Ca^{2+} regulates the CTL killing efficiency is not yet fully understood. The second part of this work shows that the optimum concentration of extracellular Ca^{2+} for CTL-mediated cytotoxicity is between 130-800 μ M, much lower than the physiological concentration, which is about 1 mM. These findings were reproduced from findings in our laboratory by Friedmann, Hoxha, Knörck and Schwarz. Concomitantly, LG, the major killing machinery in CTL, is released the most in 132 μ M $[Ca^{2+}]_{ex}$ than at lower or higher $[Ca^{2+}]_{ex}$.

5.2.1. Optimal $[Ca^{2+}]_{ex}$ dependence for killer cell function

We have shown in the lab that $[Ca^{2+}]_{in}$ monotonically rises with increasing $[Ca^{2+}]_{ex}$ but not in a linear manner (Sebastian Mang, unpublished). ORAI1 is the main component of CRAC channel, which regulates Ca^{2+} influx [135]. It has been shown by the others [136] and us (Carmen Mangerich, Eva Schwarz and Carsten Kummerow, unpublished) that when ORAI1 is downregulated, the increase of intracellular Ca^{2+} in CTL is reduced upon stimulation. This

reduction in Ca^{2+} influx results in a significantly enhanced killing efficiency (Kim Friedmann, Fig. 28G). This observation is in line with the finding that CTL killing efficiency is higher in lower extracellular Ca^{2+} range (130-800 μM) compared to the physiological extracellular Ca^{2+} concentration (1 mM) (Fig. 25A). Taken together, these findings suggest that to eliminate target cells more efficiently, CTL requires lower intracellular Ca^{2+} concentration after target recognition, which can be mediated either with a low extracellular Ca^{2+} concentration in the environment or with a reduced CRAC/Orai1 Ca^{2+} channel activity.

Whether NK cells exhibit the same $[\text{Ca}^{2+}]_{\text{ex}}$ dependence is also of great importance. Finds by coworkers show that the primary NK cells and the NK cell line, NK92, have the best killing efficiency at the $[\text{Ca}^{2+}]_{\text{ex}}$ of around 1.7 mM (Yan Zhou and Rouven Schoppmeyer, unpublished). Different dependence of $[\text{Ca}^{2+}]_{\text{ex}}$ between CTL and NK cells suggests that the key regulator(s) or pathways to modulate Ca^{2+} dependent killing may differ in CTL and NK cells.

Is optimal $[\text{Ca}^{2+}]_{\text{ex}}$ different for different cell functions? Carpentieri *et al.* show that the optimal $[\text{Ca}^{2+}]_{\text{ex}}$ concentrations for thymidine incorporation of T cell is 2 mM [137]. CTLs have an optimal migration velocity at around 0.5 mM $[\text{Ca}^{2+}]_{\text{ex}}$ (Helene Lyrman and Carsten Kummerow *et al.*, unpublished). The proliferation of CTL requires an optimal $[\text{Ca}^{2+}]_{\text{ex}}$ higher than 4 μM (Arne Knörck, unpublished). These different optimal $[\text{Ca}^{2+}]_{\text{ex}}$ for different functions indicate that Ca^{2+} is a very versatile regulator of cell function. Different $[\text{Ca}^{2+}]_{\text{in}}$, mediated by different Ca^{2+} influx or extrusion activity and/or mediated by different $[\text{Ca}^{2+}]_{\text{ex}}$, can be used to differentiate between cell functions as has for instance also recently shown in melanoma cells, in which Ca^{2+} differentially regulates proliferation and metastasis [138].

5.2.2. Potential mechanism(s) mediating the $[Ca^{2+}]_{ex}$ dependence in killer cells

Coworkers and I have shown that killer cells elicit optimal cytotoxicity in a $[Ca^{2+}]_{ex}$ -dependent manner, however, the mechanism regulating the Ca^{2+} dependent killing remains unclear. First of all, what channel is involved in mediating the $[Ca^{2+}]_{ex}$ dependence is interesting. Calcium release-activated calcium (CRAC) channels, which consist of STIM and Orai proteins, are a major Ca^{2+} influx pathway in immune cells [139]. Since ORAI channels are Ca^{2+} -dependent inactivated, and the STIM1/Orai1 expression ratio influences the extent of Ca^{2+} -dependent inactivated [140], it is highly possible that intracellular Ca^{2+} does not increase monotonously with increasing extracellular Ca^{2+} concentrations. Apart from the CRAC channel ORAI1, other channels may also play a role in Ca^{2+} -dependent CTL killing. It is reported that the activation of Ca^{2+} -activated K^+ channels (K(Ca)) also has a strict dependence on the $[Ca^{2+}]_{in}$. Decreasing the $[Ca^{2+}]_{in}$ from 10 μ M to 1 μ M results in a higher open probability of K(Ca) channels [141]. Therefore, K(Ca) channels is also a good candidate to act independently or along with ORAI to regulate Ca^{2+} -optimized CTL killing.

In addition to $[Ca^{2+}]_{ex}$ channels, molecule(s) that respond to the $[Ca^{2+}]_{ex}$ variation and finely control LG fusion need to be considered. For the LG fusion step, there are probably molecules, which might sense the Ca^{2+} change. Among numerous Ca^{2+} sensors, synaptotagmins are found to be the major player in the SNARE complex to mediating the fast Ca^{2+} sensing [142]. Another Ca^{2+} sensor, synaptotagmin-like protein (SLP) that interact with different molecules in the fusion zipper complex of the vesicles, may also be involved in the regulation of $[Ca^{2+}]_{ex}$ dependent LG fusion [143].

LG pathway and the Fas/FasL are the two important pathways killer cells utilize to elicit the cytotoxicity [144], [145]. Whether Fas/FasL pathway has the same Ca^{2+} dependence is unclear,

although evidence shows that Fas/FasL pathway is regulated by Ca^{2+} . It is known that IP_3R , the Ca^{2+} regulated effector molecule, is involved in regulating the release of Fas molecules pathway, and increased $[\text{Ca}^{2+}]_{\text{ex}}$ notably increases the expression of both Fas and FasL molecules on T-cell hybridomas [146]–[149]. Noticeably, although still under debate, some studies show that the induced Fas upon immunoreceptor activation is stored in the lytic granules [150], [151]. Since GZB and PFN in the LG have the same $[\text{Ca}^{2+}]_{\text{ex}}$ dependent release kinetics, it is likely that the Fas molecules in the LG are also released with the same $[\text{Ca}^{2+}]_{\text{ex}}$ dependence as GZB and PFN. Given the fact that the optimal $[\text{Ca}^{2+}]_{\text{ex}}$ concentration for LG release is the same as for CTL killing, even if Fas has a different $[\text{Ca}^{2+}]_{\text{ex}}$ dependence, it would have only a very limited impact on $[\text{Ca}^{2+}]_{\text{ex}}$ -regulated CTL killing efficiency.

In summary, by the results observed and discussed above, I conclude for part 1 that bystander cells enhance killer cell mediated cytotoxicity via H_2O_2 -mediated migration velocity enhancement and $\beta 1$, 2, and 7 integrin-mediated persistence enhancement. I revealed a positive role of bystander cells in killer cell cytotoxicity. In part 2, coworkers and I show the optimal range of Ca^{2+} for CTL to elicit the killing machinery. These findings broaden our knowledge of the role of bystander cell as well as Ca^{2+} in regulating killer cell function, therefore allow new insights into the possible impact of the microenvironment on immune surveillance.

6. References

- [1] G. Gasteiger and A. Y. Rudensky, “Opinion: Interactions of innate and adaptive lymphocytes,” *Nat. Rev. Immunol.*, vol. 14, no. 9, pp. 631–639, Sep. 2014.
- [2] R. L. Gallo and T. Nakatsuji, “Microbial Symbiosis with the Innate Immune Defense System of the Skin,” *J. Invest. Dermatol.*, vol. 131, no. 10, pp. 1974–1980, Oct. 2011.
- [3] M. Ezzat Alnakip *et al.*, “The Immunology of Mammary Gland of Dairy Ruminants between Healthy and Inflammatory Conditions,” *J. Vet. Med.*, vol. 2014, 2014.
- [4] L. V. Hooper, D. R. Littman, and A. J. Macpherson, “Interactions between the microbiota and the immune system,” *Science*, vol. 336, no. 6086, pp. 1268–1273, Jun. 2012.
- [5] M. E. V. Johansson, H. Sjövall, and G. C. Hansson, “The gastrointestinal mucus system in health and disease,” *Nat. Rev. Gastroenterol. Hepatol.*, vol. 10, no. 6, pp. 352–361, Jun. 2013.
- [6] C. R. Gomez, V. Nomellini, D. E. Faunce, and E. J. Kovacs, “Innate immunity and aging,” *Exp. Gerontol.*, vol. 43, no. 8, pp. 718–728, Aug. 2008.
- [7] G. N. Kaufman, A. H. Massoud, M. Dembele, M. Yona, C. A. Piccirillo, and B. D. Mazer, “Induction of Regulatory T Cells by Intravenous Immunoglobulin: A Bridge between Adaptive and Innate Immunity,” *Front. Immunol.*, vol. 6, p. 469, 2015.
- [8] R. S. Raj, E. A. Bonney, and M. Phillippe, “Influenza, immune system, and pregnancy,” *Reprod. Sci. Thousand Oaks Calif*, vol. 21, no. 12, pp. 1434–1451, Dec. 2014.
- [9] R. Medzhitov and C. A. Janeway, “Innate immunity: Impact on the adaptive immune response,” *Curr. Opin. Immunol.*, vol. 9, no. 1, pp. 4–9, Feb. 1997.
- [10] S. Marusicgalesic, D. Stephany, D. Longo, and A. Kruisbeek, “Development of Cd4-Cd8+ Cyto-Toxic T-Cells Requires Interactions with Class-I Mhc Determinants,” *Nature*, vol. 333, no. 6169, pp. 180–183, May 1988.
- [11] S. M. Kaech and R. Ahmed, “Memory CD8+ T cell differentiation: initial antigen encounter triggers a developmental program in naïve cells,” *Nat. Immunol.*, vol. 2, no. 5, pp. 415–422, May 2001.
- [12] F. Sallusto, J. Geginat, and A. Lanzavecchia, “Central memory and effector memory T cell subsets: Function, generation, and maintenance,” *Annu. Rev. Immunol.*, vol. 22, pp. 745–763, 2004.
- [13] T. Boehm and J. B. Swann, “Origin and evolution of adaptive immunity,” *Annu. Rev. Anim. Biosci.*, vol. 2, pp. 259–283, Feb. 2014.
- [14] R. W. Dutton, L. M. Bradley, and S. L. Swain, “T Cell Memory,” *Annu. Rev. Immunol.*, vol. 16, no. 1, pp. 201–223, 1998.
- [15] O. Dushek and P. A. van der Merwe, “An induced rebinding model of antigen discrimination,” *Trends Immunol.*, vol. 35, no. 4, pp. 153–158, Apr. 2014.
- [16] H. Spits *et al.*, “Early stages in the development of human T, natural killer and thymic dendritic cells,” *Immunol. Rev.*, vol. 165, pp. 75–86, Oct. 1998.
- [17] A. G. Rolink, S. Massa, G. Balciunaite, and R. Ceredig, “Early lymphocyte development in bone marrow and thymus,” *Swiss Med. Wkly.*, vol. 137 Suppl 155, p. 20S–24S, Mar. 2007.
- [18] H. von Boehmer and H. J. Fehling, “Structure and function of the pre-T cell receptor,” *Annu. Rev. Immunol.*, vol. 15, pp. 433–452, 1997.
- [19] J. Nedjic, M. Aichinger, and L. Klein, “Autophagy and T cell education in the thymus Eat yourself to know yourself,” *Cell Cycle*, vol. 7, no. 23, pp. 3625–3628, Dec. 2008.

- [20] Timothy K. Starr, Stephen C. Jameson, and K. A. Hogquist, "Positive and Negative Selection of T Cells," *Annu. Rev. Immunol.*, vol. 21, no. 1, pp. 139–176, 2003.
- [21] M. Wencker, L. Gazzolo, and M. Duc Dodon, "The leukemogenic activity of TaxHTLV-1 during human alphabeta T cell development," *Front. Biosci. Sch. Ed.*, vol. 1, pp. 194–204, 2009.
- [22] K. K. Baldwin, B. P. Trenchak, J. D. Altman, and M. M. Davis, "Negative selection of T cells occurs throughout thymic development," *J. Immunol. Baltim. Md 1950*, vol. 163, no. 2, pp. 689–698, Jul. 1999.
- [23] S. Balkow *et al.*, "Concerted Action of the FasL/Fas and Perforin/Granzyme A and B Pathways Is Mandatory for the Development of Early Viral Hepatitis but Not for Recovery from Viral Infection," *J. Virol.*, vol. 75, no. 18, pp. 8781–8791, Sep. 2001.
- [24] M. L. Dustin, "The immunological synapse," *Cancer Immunol. Res.*, vol. 2, no. 11, pp. 1023–1033, Nov. 2014.
- [25] S. Radoja, M. Saio, D. Schaer, M. Koneru, S. Vukmanovic, and A. B. Frey, "CD8(+) tumor-infiltrating T cells are deficient in perforin-mediated cytolytic activity due to defective microtubule-organizing center mobilization and lytic granule exocytosis," *J. Immunol.*, vol. 167, no. 9, pp. 5042–5051, Nov. 2001.
- [26] T. N. Sims *et al.*, "Opposing effects of PKC theta and WASp on symmetry breaking and relocation of the immunological synapse," *Cell*, vol. 129, no. 4, pp. 773–785, May 2007.
- [27] G. de Saint Basile, G. Ménasché, and A. Fischer, "Molecular mechanisms of biogenesis and exocytosis of cytotoxic granules," *Nat. Rev. Immunol.*, vol. 10, no. 8, pp. 568–579, Aug. 2010.
- [28] P. Anton van der Merwe, S. J. Davis, A. S. Shaw, and M. L. Dustin, "Cytoskeletal polarization and redistribution of cell-surface molecules during T cell antigen recognition," *Semin. Immunol.*, vol. 12, no. 1, pp. 5–21, Feb. 2000.
- [29] M. J. Pinkoski *et al.*, "Entry and trafficking of granzyme B in target cells during granzyme B-perforin-mediated apoptosis," *Blood*, vol. 92, no. 3, pp. 1044–1054, Aug. 1998.
- [30] A. Grakoui *et al.*, "Pillars article: The immunological synapse: a molecular machine controlling T cell activation. Science. 1999. 285: 221-227," *J. Immunol. Baltim. Md 1950*, vol. 194, no. 9, pp. 4066–4072, May 2015.
- [31] M. Oh-hora and A. Rao, "Calcium signaling in lymphocytes," *Curr. Opin. Immunol.*, vol. 20, no. 3, pp. 250–258, Jun. 2008.
- [32] L. M. Kingeter, S. Paul, S. K. Maynard, N. G. Cartwright, and B. C. Schaefer, "Cutting edge: TCR ligation triggers digital activation of NF-kappaB," *J. Immunol. Baltim. Md 1950*, vol. 185, no. 8, pp. 4520–4524, Oct. 2010.
- [33] M. Hoth and R. Penner, "Depletion of intracellular calcium stores activates a calcium current in mast cells," *Nature*, vol. 355, no. 6358, pp. 353–356, Jan. 1992.
- [34] S. Feske, "Calcium signalling in lymphocyte activation and disease," *Nat. Rev. Immunol.*, vol. 7, no. 9, pp. 690–702, Sep. 2007.
- [35] L. L. Nohara, S. R. Stanwood, K. D. Omilusik, and W. A. Jefferies, "Tweeters, Woofers and Horns: The Complex Orchestration of Calcium Currents in T Lymphocytes," *Front. Immunol.*, vol. 6, p. 234, 2015.
- [36] R. B. Martin, "Calcium in biological systems," *Inorganica Chim. Acta*, vol. 79, p. 39, Jan. 1983.
- [37] M. Yáñez, J. Gil-Longo, and M. Campos-Toimil, "Calcium binding proteins," *Adv. Exp. Med. Biol.*, vol. 740, pp. 461–482, 2012.
- [38] R. S. Lewis, "Calcium signaling mechanisms in T lymphocytes," *Annu. Rev. Immunol.*, vol. 19, pp. 497–521, 2001.

- [39] M. J. Berridge, "The versatility and complexity of calcium signalling," *Novartis Found. Symp.*, vol. 239, pp. 52-64-67, 150-159, 2001.
- [40] D. R. Davila, J. L. Lane, F. T. Lauer, and S. W. Burchiel, "Protein tyrosine kinase activation by polycyclic aromatic hydrocarbons in human HPB-ALL T cells," *J. Toxicol. Environ. Health A*, vol. 56, no. 4, pp. 249-261, Feb. 1999.
- [41] J. Jacobelli, S. A. Chmura, D. B. Buxton, M. M. Davis, and M. F. Krummel, "A single class II myosin modulates T cell motility and stopping, but not synapse formation," *Nat. Immunol.*, vol. 5, no. 5, pp. 531-538, May 2004.
- [42] M. Savignac, B. Mellström, and J. R. Naranjo, "Calcium-dependent transcription of cytokine genes in T lymphocytes," *Pflüg. Arch. Eur. J. Physiol.*, vol. 454, no. 4, pp. 523-533, Jul. 2007.
- [43] P. J. Shaw and S. Feske, "Physiological and pathophysiological functions of SOCE in the immune system," *Front. Biosci. Elite Ed.*, vol. 4, pp. 2253-2268, 2012.
- [44] G. R. Monteith, F. M. Davis, and S. J. Roberts-Thomson, "Calcium Channels and Pumps in Cancer: Changes and Consequences," *J. Biol. Chem.*, vol. 287, no. 38, pp. 31666-31673, Sep. 2012.
- [45] M. C. Curry, S. J. Roberts-Thomson, and G. R. Monteith, "Plasma membrane calcium ATPases and cancer," *BioFactors Oxf. Engl.*, vol. 37, no. 3, pp. 132-138, Jun. 2011.
- [46] M. Feng *et al.*, "Store-independent activation of orai1 by SPCA2 in mammary tumors," *Cell*, vol. 143, no. 1, pp. 84-98, 2010.
- [47] K. Kunzelmann, "Ion Channels and Cancer," *J. Membr. Biol.*, vol. 205, no. 3, pp. 159-173, Jun. 2005.
- [48] P. H. Ratz, K. M. Berg, N. H. Urban, and A. S. Miner, "Regulation of smooth muscle calcium sensitivity: KCl as a calcium-sensitizing stimulus," *Am. J. Physiol. Cell Physiol.*, vol. 288, no. 4, pp. C769-783, Apr. 2005.
- [49] K. Shibao *et al.*, "The type III inositol 1,4,5-trisphosphate receptor is associated with aggressiveness of colorectal carcinoma," *Cell Calcium*, vol. 48, no. 6, pp. 315-323, Dec. 2010.
- [50] F. D. Virgilio, "Purines, Purinergic Receptors, and Cancer," *Cancer Res.*, vol. 72, no. 21, pp. 5441-5447, Nov. 2012.
- [51] F. Li *et al.*, "Intracellular Released Payload Influences Potency and Bystander-Killing Effects of Antibody-Drug Conjugates in Preclinical Models," *Cancer Res.*, vol. 76, no. 9, pp. 2710-2719, May 2016.
- [52] J. Yang and R. A. Weinberg, "Epithelial-mesenchymal transition: At the crossroads of development and tumor metastasis," *Dev. Cell*, vol. 14, no. 6, pp. 818-829, Jun. 2008.
- [53] A. P. West *et al.*, "TLR signalling augments macrophage bactericidal activity through mitochondrial ROS," *Nature*, vol. 472, no. 7344, pp. 476-480, Apr. 2011.
- [54] T. Celhar *et al.*, "TLR7 and TLR9 ligands regulate antigen presentation by macrophages," *Int. Immunol.*, vol. 28, no. 5, pp. 223-232, May 2016.
- [55] T. H. Schreiber, D. Wolf, M. Boder, and E. Podack, "Tumor antigen specific iTreg accumulate in the tumor microenvironment and suppress therapeutic vaccination," *Oncoimmunology*, vol. 1, no. 5, pp. 642-648, Aug. 2012.
- [56] "Regulating the immune system: the induction of ..." [Online]. Available: http://xueshu.baidu.com/s?wd=paperuri%3A%28abbca6654f92d441b952640780c861d6%29&filter=sc_long_sign&tn=SE_xueshusource_2kduw22v&sc_vurl=http%3A%2F%2Fwww.ncbi.nlm.nih.gov%2Fpmc%2Farticles%2FPMC546291%2F&ie=utf-8&sc_us=2524338631630888772. [Accessed: 04-Feb-2017].
- [57] M. Cao *et al.*, "Kinase inhibitor Sorafenib modulates immunosuppressive cell populations in a murine liver cancer model," *Lab. Invest. J. Tech. Methods Pathol.*, vol. 91, no. 4, pp. 598-608, Apr. 2011.

- [58] K. Sakakura and K. Chikamatsu, “Immune suppression and evasion in patients with head and neck cancer,” *Adv. Cell. Mol. Otolaryngol.*, vol. 1, no. 0, Jul. 2013.
- [59] T. Martin, S. F. Duffy, D. A. Carson, and T. J. Kipps, “Evidence for somatic selection of natural autoantibodies,” *J. Exp. Med.*, vol. 175, no. 4, pp. 983–991, Apr. 1992.
- [60] T. Blankenstein, M. Leisegang, W. Uckert, and H. Schreiber, “Targeting cancer-specific mutations by T cell receptor gene therapy,” *Curr. Opin. Immunol.*, vol. 33, pp. 112–119, Apr. 2015.
- [61] K. G. Lucas, L. Bao, R. Bruggeman, K. Dunham, and C. Specht, “The detection of CMV pp65 and IE1 in glioblastoma multiforme,” *J. Neurooncol.*, vol. 103, no. 2, pp. 231–238, Jun. 2011.
- [62] R. Biassoni *et al.*, “Human natural killer cell receptors and co-receptors,” *Immunol. Rev.*, vol. 181, pp. 203–214, Jun. 2001.
- [63] E. C. Schwarz *et al.*, “Calcium dependence of T cell proliferation following focal stimulation,” *Eur. J. Immunol.*, vol. 37, no. 10, pp. 2723–2733, Oct. 2007.
- [64] C. Kummerow, E. C. Schwarz, B. Bufe, F. Zufall, M. Hoth, and B. Qu, “A simple, economic, time-resolved killing assay,” *Eur. J. Immunol.*, vol. 44, no. 6, pp. 1870–1872, Jun. 2014.
- [65] S. S. Bhat *et al.*, “Syntaxin 8 is required for efficient lytic granule trafficking in cytotoxic T lymphocytes,” *Biochim. Biophys. Acta*, vol. 1863, no. 7 Pt A, pp. 1653–1664, Jul. 2016.
- [66] C. Kummerow, E. C. Schwarz, B. Bufe, F. Zufall, M. Hoth, and B. Qu, “A simple, economic, time-resolved killing assay,” *Eur. J. Immunol.*, vol. 44, no. 6, pp. 1870–1872, Jun. 2014.
- [67] G. V. Z. Dedoussis, A. C. Kaliora, and N. K. Andrikopoulos, “Effect of phenols on natural killer (NK) cell-mediated death in the K562 human leukemic cell line,” *Cell Biol. Int.*, vol. 29, no. 11, pp. 884–889, Nov. 2005.
- [68] Z. Xiao *et al.*, “Bystander cells enhance NK cytotoxic efficiency by reducing search time,” *Sci. Rep.*, Feb. 2017.
- [69] K. Franciszkiewicz *et al.*, “Synaptic release of CCL5 storage vesicles triggers CXCR4 surface expression promoting CTL migration in response to CXCL12,” *J. Immunol. Baltim. Md 1950*, vol. 193, no. 10, pp. 4952–4961, Nov. 2014.
- [70] A. C. Repp, E. S. Mayhew, S. Apte, and J. Y. Niederkorn, “Human uveal melanoma cells produce macrophage migration-inhibitory factor to prevent lysis by NK cells,” *J. Immunol. Baltim. Md 1950*, vol. 165, no. 2, pp. 710–715, Jul. 2000.
- [71] T. Oettel and M. Dzugasov, “Anomalous diffusion in supercooled liquids: a long-range localization in particle trajectories,” *J. Chem. Phys.*, vol. 131, no. 4, p. 44510, Jul. 2009.
- [72] J. S. van Zon and P. R. ten Wolde, “Green’s-function reaction dynamics: a particle-based approach for simulating biochemical networks in time and space,” *J. Chem. Phys.*, vol. 123, no. 23, p. 234910, Dec. 2005.
- [73] M. J. Saxton, “Lateral diffusion in an archipelago. Distance dependence of the diffusion coefficient,” *Biophys. J.*, vol. 56, no. 3, pp. 615–622, Sep. 1989.
- [74] S. Alampour-Rajabi *et al.*, “MIF interacts with CXCR7 to promote receptor internalization, ERK1/2 and ZAP-70 signaling, and lymphocyte chemotaxis,” *FASEB J. Off. Publ. Fed. Am. Soc. Exp. Biol.*, vol. 29, no. 11, pp. 4497–4511, Nov. 2015.
- [75] G. Cinamon, V. Shinder, R. Shamri, and R. Alon, “Chemoattractant signals and beta 2 integrin occupancy at apical endothelial contacts combine with shear stress signals to promote transendothelial neutrophil migration,” *J. Immunol. Baltim. Md 1950*, vol. 173, no. 12, pp. 7282–7291, Dec. 2004.

- [76] S. Gonzalvo-Feo *et al.*, “Endothelial cell-derived chemerin promotes dendritic cell transmigration,” *J. Immunol. Baltim. Md 1950*, vol. 192, no. 5, pp. 2366–2373, Mar. 2014.
- [77] J. M. Roda, R. Parihar, A. Lehman, A. Mani, S. Tridandapani, and W. E. Carson, “Interleukin-21 enhances NK cell activation in response to antibody-coated targets,” *J. Immunol. Baltim. Md 1950*, vol. 177, no. 1, pp. 120–129, Jul. 2006.
- [78] C. Collins and W. J. Nelson, “Running with neighbors: coordinating cell migration and cell-cell adhesion,” *Curr. Opin. Cell Biol.*, vol. 36, pp. 62–70, Oct. 2015.
- [79] F. Kukulski, F. Ben Yebdri, F. Bahrami, M. Fausther, A. Tremblay, and J. Sévigny, “Endothelial P2Y2 receptor regulates LPS-induced neutrophil transendothelial migration in vitro,” *Mol. Immunol.*, vol. 47, no. 5, pp. 991–999, Feb. 2010.
- [80] W. Razzell, I. R. Evans, P. Martin, and W. Wood, “Calcium flashes orchestrate the wound inflammatory response through DUOX activation and hydrogen peroxide release,” *Curr. Biol. CB*, vol. 23, no. 5, pp. 424–429, Mar. 2013.
- [81] M. Skinner, “Cell migration. H₂O₂ sensing: the missing ‘Lynk,’” *Nat. Rev. Mol. Cell Biol.*, vol. 13, no. 1, pp. 2–3, Jan. 2012.
- [82] D. Sieger, C. Moritz, T. Ziegenhals, S. Prykhozhij, and F. Peri, “Long-range Ca²⁺ waves transmit brain-damage signals to microglia,” *Dev. Cell*, vol. 22, no. 6, pp. 1138–1148, Jun. 2012.
- [83] H. Y. Wang and R.-F. Wang, “Regulatory T cells and cancer,” *Curr. Opin. Immunol.*, vol. 19, no. 2, pp. 217–223, Apr. 2007.
- [84] C.-Y. Zhang *et al.*, “The role of CCL20/CCR6 axis in recruiting Treg cells to tumor sites of NSCLC patients,” *Biomed. Pharmacother. Bioméd. Pharmacothérapie*, vol. 69, pp. 242–248, Feb. 2015.
- [85] E. O. Long, H. S. Kim, D. Liu, M. E. Peterson, and S. Rajagopalan, “Controlling Natural Killer Cell Responses: Integration of Signals for Activation and Inhibition,” *Annu. Rev. Immunol.*, vol. 31, no. 1, pp. 227–258, 2013.
- [86] E. D. Hall, K. E. Pazara, and J. M. Braugher, “Effects of tirilazad mesylate on postischemic brain lipid peroxidation and recovery of extracellular calcium in gerbils,” *Stroke*, vol. 22, no. 3, pp. 361–366, Mar. 1991.
- [87] R. Sauerheber, “Physiologic Conditions Affect Toxicity of Ingested Industrial Fluoride,” *J. Environ. Public Health*, vol. 2013, 2013.
- [88] M. Peacock, “Calcium Metabolism in Health and Disease,” *Clin. J. Am. Soc. Nephrol.*, vol. 5, no. Supplement 1, pp. S23–S30, Jan. 2010.
- [89] S. I. Djomehri *et al.*, “Mineral density volume gradients in normal and diseased human tissues,” *PLoS One*, vol. 10, no. 4, p. e0121611, 2015.
- [90] C. Steenbergen, T. A. Fralix, and E. Murphy, “Role of increased cytosolic free calcium concentration in myocardial ischemic injury,” *Basic Res. Cardiol.*, vol. 88, no. 5, pp. 456–470, Oct. 1993.
- [91] F. M. Davis *et al.*, “Induction of epithelial-mesenchymal transition (EMT) in breast cancer cells is calcium signal dependent,” *Oncogene*, vol. 33, no. 18, pp. 2307–2316, May 2014.
- [92] T. Kohno *et al.*, “High-mobility group box 1 protein blockade suppresses development of abdominal aortic aneurysm,” *J. Cardiol.*, vol. 59, no. 3, pp. 299–306, May 2012.
- [93] N. Prevarskaya, R. Skryma, and Y. Shuba, “Calcium in tumour metastasis: new roles for known actors,” *Nat. Rev. Cancer*, vol. 11, no. 8, pp. 609–618, Aug. 2011.
- [94] V. Robert, E. Triffaux, M. Savignac, and L. Pelletier, “Singularities of calcium signaling in effector T-lymphocytes,” *Biochim. Biophys. Acta*, vol. 1833, no. 7, pp. 1595–1602, Jul. 2013.

- [95] J. A. Lopez *et al.*, “Perforin forms transient pores on the target cell plasma membrane to facilitate rapid access of granzymes during killer cell attack,” *Blood*, vol. 121, no. 14, pp. 2659–2668, Apr. 2013.
- [96] M. R. Marshall *et al.*, “VAMP8-dependent fusion of recycling endosomes with the plasma membrane facilitates T lymphocyte cytotoxicity,” *J. Cell Biol.*, vol. 210, no. 1, pp. 135–151, Jul. 2015.
- [97] Y. Nakanishi, B. Lu, C. Gerard, and A. Iwasaki, “CD8(+) T lymphocyte mobilization to virus-infected tissue requires CD4(+) T-cell help,” *Nature*, vol. 462, no. 7272, pp. 510–513, Nov. 2009.
- [98] C. Savarin, S. A. Stohlman, R. Atkinson, R. M. Ransohoff, and C. C. Bergmann, “Monocytes Regulate T Cell Migration through the Glia Limitans during Acute Viral Encephalitis,” *J. Virol.*, vol. 84, no. 10, pp. 4878–4888, May 2010.
- [99] J. Watt and H. M. Kocher, “The desmoplastic stroma of pancreatic cancer is a barrier to immune cell infiltration,” *Oncoimmunology*, vol. 2, no. 12, p. e26788, Dec. 2013.
- [100] A. Schietinger, M. Philip, R. B. Liu, K. Schreiber, and H. Schreiber, “Bystander killing of cancer requires the cooperation of CD4(+) and CD8(+) T cells during the effector phase,” *J. Exp. Med.*, vol. 207, no. 11, pp. 2469–2477, Oct. 2010.
- [101] S. I. Grivennikov, F. R. Greten, and M. Karin, “Immunity, Inflammation, and Cancer,” *Cell*, vol. 140, no. 6, pp. 883–899, Mar. 2010.
- [102] J. Jiang, C. Wu, and B. Lu, “Cytokine-induced killer cells promote antitumor immunity,” *J. Transl. Med.*, vol. 11, p. 83, Mar. 2013.
- [103] S. Wang *et al.*, “ α -Synuclein, a chemoattractant, directs microglial migration via H₂O₂-dependent Lyn phosphorylation,” *Proc. Natl. Acad. Sci. U. S. A.*, vol. 112, no. 15, pp. E1926–E1935, Apr. 2015.
- [104] P. Niethammer, C. Grabher, A. T. Look, and T. J. Mitchison, “A tissue-scale gradient of hydrogen peroxide mediates rapid wound detection in zebrafish,” *Nature*, vol. 459, no. 7249, pp. 996–999, Jun. 2009.
- [105] R. Ananthkrishnan and A. Ehrlicher, “The Forces Behind Cell Movement,” *Int. J. Biol. Sci.*, vol. 3, no. 5, pp. 303–317, Jun. 2007.
- [106] S. P. Chaki *et al.*, “Nck enables directional cell migration through the coordination of polarized membrane protrusion with adhesion dynamics,” *J Cell Sci*, vol. 126, no. 7, pp. 1637–1649, Apr. 2013.
- [107] S. L. Gupton *et al.*, “Cell migration without a lamellipodium translation of actin dynamics into cell movement mediated by tropomyosin,” *J. Cell Biol.*, vol. 168, no. 4, pp. 619–631, Feb. 2005.
- [108] W. T. Gerthoffer, “Mechanisms of Vascular Smooth Muscle Cell Migration,” *Circ. Res.*, vol. 100, no. 5, pp. 607–621, Mar. 2007.
- [109] A. V. Kuznetsov *et al.*, “Mitochondrial ROS production under cellular stress: comparison of different detection methods,” *Anal. Bioanal. Chem.*, vol. 400, no. 8, pp. 2383–2390, Jun. 2011.
- [110] S. G. Rhee, T.-S. Chang, W. Jeong, and D. Kang, “Methods for detection and measurement of hydrogen peroxide inside and outside of cells,” *Mol. Cells*, vol. 29, no. 6, pp. 539–549, Jun. 2010.
- [111] M. Malinouski, Y. Zhou, V. V. Belousov, D. L. Hatfield, and V. N. Gladyshev, “Hydrogen Peroxide Probes Directed to Different Cellular Compartments,” *PLOS ONE*, vol. 6, no. 1, p. e14564, Jan. 2011.
- [112] M. Ott, V. Gogvadze, S. Orrenius, and B. Zhivotovsky, “Mitochondria, oxidative stress and cell death,” *Apoptosis Int. J. Program. Cell Death*, vol. 12, no. 5, pp. 913–922, May 2007.

- [113] M. P. Murphy, “How mitochondria produce reactive oxygen species,” *Biochem. J.*, vol. 417, no. Pt 1, pp. 1–13, Jan. 2009.
- [114] K. Bedard and K.-H. Krause, “The NOX family of ROS-generating NADPH oxidases: physiology and pathophysiology,” *Physiol. Rev.*, vol. 87, no. 1, pp. 245–313, Jan. 2007.
- [115] A. B. Al-Mehdi, H. Shuman, and A. B. Fisher, “Intracellular generation of reactive oxygen species during nonhypoxic lung ischemia,” *Am. J. Physiol.*, vol. 272, no. 2 Pt 1, pp. L294–300, Feb. 1997.
- [116] T. A. Young, C. C. Cunningham, and S. M. Bailey, “Reactive oxygen species production by the mitochondrial respiratory chain in isolated rat hepatocytes and liver mitochondria: studies using myxothiazol,” *Arch. Biochem. Biophys.*, vol. 405, no. 1, pp. 65–72, Sep. 2002.
- [117] M. Sedeek, R. Nasrallah, R. M. Touyz, and R. L. Hébert, “NADPH oxidases, reactive oxygen species, and the kidney: friend and foe,” *J. Am. Soc. Nephrol. JASN*, vol. 24, no. 10, pp. 1512–1518, Oct. 2013.
- [118] R. C. N. Melo, D. L. Fabrino, H. D’Avila, H. C. Teixeira, and A. P. Ferreira, “Production of hydrogen peroxide by peripheral blood monocytes and specific macrophages during experimental infection with *Trypanosoma cruzi* in vivo,” *Cell Biol. Int.*, vol. 27, no. 10, pp. 853–861, 2003.
- [119] A. Huttenlocher and A. R. Horwitz, “Integrins in cell migration,” *Cold Spring Harb. Perspect. Biol.*, vol. 3, no. 9, p. a005074, Sep. 2011.
- [120] M. E. Janik, A. Lityńska, and P. Vereecken, “Cell migration—the role of integrin glycosylation,” *Biochim. Biophys. Acta*, vol. 1800, no. 6, pp. 545–555, Jun. 2010.
- [121] D. Liu, Y. T. Bryceson, T. Meckel, G. Vasiliver-Shamis, M. L. Dustin, and E. O. Long, “Integrin-dependent organization and bidirectional vesicular traffic at cytotoxic immune synapses,” *Immunity*, vol. 31, no. 1, pp. 99–109, Jul. 2009.
- [122] P. Costa, T. M. E. Scales, J. Ivaska, and M. Parsons, “Integrin-specific control of focal adhesion kinase and RhoA regulates membrane protrusion and invasion,” *PLoS One*, vol. 8, no. 9, p. e74659, 2013.
- [123] M. A. Schwartz and A. R. Horwitz, “Integrating adhesion, protrusion, and contraction during cell migration,” *Cell*, vol. 125, no. 7, pp. 1223–1225, Jun. 2006.
- [124] M. Shafaq-Zadah *et al.*, “Persistent cell migration and adhesion rely on retrograde transport of $\beta(1)$ integrin,” *Nat. Cell Biol.*, vol. 18, no. 1, pp. 54–64, Jan. 2016.
- [125] D. P. White, P. T. Caswell, and J. C. Norman, “ $\alpha v \beta 3$ and $\alpha 5 \beta 1$ integrin recycling pathways dictate downstream Rho kinase signaling to regulate persistent cell migration,” *J. Cell Biol.*, vol. 177, no. 3, pp. 515–525, May 2007.
- [126] B. D. Harms, G. M. Bassi, A. R. Horwitz, and D. A. Lauffenburger, “Directional Persistence of EGF-Induced Cell Migration Is Associated with Stabilization of Lamellipodial Protrusions,” *Biophys. J.*, vol. 88, no. 2, pp. 1479–1488, Feb. 2005.
- [127] J. E. Burdizzo, Á. González, and C. O. Arregui, “PTP1B promotes focal complex maturation, lamellar persistence and directional migration,” *J Cell Sci*, vol. 126, no. 8, pp. 1820–1831, Apr. 2013.
- [128] S. Kuriyama and R. Mayor, “Molecular analysis of neural crest migration,” *Philos. Trans. R. Soc. Lond. B Biol. Sci.*, vol. 363, no. 1495, pp. 1349–1362, Apr. 2008.
- [129] R. Pankov *et al.*, “A Rac switch regulates random versus directionally persistent cell migration,” *J. Cell Biol.*, vol. 170, no. 5, pp. 793–802, Aug. 2005.
- [130] S. Wiesner, K. R. Legate, and R. Fässler, “Integrin-actin interactions,” *Cell. Mol. Life Sci. CMLS*, vol. 62, no. 10, pp. 1081–1099, May 2005.
- [131] S. Dai *et al.*, “Enhanced induction of dendritic cell maturation and HLA-A*0201-restricted CEA-specific CD8(+) CTL response by exosomes derived from IL-18 gene-

- modified CEA-positive tumor cells,” *J. Mol. Med. Berl. Ger.*, vol. 84, no. 12, pp. 1067–1076, Dec. 2006.
- [132] C. Kahlert and R. Kalluri, “Exosomes in Tumor Microenvironment Influence Cancer Progression and Metastasis,” *J. Mol. Med. Berl. Ger.*, vol. 91, no. 4, pp. 431–437, Apr. 2013.
- [133] O. Rechavi, I. Goldstein, and Y. Kloog, “Intercellular exchange of proteins: The immune cell habit of sharing,” *FEBS Lett.*, vol. 583, no. 11, pp. 1792–1799, Jun. 2009.
- [134] C. Théry, L. Duban, E. Segura, P. Véron, O. Lantz, and S. Amigorena, “Indirect activation of naïve CD4+ T cells by dendritic cell-derived exosomes,” *Nat. Immunol.*, vol. 3, no. 12, pp. 1156–1162, Dec. 2002.
- [135] “PubMed entry.”
- [136] H. Kito *et al.*, “Regulation of store-operated Ca²⁺ entry activity by cell cycle dependent up-regulation of Orai2 in brain capillary endothelial cells,” *Biochem. Biophys. Res. Commun.*, vol. 459, no. 3, pp. 457–462, Apr. 2015.
- [137] U. Carpentieri, J. Myers, C. W. Daeschner, and M. E. Haggard, “Effects of iron, copper, zinc, calcium, and magnesium on human lymphocytes in culture,” *Biol. Trace Elem. Res.*, vol. 16, no. 2, pp. 165–176, Jul. 1988.
- [138] H. Stanisz, A. Vultur, M. Herlyn, A. Roesch, and I. Bogeski, “The role of Orai-STIM calcium channels in melanocytes and melanoma,” *J. Physiol.*, vol. 594, no. 11, pp. 2825–2835, Jun. 2016.
- [139] M. Hoth, “CRAC channels, calcium, and cancer in light of the driver and passenger concept,” *Biochim. Biophys. Acta BBA - Mol. Cell Res.*, vol. 1863, no. 6, Part B, pp. 1408–1417, Jun. 2016.
- [140] P. J. Hoover and R. S. Lewis, “Stoichiometric requirements for trapping and gating of Ca²⁺ release-activated Ca²⁺ (CRAC) channels by stromal interaction molecule 1 (STIM1),” *Proc. Natl. Acad. Sci. U. S. A.*, vol. 108, no. 32, pp. 13299–13304, Aug. 2011.
- [141] S. Grissmer, A. N. Nguyen, and M. D. Cahalan, “Calcium-activated potassium channels in resting and activated human T lymphocytes. Expression levels, calcium dependence, ion selectivity, and pharmacology,” *J. Gen. Physiol.*, vol. 102, no. 4, pp. 601–630, Oct. 1993.
- [142] S. D. Meriney, J. A. Umbach, and C. B. Gundersen, “Fast, Ca²⁺-dependent exocytosis at nerve terminals: shortcomings of SNARE-based models,” *Prog. Neurobiol.*, vol. 121, pp. 55–90, Oct. 2014.
- [143] T. S. Kuroda, M. Fukuda, H. Ariga, and K. Mikoshiba, “The Slp homology domain of synaptotagmin-like proteins 1–4 and Slac2 functions as a novel Rab27A binding domain,” *J. Biol. Chem.*, vol. 277, no. 11, pp. 9212–9218, Mar. 2002.
- [144] J. H. Russell and T. J. Ley, “Lymphocyte-mediated cytotoxicity,” *Annu. Rev. Immunol.*, vol. 20, pp. 323–370, 2002.
- [145] Y. Zou *et al.*, “Increased killing of liver NK cells by Fas/Fas ligand and NKG2D/NKG2D ligand contributes to hepatocyte necrosis in virus-induced liver failure,” *J. Immunol. Baltim. Md 1950*, vol. 184, no. 1, pp. 466–475, Jan. 2010.
- [146] T. Brunner *et al.*, “Cell-autonomous Fas (CD95)/Fas-ligand interaction mediates activation-induced apoptosis in T-cell hybridomas,” *Nature*, vol. 373, no. 6513, pp. 441–444, Feb. 1995.
- [147] K. Ayub, I. Laffafian, S. Dewitt, and M. B. Hallett, “Ca influx shutdown in neutrophils induced by Fas (CD95) cross-linking,” *Immunology*, vol. 112, no. 3, pp. 454–460, Jul. 2004.
- [148] D. Boehning, D. B. van Rossum, R. L. Patterson, and S. H. Snyder, “A peptide inhibitor of cytochrome c/inositol 1,4,5-trisphosphate receptor binding blocks intrinsic and

References

- extrinsic cell death pathways,” *Proc. Natl. Acad. Sci. U. S. A.*, vol. 102, no. 5, pp. 1466–1471, Feb. 2005.
- [149] A. L. Wozniak, X. Wang, E. S. Stieren, S. G. Scarbrough, C. J. Elferink, and D. Boehning, “Requirement of biphasic calcium release from the endoplasmic reticulum for Fas-mediated apoptosis,” *J. Cell Biol.*, vol. 175, no. 5, pp. 709–714, Dec. 2006.
- [150] J.-S. He and H. L. Ostergaard, “CTLs Contain and Use Intracellular Stores of FasL Distinct from Cytolytic Granules,” *J. Immunol.*, vol. 179, no. 4, pp. 2339–2348, Aug. 2007.
- [151] E. Rouvier, M. F. Luciani, and P. Golstein, “Fas involvement in Ca(2+)-independent T cell-mediated cytotoxicity,” *J. Exp. Med.*, vol. 177, no. 1, pp. 195–200, Jan. 1993.

7. Publications

1. Jessica Law, Anna Susloparova, Xuan Thang Vu, **Xiao Zhou**, Felix Hempel, Bin Qu, Markus Hoth, and Sven Ingebrandt. 2015. Human T cells monitored by impedance spectrometry using field-effect transistor arrays: A novel tool for single-cell adhesion and migration studies. *Biosens. Bioelectron.* 67: 170–176.
2. **Xiao Zhou**, Rengping Zhao, Karsten Schwarz, Matthieu Mangeat, Eva C. Schwarz, Mohamed Hamed, Ivan Bogeski, Volkhard Helms, Heiko Rieger, Bin Qu. 2017. Bystander cells enhance NK cytotoxic efficiency by reducing search time. *Scientific Reports*.
3. Rouven Schoppmeyer*, Rengping Zhao*, He Cheng, Chen Liu, **Xiao Zhou**, Eva C. Schwarz¹, Yan Zhou, Arne Knörck, Mohamed Hamed, Gertrud Schwär¹, Shunrong Ji, Liang Liu, Jiang Long, Volkhard Helms, Markus Hoth, Xianjun Yu, Bin Qu. Characterization of profilin1 functions in cytotoxic T lymphocytes. (Submitted)
4. **Xiao Zhou**, Eva C. Schwarz, Carsten Kummerow, Bin Qu, Hélène Lyrmann, Annette Lis, Christian Barhers, Cora Hoxha, Gertrud Schwär, Kim Friedmann, Rouven Schoppmeyer, Yan Zhou, Rengping Zhao, Adrian Angenendt, Arne Knörck, Sebastian Mang, Sabrina Capello, Shruthi S. Bhat, Carmen Mangerich, Markus Hoth. Efficient target cell killing by human CTL and NK cells at their respective Ca²⁺ optimum. (In preparation)

8. Acknowledgements

My deepest gratitude goes foremost to Prof. Dr. Markus Hoth, my supervisor, for the constant encouragement and guidance. Without his consistent support, patience and understanding, this thesis would not have reached its present form. Prof. Hoth is like a guiding star, and by following him one will sincerely enjoy the journey in science as well as in life.

My sincere gratitude also goes to Dr. Bin Qu for her extraordinary talent and guidance. Dr. Qu is always being supportive, motivated and encouraging. As a supervisor, she is smart and inspirational, as a friend, she is also always reliable and full of humor.

I would also sincerely thank Dr. Eva Schwarz, who is always encouraging and supportive. Dr. Schwarz is the person with a great and glorious personality that I can always look up to.

I am also greatly indebted to the entire group, with special thanks to Yan Zhou, Renping Zhao, Carsten Kummerow, Ivan Bogeski, Christian Bakes, Dalia Alansary, Shruthi Bhat, Kim Friedmann, Arne Knoerck, Cora Hoxha, Carmen Haessig, Gertrud Schwaer, Sandra Janku and our secretary Regine Kaleja.

I am also grateful to Prof. Dr. Heiko Rieger for formulating the compartment model. My sincere thanks go to the graduate school of Calcium Signalling and Cellular Nanodomains (GK1326) for the generous financial support and for the helpful scientific training courses arranged and coordinated by Prof. Dr. Dieter Bruns and Judith Wolf.

And finally, I cannot thank my beloved family enough for their deep love and constant belief in me through all these years.